GAS-SURFACE INTERACTIONS OCCURRING ON MATERIALS WITHIN ULTRAHIGH VACUUM

by

Ronald Allen Outlaw

Thesis submitted to the Graduate Faculty of the
Virginia Polytechnic Institute and State University
in partial fulfillment of the requirements for the degree of

DOCTOR OF PHILOSOPHY

of

MATERIALS ENGINEERING SCIENCE

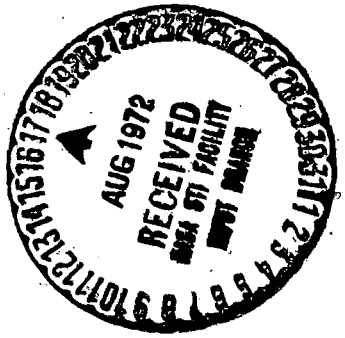

APPROVED:

Dr. J. P. Wightman, Chairman

Dr. J. L. Lytton

Dr. C. R. Houska

Dr. J. H. Steele, Jr.

Dr. L. H. Slack

May 1972

Blacksburg, Virginia

Details of illustrations in this document may be better studied on microfiche

(NASA-TM-X-68689) GAS SURFACE INTERACTIONS OCCURRING ON MATERIALS WITHIN ULTRAHIGH VACUUM Ph.D. Thesis - Va. Polytechnic Inst. R.A. Outlaw (NASA) May 1972 127 p CSCL 11D G3/18

N72-28573

Unclas 36800

GAS-SURFACE INTERACTIONS OCCURRING ON MATERIALS WITHIN ULTRAHIGH VACUUM

by

Ronald Allen Outlaw

(ABSTRACT)

The physical adsorption of nitrogen on the chemically cleaned surfaces of Pyrex, 347 stainless steel and polycrystalline nickel was investigated over the pressure range 1×10^{-12} to 3×10^{-7} torr and for temperatures 77.4° and 87.4°K. The adsorption data were linearized by the Dubinin-Radushkevich equation. The metal surfaces were cleaned by electron impact desorption (EID) and the desorbed gases analyzed by mass spectrometry. Work function measurements were also used to indicate changes in the surface condition following an EID dose. At least a monolayer of gas was observed to desorb from the metal surfaces. The isotherms revealed that the metal surfaces were very heterogeneous and that the Pyrex surface had been leached. The calculated isosteric heats of adsorption indicated that the relative order of the physical binding of nitrogen to the solids was 347 stainless steel > Pyrex > nickel.

A relationship was observed to exist in the dynamic technique between the equilibration time and the pressure above the adsorbed layer. The slope of the log-log plot of these parameters was found to

be sensitive to the surface heterogeneity and may be related to the activation energy for surface diffusion of physically adsorbed molecules.

Work function measurements indicated that oxygen adsorption occurred at 298^{o}K on the oxide covered surfaces of stainless steel and nickel and was followed by incorporation into the bulk. The incorporation appeared to be rapidly promoted by low energy electron impact.

ACKNOWLEDGMENTS

The author wishes to express his appreciation for the guidance provided by his advisory committee: Professor J. P. Wightman, Chairman; Professor J. L. Lytton, Professor C. R. Houska, Assistant Professor L. H. Slack, and Assistant Professor J. H. Steele, Jr. The author is especially grateful to Professor Wightman for his consistent encouragement and direction. A special thanks is extended to Mr. F. J. Brock of the Physics Department, Old Dominion University for his many helpful and enlightening discussions and for his assistance in various constructions on the apparatus.

The author would also like to express his appreciation to his Langley Research Center supervisor, Mr. Paul R. Yeager, for his patience and consideration over the past 2 years this work has been in progress. The author is indebted to Dr. W. S. Lassiter for allowing the use of his Auger Electron Spectrometer to conduct the EID experiment on nickel. Special gratitude is extended to Mr. Ronald F. Hoyt who has been of great assistance in maintaining and operating the apparatus. In addition, the following NASA employees have been helpful in many ways to the completion of this work: Mr. Paul G. Sandefur, Mr. Theodore E. Larson, Mr. W. F. Presson, and Mrs. Arlene R. Mitchell who typed this manuscript. Finally, the author wishes to express his thanks to his wife, Theresa, for her understanding, encouragement, and patience.

TABLE OF CONTENTS

		Page
I.	INTRODUCTION	1
II.	PREVIOUS INVESTIGATIONS	3
	A. Pyrex Glass	3
	B. Stainless Steel	5
	C. Polycrystalline Nickel	6
	D. Electron Impact Desorption (EID)	9
	E. Work Function Studies	12
III.	EXPERIMENTAL APPARATUS AND MATERIAL SURFACES	14
	A. Apparatus	14
	1. Main chamber	14
	2. Forechamber	14
	3. Pumps	17
	4. Short tube molecular leak	17
	5. Ionization gages	18
	6. Quadrupole mass spectrometer (QMS)	19
	7. Thermocouple gage	20
	8. Special electronics	20
	9. Valves	20
	10. EID/Work function cathode	20
	B. Material Surfaces	22
	1. 7740 Pyrex	22
	2. 347 Stainless Steel	23
	3. Polycrystalline Nickel	24
IV.	OPERATIONAL THEORY AND PROCEDURE	26
	A. Dynamic Technique	26
	B. Electron Impact Desorption	33
	C. Work Function Measurements	38
	D. Procedure	46
V.	RESULTS AND DISCUSSION	51
	A. N_2/Pyrex	51
	B. N_2/347 Stainless Steel	56
	C. Oxygen Reactions With 347 Stainless Steel	71
	D. N_2/Polycrystalline Nickel	72
	E. Oxygen Reaction With Nickel	86

Page

F. Equilibrium Time Study 91
1. N_2/Pyrex 91
2. N_2/347 Stainless Steel 95
3. N_2/Nickel 97

G. Surface Mobility and Clustering 98

VI. CONCLUSIONS 104

VII. BIBLIOGRAPHY 106

VIII. APPENDICES 110

A. An AES Experiment 110
B. Error Analysis 115

IX. VITA 117

LIST OF FIGURES

Figure		Page
1.	Isometric Drawing of Ultrahigh Vacuum System	15
2.	Schematic of Ultrahigh Vacuum System	16
3.	Schematic of Adsorption Vessels	21
4.	Schematic of Main Chamber, Adsorption Vessel and Electrostatic Ion Pump	28
5.	Typical Pressure - Time and Temperature-Time Behavior, Characteristic of the Dynamic Technique	31
6.	Potential Diagram Illustrating the Phenomena of EID	35
7.	Simplified Schematic of the EID and Work Function Circuitry to the Adsorption Vessel	39
8.	Potential Diagram Illustrating the Retarding Field Region for This Adsorption Vessel Geometry	43
9.	Typical Emission Current Versus Anode Voltage Plots Illustrating Change In Work Function	47
10.	Physical Adsorption Isotherms of Nitrogen On Pyrex	52
11.	Dubinin-Radushkevich Plots of Nitrogen On Pyrex	54
12.	Work Function Variation, $\Delta\varphi$, 347 Stainless Steel Versus EID Dosage, jt	58
13.	Mass Spectra of the Gas Composition During and After EID of 347 Stainless Steel	59
14.	The Unresolved Desorption Efficiency $\theta\eta'$, Versus Electron Energy, E, for 347 Stainless Steel	61
15.	Physical Adsorption Isotherms of Nitrogen On 347 Stainless Steel for Two Surface Conditions	63
16.	Dubinin-Radushkevich Plots of Nitrogen On 347 Stainless Steel for Two Surface Conditions	65
17.	Isosteric Heats of Adsorption, q_{st}, Versus σ of Nitrogen On 347 Stainless Steel for Two Surface Conditions	69

Figure Page

18. Work Function Variation, $\Delta\varphi$, Versus Exposure Time, t, of Oxygen On 347 Stainless Steel at 298°K 73

19. Work Function Variation, $\Delta\varphi$, Versus Exposure Time, t, of Oxygen On 347 Stainless Steel at Several Pressures (298°K). 74

20. The Variation in Pressure δ_p, Versus EID of 100 eV, 300 eV and 560 eV Electron Energies 76

21. Work Function Variation, $\Delta\varphi$, of Nickel Versus EID Dosage, jt 78

22. Physical Adsorption Isotherms of Nitrogen On Nickel for Two Surface Conditions 80

23. Dubinin-Radushkevich Plots of Nitrogen On Nickel for Two Surface Conditions 82

24. Isosteric Heats of Adsorption, q_{st}, Versus σ of Nitrogen On Nickel for Two Surface Conditions 85

25. Work Function Variation, $\Delta\varphi$, Versus Exposure Time, t, of Oxygen On Nickel at 298°K. 87

26. Work Function Variation, $\Delta\varphi$, Versus Time, t, Following Oxygen Exposure On Nickel at 298°K 90

27. Equilibrium Time, t_{eq}, Determination of Nitrogen On Pyrex for Several Equilibrium Pressures. 92

28. Linear Relationship Between the Equilibrium Time, t_{eq}, and the Pressure Above the Adsorbed Layer, p, of Nitrogen On Pyrex. 93

29. Variation in Equilibrium Time, t_{eq}, With Ion Current, i^+, of Nitrogen On 347 Stainless Steel for Different System Conditions 96

30. Variation in Equilibrium Time, t_{eq}, With Ion Current, i^+, of Nitrogen On Nickel for Two Surface Conditions 99

A-1. Auger Spectrum of Polycrystalline Nickel Before (a) and After (b) EID Cleaning 111

A-2. Variation of Auger Peak to Peak (PTP) Signals of Carbon, Sulfur and Oxygen Relative to Nickel with EID Time 113

LIST OF TABLES

Table		Page
I.	Temperature Dependence of D-R Constants for the System N_2/Pyrex	55
II.	A Comparison of σ at 1 x 10^{-9} Torr for N_2 on Several Adsorbents	66
III.	Temperature Dependence of D-R Constants for the System N_2/347 Stainless Steel	67
IV.	Temperature Dependence of D-R Constants for the System N_2/Nickel	83
V.	The Growth Rate of Clusters as a Function of Pressure	103

I. INTRODUCTION

This work is principally a study of the physical adsorption of nitrogen at very low pressures on Pyrex, 347 stainless steel, and polycrystalline nickel. A thorough study of surface chemical cleaning techniques was made to minimize the probability of surface contaminants introducing ambiguity in the experimental results of this work. The technique considered most reliable was applied to all experimental surfaces as well as to the interior of the entire vacuum system. In this study, adsorption was investigated over the pressure range 1×10^{-12} to 3×10^{-7} torr and at surface temperature $77.4^{\circ}K$ and $87.4^{\circ}K$. The Dubinin-Radushkevich equation is used to analyze the experimental data. It has been demonstrated repeatedly that this equation is satisfied by the physical adsorption data from a wide variety of gas-surface systems in the low pressure region. Work function measurements were made to monitor the variation of surface potential with coverage during electron impact desorption (EID) and to monitor the variation of surface potential with oxygen exposure (coverage). An ancillary Auger electron spectroscopy (AES) experiment on nickel was conducted to determine the efficiency of EID in cleaning the nickel surface.

Pyrex, stainless, and nickel were selected as adsorbents since these materials are commonly used in the construction of scientific instruments such as mass spectrometers and ion gages. Surfaces are covered with layers of adsorbed gases under ordinary conditions. During normal instrument operation these gases desorb and frequently compromise the data dealing with a specific experiment. It is not uncommon

to find that spurious surface effects completely obscure expected results of an experiment. Nitrogen, for example, adsorbed on an ordinary metal surface often reacts with surface contaminants such as carbon and hydrogen to form hydrogen cyanide. Adsorbed oxygen frequently yields carbon monoxide, carbon dioxide, and water. Atomic oxygen adsorbed on a metal surface is quite reactive, in fact, it is rarely detected in the neighborhood of a metal surface. Several classes of instruments have at least one high temperature surface. The thermal energy available at a hot filament has been known to dissociate an incident molecular species or to actually form a new species, e.g., hydrogen combines with the surface carbon to form methane. These examples are representative of the few that are understood.

Thus, an understanding of gas-solid interactions is important both from a fundamental and a technological viewpoint.

II. PREVIOUS INVESTIGATIONS

General reviews of gas-surface interactions pertinent to this research can be found in books by Young and Crowell[1]; Flood[2]; Ross and Olivier[3]; Hayward and Trapnell[4]; and Green[5]; Saltzburg, Smith, and Rogers[6]; Samorjai[7]; de Boer[8]; and Kaminsky[9]. Some of the procedures utilized in this work such as electron impact desorption techniques, mass spectrometric techniques, and work function measurement techniques are also included in these reviews. A discussion of the literature dealing with the specific surfaces studied is presented below.

A. Pyrex Glass

The adsorption properties of Pyrex have been frequently studied in the past because of its common use and convenience. Since many experimental vacuum systems are constructed of Pyrex, an adsorption vessel can be easily fashioned into a desired geometry and made an integral part of the system. Physical adsorption of various gases on Pyrex at pressures as low as 1×10^{-11} torr, and at temperatures as low as $4.20^{\circ}K$, using both static and dynamic techniques have been reported.[10-15]

A significant result developed by much of this work is that the data obtained fits well the Dubinin-Radushkevich equation

$$\sigma = \sigma_m \exp -B\varepsilon^2 \qquad (1)$$

where the Polanyi energy, ε, is given by

$$\varepsilon = RT \ln(p/p_o)$$

and σ = number of molecules adsorbed per unit area

σ_m = number of molecules adsorbed per unit area forming a complete monolayer

T = temperature of adsorbent/adsorbate

p = equilibrium pressure of adsorbate

p_o = saturation vapor pressure of adsorbate at T

R = gas constant

The apparent utility of this equation has focused a great deal of interest on its constants, σ_m and B. Kaganer[16], for example, has interpreted the constant σ_m to be the value of adsorption at monolayer coverage. Hobson and Armstrong[17], experimentally supporting this interpretation, found their nitrogen on Pyrex data to be very near the accepted monolayer density for nitrogen, 6.2×10^{14} molecules per cm^2. The constant B, which is characteristic of the gas-solid system, has been related to the mean energy of adsorption ($B^{-1/2}$) over the range of coverage investigated[18]. Attempts at analytically finding an accurate expression for B have been made by several authors[19-20], but at the present the D-R equation remains on a semi-empirical basis. Schram[21] has theoretically and experimentally questioned the interpretation of constant temperature in the Polanyi energy. When $\ln \sigma$ is plotted versus ε^2, the data obtained at all temperatures, if independent of temperature variation, should fall on the same straight line, but Schram has noted a small deviation in slope for different

temperature isotherms. He reported that this result should be expected if $\partial\varepsilon/\partial T$ is not a function of temperature. Others have also observed this deviation experimentally on Pyrex.

Another observation of significance is that Pyrex (roughness factor between 1 and 2) does not appear to be a homogeneous surface. This is implied by the ascending isosteric heat of adsorption curves with decreasing coverage[22]. For example, isosteric heats for nitrogen on Pyrex vary from approximately 3.5 to 6.0 kcal/mole for coverages between 2×10^{-1} and 1×10^{-3} [23]. This apparent surface heterogeneity probably accounts for the fact that Henry's Law is not observed in the isotherm data obtained by the above authors.

B. Stainless Steel

In recent years, stainless steel has become a material of great concern to the surface scientist because of its common use in space flight applications and ultra-high vacuum instrumentation. Instruments constructed of stainless provide surfaces of complex and unknown adsorptive properties, which, at low pressure, can severely alter the gas composition and make it difficult or impossible to correctly interpret the experimental data.

Troy and Wightman[24] have recently reported physical adsorption data of N_2, CH_4, Ar, and Kr on 304 stainless steel in the pressure range 10^{-9} to 10^{-4} torr using a static technique. The stainless was used in the as received condition with the exception that it was baked (~ 250°C) following system evacuation. Since no other cleaning techniques were used, the surface was most likely a complex arrangement of the oxides

of iron, chromium, and nickel interspersed with the contaminants carbon and sulfur, and partially covered with adsorbed gases such as hydrogen and carbon monoxide. This surface condition is frequently typical of instrument surfaces in normal operation. Troy and Wightman found that the relative order of binding strength of the gases investigated is $Ar < Kr < N_2 < CH_4$. The excess isosteric heats (difference between isosteric heat and heat of vaporization) obtained for nitrogen as calculated from the D-R equation, varied from 5 to 1.6 kcal/mole over a range of coverage 10^{-3} to 6×10^{-1}. The contribution to adsorption energy of the nitrogen quadrupole moment was found to be about 30% of the total interaction. They found also that all their data could be linearized by fitting to the D-R equation but, as previously reported by Schram, they did not find complete temperature correlation. Their BET determination of the surface area indicated a roughness factor somewhere between 2 and 5.

Degras, Schram, Lux and Petermann[25] found, using flashed clean 304 stainless ribbon, adsorption heats of 6 kcal/mole for H_2 and about 4 to 5 kcal/mole for CO. Hydrogen is commonly found as the prominent residual gas in a metal vacuum system and carbon monoxide is usually present in all vacuum systems because of its generation by instrument hot filaments.

C. Polycrystalline Nickel

Pure nickel and nickel alloys are also often used in the construction of instrumentation for low pressure measurements. Unlike stainless, however, a great deal of research has been done on both

crystalline and polycrystalline nickel[26]. Unfortunately, little has been done to establish the properties of physical adsorption of gases on nickel at space-like pressures ($< 1 \times 10^{-9}$ torr). This, of course, is a very important pressure threshold since it is common to space and the lunar atmosphere.

Early physical adsorption studies by Zettlemoyer, Yung-Fang Yu, and Chessick[27] of argon on oxide coated and reduced nickel powders resulted in heats of adsorption of 4.7 kcal/mole and 3 kcal/mole, respectively. Later, low pressure studies by Schram[28] of argon on nickel foil, mounted within a Pyrex envelope, gave isosteric heats of 7.2 to 3.5 kcal/mole corresponding to coverages of 10^{-6} and 10^{-1}. The nickel foil was cleaned by rf heating at 800°C in an environment of 10^{-10} torr. The data was obtained using the static technique and subtracting the Pyrex isotherm data from the nickel-plus Pyrex isotherm data. Schram concluded from this work that the slopes of the D-R equation are, in fact, temperature dependent as predicted by his theoretical analysis. This effect appeared to be small ($dB/dT \sim 10^{-9}$). A similar but substantially larger temperature effect has been noted experimentally by Troy and Wightman[29] with the adsorption of Ar and CH_4 on 304 stainless steel. Troy and Wightman, however, did not suggest Schram's rationale as a possible explanation for this anomaly.

Baker and Fox[30] have dynamically studied the physical adsorption of krypton and xenon on nickel films deposited on Pyrex. Their data covered the pressure range 10^{-9} to 10^{-5} torr at temperatures between 77°K and 90°K. Isosteric heats obtained for krypton were linear over

the coverage investigated and varied from 5.2 to 4.5 kcal/mole. Oddly, the isosteric heats for xenon were also in this range. The authors made no comparison with the D-R equation, but did compare their data to the Freundlich isotherm, $\theta^n = k\ p$.

One of the most interesting gas-surface interactions is that of nitrogen adsorption on nickel at room temperature. It has been reported by many that molecular nitrogen does not chemisorb on the surface of nickel and by many that it does; both groups using a variety of methods to substantiate their conclusion[31-36]. This question is of importance to this work because chemisorbed nitrogen would occupy surface sites on the nickel. Winters, Horne, and Donaldson[37] reported nitrogen chemisorption on nickel at room temperature after the gas had been "activated" by electron impact. Chemisorption, in their experiment was attributed to N and N_2^+ reacting with the surface; both species resulted from electron bombardment of N_2 in the gas phase. It was their opinion that no activation energy was necessary for the chemisorption of atomic nitrogen, and that the ionized molecule probably receives the necessary energy to dissociate by Auger neutralization at the nickel surface. A recent electron energy loss spectroscopy paper by Steinrisser and Sickafus[38] reported at the 1971 International Solid Surface Conference, revealed an unordered adlayer of nitrogen on the nickel (110) face. No evidence was given as to whether the nitrogen was in an excited, atomic, or ionic state prior to adsorption. Gregory and Hayward[35] have reported the chemisorption of "activated" nitrogen on nickel thin films and nickel ribbons at room

temperature. The nitrogen was "activated" by thermal dissociation on tungsten and by an rf discharge. The adsorbing gas was probably comprised of N, N^+, N_2^+ (the three dominant species), and N^{++}, N_3^+, and N_4^+. They found two adsorption states, termed α and β, with a desorption energy of 28 ± 4 kcal/mole for both states. This value is very near the decomposition energy of Ni_3N (25.5 kcal/mole). The authors suggest that the β state is Ni_3N because of this energy comparison and because the desorption and decomposition temperatures are both within the range, 250^o - 300^oC. No discussion was presented as to the energetics of the adsorbing species or to the fractions of N, N^+, and N_2^+, thus making it impossible to interpret whether N will chemically adsorb in its ground state on the nickel.

D. Electron Impact Desorption (EID)

Low energy electrons (< 1 keV) incident on a solid surface are known to induce the desorption of energetic neutrals and ions from the surface. This phenomena has become a common tool for the study of chemisorbed species on solids since it can yield valuable information about the nature of the bonding between adatom and the surface. Results of such studies and their associated techniques have recently been reviewed by Madey and Yates[39].

In this research, EID has been used to clean the metal surface. Although EID is not as efficient as ion bombardment in cleaning a surface, it does not destroy the surface order and does not increase the density of lattice defects as does the ion bombardment. Surface

contaminants such as water, sulfur, carbon, and the oxides of nickel must be removed in order to measure true nitrogen binding energies on polycrystalline nickel.

Klopfer[40] has noted the disappearance of chemisorbed oxygen and NiO on nickel by heating to temperatures of about 500°K. This occurs, however, only when the oxygen concentration dissolved in the metal is low. Thus, a simple bakeout on a nickel specimen, with relatively little oxygen in the bulk, could leave the nickel surface virtually free of oxygen. Horgan and King[41] have observed a remarkable transition of the capture probability at 0.25 monolayers when a nickel film is exposed to oxygen. Initially, the oxygen is nondissociatively adsorbed into an unordered state with a heat of adsorption of 50 kcal/mole. At the quarter monolayer point, the transition, termed β' to β, occurs and a stronger, more ordered state with a heat of adsorption of 110 kcal/mole results. By increasing the temperature of the surface the transition disappears since according to Klopfer's interpretation the oxygen has diffused into the bulk at the higher temperature. Horgan and King indicate a third stage occurring at a coverage of one oxygen atom for one nickel atom. At this point a sharp drop in capture probability is evident and an oxide film begins to form slowly. A general interpretation of this slow process is that the excess oxygen is penetrating into the metal lattice. Delchar and Tompkins[47] observed oxygen uptake in nickel films exceeding a monolayer at 298°K and have interpreted this as oxygen incorporation.

Klopfer's[40] EID studies revealed the startling fact that no atomic oxygen was desorbed, only O_2 and O^+. He determined that the desorption efficiency was very small until a coverage of 7.5×10^{14} molecules/cm^2 had been adsorbed and from that point obtained a desorption efficiency which increased linearly with coverage. Klopfer considered that the low desorption efficiency ($\eta' < 10^{-5}$ molecules/electron) is connected with the previously discussed oxygen incorporation.

Klopfer[43] has also studied the effects of adsorbed water on nickel by EID. The salient result coming from this work is that at partial pressures of water below 10^{-8} torr, the efficiency decreases linearly. At a current density of 1 ma/cm^2, an electron energy of 400 eV, and a pressure of 10^{-8} torr, about 10^{12} molecules/cm^2-sec is desorbed. Water is not usually a problem after a good bakeout, however.

Sickafus[44], using AES and LEED, has studied the contaminants sulfur and carbon on nickel. The nickel was cleaned by argon ion bombardment. He observed that the sulfur and carbon on the nickel form separate patches or regions which do not overlap. He found that the desorption energy of carbon is 0.60 eV and that desorption (as CO) occurs at temperatures greater than 400°C. This corresponds well to the desorption of CO on nickel. It was speculated from this result that oxygen reacts at the edge of the small carbon regions to form CO which can then desorb. Sickafus reasoned that the carbon may have been externally added to his nickel surface by the AES beam dissociating carbon bearing adsorbates. Coad and Riviére[45] have also studied carbon on nickel by AES. They found the ordering of carbon with nickel in the proportion Ni_3C below

400°C, but that its dissociation occurs above that temperature.

Hydrogen adsorption on nickel has been studied by many with a wide variation in data, but only H^+ ions have been observed as the desorption species from EID[39]. There has not yet been a report of neutral desorption. Williams and Gasser[46] obtained a total desorption cross section less than 5×10^{-18} cm^2 with the CO contamination less than 1% of the hydrogen pressure, but the cross section climbs to 2×10^{-16} cm^2 with CO 30% of the gas.

E. Work Function Studies

The surface state of metal systems can be studied by the use of its change in work function[47]. In this work the retarding field diode technique was used to monitor the effect of the EID treatments[48].

Baker and Johnson[49], adopting the photoelectric emission technique for measuring the work function of nickel thin films, also used the work function to infer surface heterogeneity and surface cleanliness. They observed marked increases in work function with CO exposures greater than 1×10^{-7} torr and that the increase was greatest on the (111) crystal plane. CO_2, O_2, and CH_4 were also found to increase the work function of nickel. Suhrmann and Wedler[50], using the same technique, found that the work function of nickel thin films decreased with decreasing substrate temperature during nickel deposition. This could be explained by noting that as the surface order decreases it is easier for electrons to escape. A value of 4.9 eV was obtained for nickel deposited at 300°K. Farnsworth and Madden[51] also noted a

decreasing work function after ion bombarding nickel single crystals. The ion bombardment produced atomic disorder and a high density of lattice defects. Cardwell[52], using the photoelectric emission technique, determined a polycrystalline nickel ribbon to have a work function of 5.06 eV. Riviére[53], using the contact potential difference, measured the work function of a nickel thin film, deposited at 300°K, to be 4.73 eV.

The significance of the above measurements points to the utility of the work function as a monitor of the relative surface condition. A rough, heterogeneous surface will give a lower work function due to the patches of disordered surfaces that are peaked or mount structured. There are simply lesser numbers of nearest neighbors to impede an electron's escape. When gas is adsorbed on a surface, however, it represents (usually) a negative charge center that tends to inhibit electron escape, thus giving rise to a higher work function.

III. EXPERIMENTAL APPARATUS AND MATERIAL SURFACES

The following section is a description of the ultrahigh vacuum system and equipment and the material surfaces.

A. Apparatus

An isometric drawing and schematic diagram of the ultrahigh vacuum system are shown in figures 1 and 2. The system consists of a main chamber, a forechamber, a turbo-molecular pump, an ion pump/titanium sublimator combination, an electrostatic ion pump, two calibrated ion gages, a quadrupole mass spectrometer, a molecular leak, a thermocouple gage, various auxillary pumps, and a variety of flanges, valves, vacuum hardware and electronics.

1. Main chamber.- The main chamber is constructed of 347 stainless steel and was chemically etched to lower its outgassing rate. The adsorption vessel is attached below this chamber. During bakeout, valves (a), (b), and (c) and (d) are open but during operation, valve (d) is closed. The pressure and gas composition in this region were monitored by a Helmer bent-beam ionization gage and a quadrupole mass spectrometer, respectively.

2. Forechamber.- The forechamber is constructed of 347 stainless and was also chemically etched. It is separated from the main chamber by a short tube molecular leak and valves (c) and (d). During bakeout all valves except (e) are open. During operation, valves (c), (e), and (g) are open. The pressure in this region is monitored by a Nottingham-type ion gage.

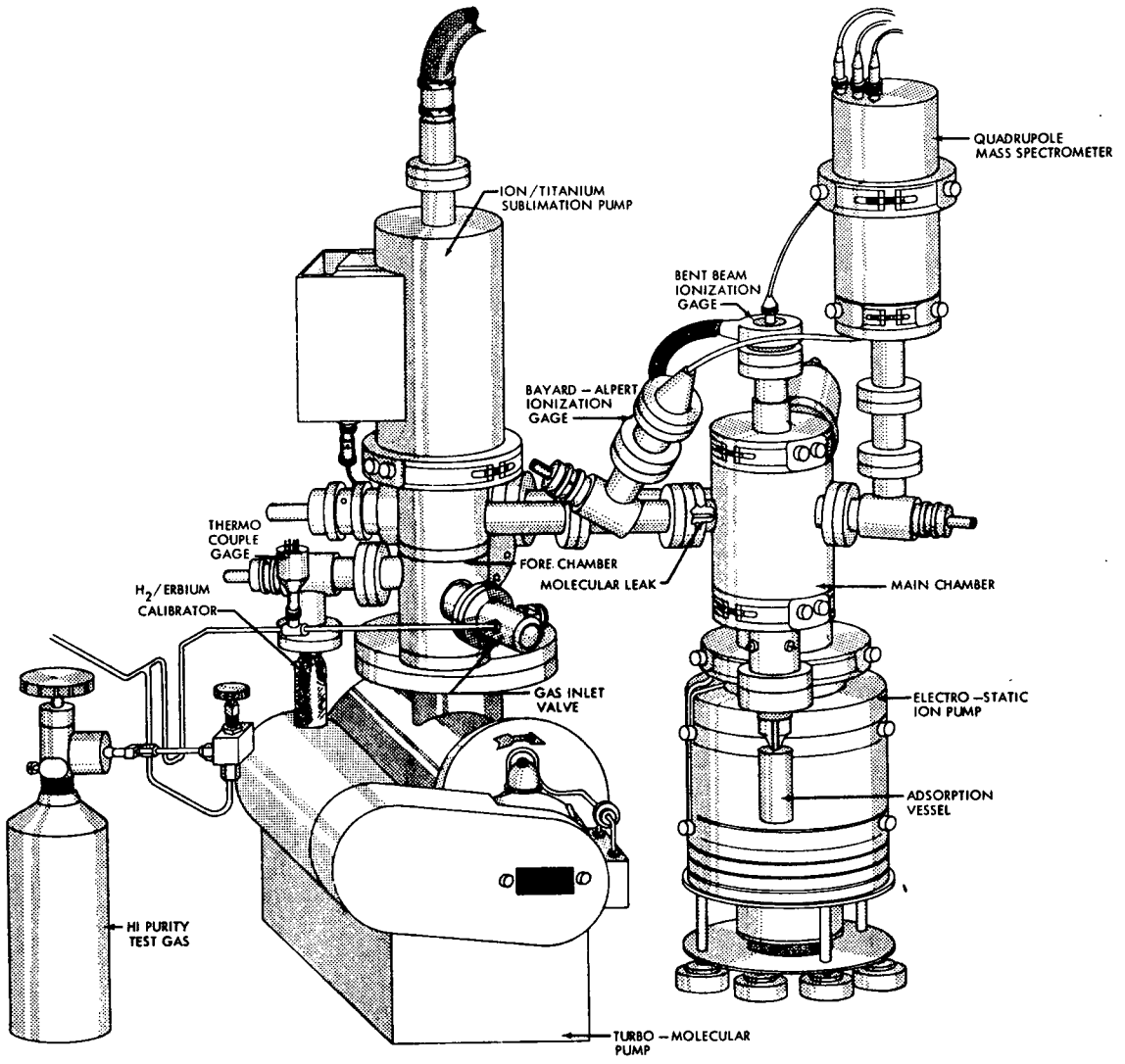

Figure 1.- Oblique Drawing of Ultrahigh Vacuum System.

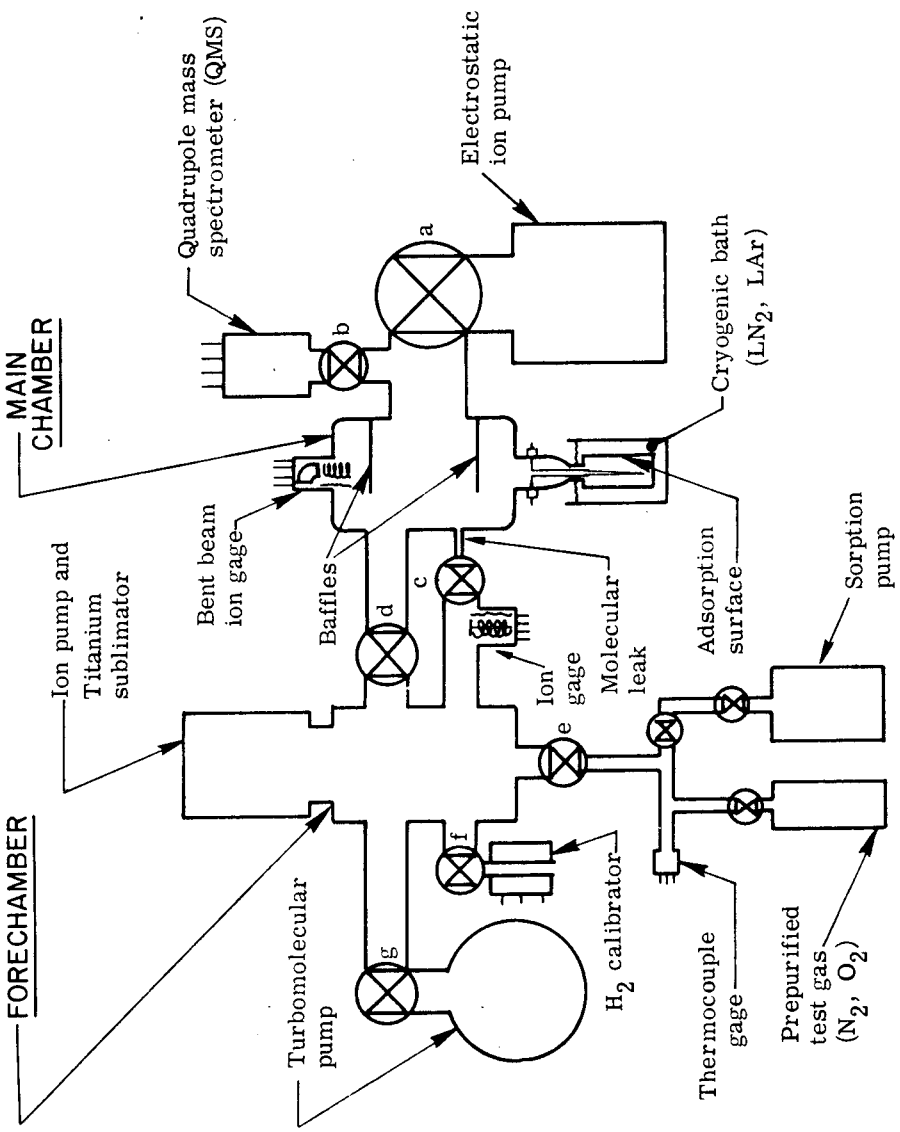

Figure 2.- Schematic of Ultrahigh Vacuum System.

3. Pumps.- The system is initially rough pumped by the 265 liter/sec (N_2) turbo-molecular pump. It is the only pump operating during bake-out. During operation, valve (g) is only slightly open so that some turbine pumping is maintained. The forechamber is primarily pumped by a 500 liter/sec (N_2) ion pump/titanium sublimator combination. The main chamber is pumped by a 1200 liter/sec (N_2) electrostatic ion pump. The pumping speed in the main chamber is regulated by adjusting the piston of the 10.16 cm bakeable valve (a).

A sorption pump in combination with a mechanical pump is used to evacuate the copper gas inlet line.

4. Short tube molecular leak.- The short tube molecular leak separates the main chamber from the forechamber during operation and provides a controlled gas flow rate into the main chamber from the forechamber. The leak is a cylindrical tube (347 stainless steel) brazed to a 7 cm blank-off insert that has knife edges machined on each side. The assembly fits between two standard 7 cm con-flat flanges. The dimensions of the leak tube are 3.81 cm in length and 0.319 cm in diameter corresponding to a conductance of 0.095 liter/sec (N_2, 298°K). The conductance of the leak (c) was determined from

$$c = 3.638\ \zeta\ A \left(\frac{T}{M}\right)^{1/2} \qquad (2)$$

where

ζ is the transmission probability

A is the cross sectional area

T is the absolute temperature of gas

M is the molecular weight of gas

The flow rate, Q, through the leak into the main chamber is

$$Q = c(p_f - p_m) \tag{3}$$

where

p_f is the pressure in the forechamber

p_m is the pressure in the main chamber

Since $p_f >> p_m$ when the test gas is admitted into the forechamber, the flow rate is

$$Q \approx c\ p_f \tag{4}$$

5. Ionization gages.- The nude Helmer bent beam ionization gage has a collector which is optically baffled from its grid ionization region. This configuration reduces the X-ray current to less than 1×10^{-14} amps. The ions are electrostatically deflected and focused onto the baffled collector. Pressure measurements on the order of 1×10^{-13} torr are thus possible. The gage is operated at an emission current of 10 milliamps and at voltages recommended by the manufacturer.

The nude Nottingham gage is capable of pressure measurements down to its X-ray limited pressure of 1×10^{-11} torr. This gage is operated

at low emission current of 40 microamps in order to preserve the gage constant at high forechamber pressures (~ 1 x 10^{-5} torr). The electrometer used for ion current measurements for the Helmer gage had a background (noise) current of about 5 x 10^{-15} amps and has current supression capability. An electrometer having a background current of about 5 x 10^{-15} was used with the Nottingham gage.

The ion current is related to the pressure by

$$\frac{i^+}{i^-} = Kp \qquad (5)$$

where

K is the gage constant

i^+ is the ion current

i^- is the emission current

p is the pressure

The gage constants for both main chamber gage K_m, and forechamber gage K_f, were determined by an orifice calibration system based on a system described by P. Clausing[54]. The value of K determined for each gage was: K_m = 8.8 $torr^{-1}$, K_f = 28.5 $torr^{-1}$.

6. Quadrupole mass spectrometer (QMS).- The instrument used for determining the residual gases remaining in the main chamber was a quadrupole mass spectrometer. The electron multiplier was modified by isolating the final collector from the ceramic boards. This was done to minimize leakage currents that become a problem at low pressures. The multiplier was also oxygen treated to rejuvenate the

gain and permit lower operational voltages (~ 2000 V). The emission current was set at 1 milliamp and the anode voltage at 70 Vdc. This instrument was not calibrated but was compared to the ionization gages.

7. Thermocouple gage.- A Pirani-type thermopile gage was used to monitor the pressure in the gas inlet line; typically, about a micron after evacuation and about 760 torr when charged with the test gas.

8. Special electronics.- An integrating digital voltmeter was used for calculating the area under the pressure-time curve. This instrument is capable of continuous integration and is used in conjunction with the suppressor electrometer to electronically determine the number of molecules adsorbed on the surface.

9. Valves.- Valve (c) is a 2.54 cm straight-through bakeable valve and is for closing off the molecular leak. Valves (d) and (g) are 5.08 cm bakeable valves; valve (d) for bakeout pumping of the main chamber, and valve (g) for closing off the turbine pump. Valve (a) is a 10.16 cm bakeable valve and was used for regulating the main chamber pumping speed. Valve (e) is a bakeable bleed valve.

10. EID/Work function cathode.- A thoria coated, 0.25 mm diameter tungsten cathode was used for both electron impact desorption and work function measurements and is shown schematically in figure 3. The cathode (1.32 cm^2) coating was sintered and cleaned (in a separate experiment) and the emission found to be approximately 10 ma/cm^2 for a temperature of 1200°C. This value agrees reasonably well with the literature[55]. During work function measurements the cathode was

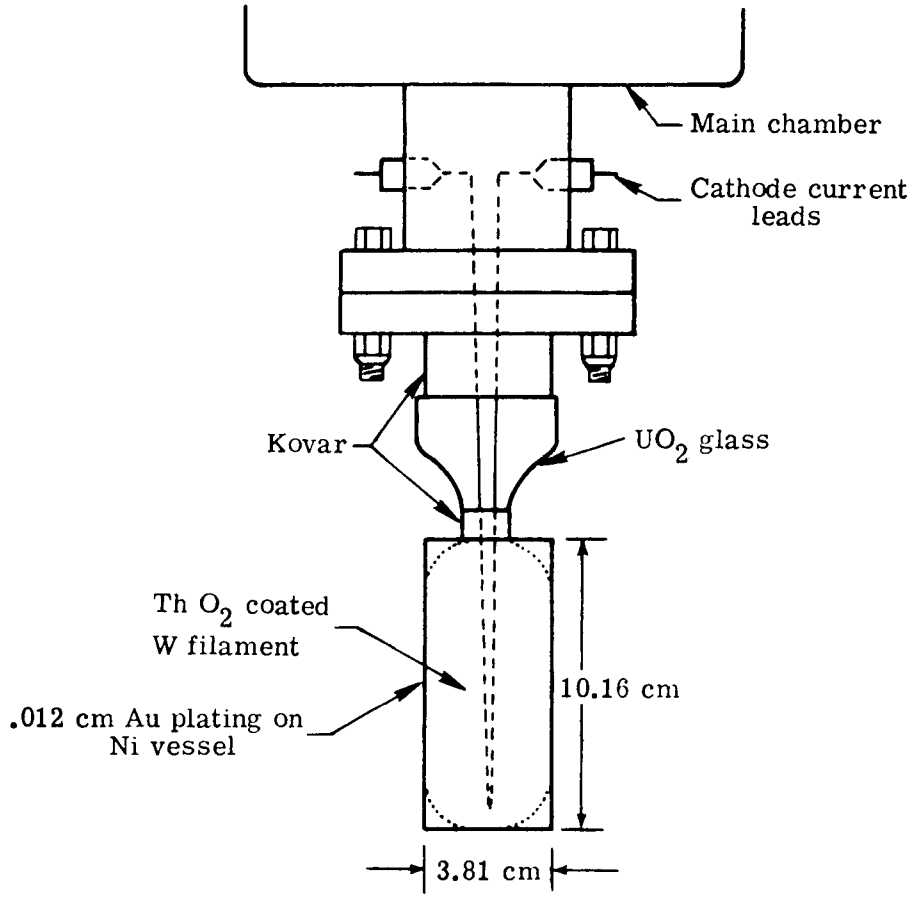

347 STAINLESS STEEL and NICKEL geometry (solid line)
A = 135 cm^2; t_w = 0.1 cm

PYREX geometry (dotted line)
A = 107.8 cm^2; t_w = 0.15 cm

Figure 3.- Schematic of Adsorption Vessels.

operated at a temperature of 900°C and during EID, the temperature did not exceed 1200°C.

These temperature constraints were used to assure that the total quantity of thorium deposited on the adsorption vessel surface during the total time that the cathode was on, was completely negligible compared to a monolayer.

B. Material Surfaces

The rationale for studying the adsorption properties of gases on 7740 Pyrex glass, 347 stainless steel and pure polycrystalline nickel, has been stated earlier. The following is a physical description of the adsorption vessels and a description of the method used to prepare the respective surfaces for ultrahigh vacuum and the surface investigation.

1. 7740 Pyrex

The Pyrex was shaped as shown (dotted line) in figure 3. Previous investigators studying Pyrex, have made no special surface preparations other than a standard degreasing before mounting on the vacuum system, and a standard bakeout. In this work, the Pyrex was chemically treated in addition to the above steps. A four step process, developed by the Diversey Company,has been found to effectively clean the surface of many metals and ceramics. The Pyrex vessel was cleaned by this process before mounting onto the vacuum system.

The four steps are:

(1) Degreaser - Essentially a noncaustic, alkaline cleaner which is heated to 75°-85°C. The immersion time is determined such that the

surface will pass the water-break test. This step is followed by a distilled water rinse.

(2) Oxidizer - A highly alkaline material containing caustic soda and an oxidant and heated to 95°-105°C. This bath sets up the surface oxides for easier removal. Immersion time is dependent on the type of material and the surface condition; usually greater than 30 minutes. This step is also followed by a distilled water rinse.

(3) Oxide remover - A mixture of acids maintained at room temperature. Immersion time is only 3-5 minutes or until the oxides are removed. The part is again rinsed in distilled water.

(4) Etchant - Concentrated acid that is heated to 80°C. Surface area of the part must be very small relative to the total volume of acid to permit a constant etchant rate. Immersion time is dependent on the material and desired amount of etching. (The Pyrex was left in this bath for 10 minutes.) Final rinse is in hot, deionized water, used in conjunction with an ultrasonic cleaner, to dislodge the product salts that are formed.

The Pyrex was then mounted on the vacuum system, evacuated to 1×10^{-8} torr and baked for 4 days at 450°C. The pressure observed during bakeout was typically 1×10^{-7} torr.

2. 347 Stainless Steel

The stainless steel was obtained from the Langley Research Center material stock and may be described as good quality. The adsorption vessel was machined from bar stock to the dimension as shown (solid line) in figure 3. The inside surface was finished by polishing with

number 600 grit silicon-carbide paper to a profilometer reading of less than 8 microinches. The stainless was then fired in vacuo to 1000°C for 30 minutes to diffuse bulk impurities to the surface and "lock" them up in surface sites. The Diversey chemical process, as described above, was then used to remove surface impurities. The stainless was etched for 10 minutes, which removed 0.017 mm and was ultrasonically scrubbed for 10 min. After mounting on the vacuum system and a bakeout similar to above, electron bombardment (EID) of the steel was initiated. After each bombardment dosage, a measure of the relative work function was made. The results of the EID and work function measurements will be discussed later.

3. Polycrystalline Nickel

The high purity nickel was obtained from the Materials Research Corporation. It was produced by vacuum casting and purified by a three-pass zone refinement. Material analysis has shown the following major impurities:

Impurity	Content (ppm)
C	37.0
N_2	3.0
O_2	18.0
P	< 15.0
Cr	1.5
Fe	12.0
Sb	< 2.0
Sn	4.0

The nickel adsorption vessel was machined to dimensions (figure 3) and the inside surface polished to a finish of less than 8 microinches using no. 1000 grit diamond paste. The nickel adsorption vessel was then vacuum fired to 1000°C for 30 minutes, removed and subjected to the Diversey cleaning process as previously described. The etching time was 10 minutes which corresponds to a removal of 0.0017 mm of nickel. Larger etching times appeared to yield the usual preferential attack of certain grains. Finally, a 0.013 mm layer of gold was electroplated onto the nickel outside surface to inhibit hydrogen (and to a lesser extent, oxygen) diffusion into the bulk from the atmosphere during bakeout.

After mounting onto the vacuum system, the vessel and system were evacuated and baked as before. Electron bombardment and work function measurements were then started, the results of which are discussed later.

IV. OPERATIONAL THEORY AND PROCEDURE

There are several ways of obtaining the data from which adsorption isotherms may be constructed. The two most often used approaches are called static and dynamic. The static technique has been commonly used for many years by many researchers[56]. This technique involves isolating the chamber by valve closure and then bleeding a test gas into a vacuum chamber where the test surface is located. The pressure in the chamber is measured and then the test surface is cooled to a prescribed temperature. The pressure in the chamber is again measured and this difference in gas phase pressure is related through the perfect gas law to the molecules adsorbed on the test surface. In this technique, corrections must be made for the ionic pumping of the gage and for the valve closure effect. The ion pumping of the gage is minimized by operating at low emission currents, but the effect is still significant, especially at low pressures.

A. Dynamic Technique

More recently, the dynamic technique has become popular[57]. As the term dynamic implies, there is gas flow. A constant number of molecules in the test chamber is established by bleeding in at a constant flow rate and pumping out at a constant rate. When the test surface in the chamber is cooled to isotherm temperature the pressure equilibrium is upset until the surface stops adsorbing and the pressure equilibrium is re-established. By integrating this change of the

pressure over time, the number of molecules adsorbed can be determined through a molecular balance equation.

The advantages of the dynamic method are essentially threefold. First, significantly lower equilibrium pressures are obtainable because the test chamber is always being pumped and the pressure contribution from the outgassing of the walls is kept much lower. Second, there are no problems from gage pumping effects since they are small compared to the primary pumping speed. A third advantage is that no valves (except the bleed valve) must be opened or closed during the experiment. The biggest disadvantage of this technique is that flow rates and pumping speeds must remain very constant in order to make precise measurements. A second disadvantage is the extremely long time that is required to reach equilibrium at low pressures.

Consider the main chamber and the adsorption vessel schematic as shown in figure 4, for which

$n_m(t)$	number density in main chamber
$n_a(t)$	number density in adsorption vessel
n_f	number density in forechamber
$n_p(t)$	number density in electro-ion pump
$\sigma(t)$	number of molecules adsorbed per cm^2 on adsorption vessel surface
c_o	conductance to pump
c_a	conductance to adsorption vessel
c'_a	conductance from adsorption vessel
c	conductance of molecular leak

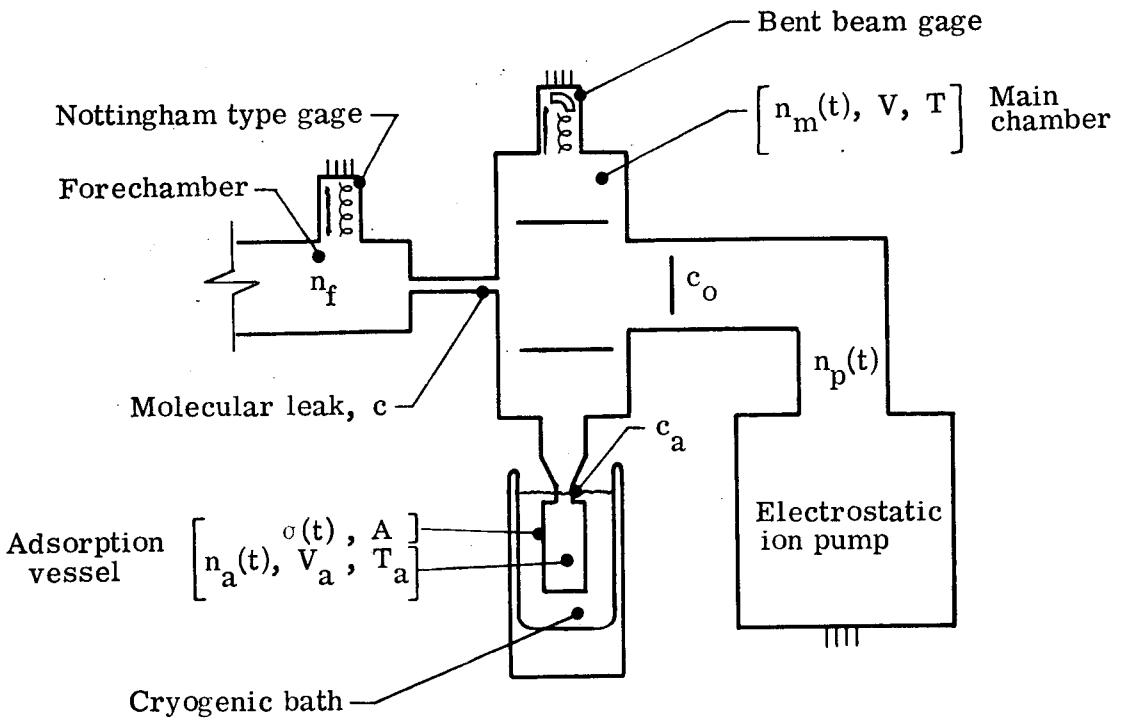

Figure 4.- Schematic of Main Chamber, Adsorption Vessel and Electrostatic Ion Pump.

V	volume of main chamber
V_a	volume of adsorption vessel
A	area of adsorption vessel
T	temperature of main chamber
T_a	temperature of adsorption vessel

Then the general equation for dynamic equilibrium molecular balance within the main chamber and within the adsorption vessel is

Rate of change of the number of molecules in chamber volume	=	Rate at which molecules enter chamber volume	=	Rate at which molecules leave chamber volume

The following conditions are applicable:

1. $n_m(t) \gg n_p(t)$ 2. $n_f \gg n_m(t)$ 3. Gage pumping is negligible

Thus the number density in the main chamber is given by

$$-\dot{n}_m(t)V + n_f c - n_m(t)c_o - n_m(t)c_a + n_a(t)c_a' = 0 \qquad (6)$$

The number density in the adsorption vessel is given by

$$-\dot{n}_a(t)V_a - A\dot{\sigma}(t) + n_m(t)c_a - n_a(t)c_a' = 0 \qquad (7)$$

Combining equation (6) and (7) gives

$$- \dot{n}_m(t)V - \dot{n}_a(t)V_a - n_m(t)c_o - A\dot{\sigma}(t) + n_f c = 0 \qquad (8)$$

and multiplying thru by dt and integrating between the limits $0 \rightarrow t$, $n_m(0) \rightarrow n_m(t)$, $n_a(0) \rightarrow n_a(t)$, $0 \rightarrow \sigma(t)$ gives

$$\sigma(t) = - \frac{V}{A}\left[n_m(t) - n_m(0)\right] - \frac{V_a}{A}\left[n_a(t) - n_m(0)\right]$$

$$+ n_f \frac{c}{A} t - \frac{c_o}{A}\int_o^t n_m(t)\, dt \qquad (9)$$

Equation (9) represents the number of molecules adsorbed at any time t. If a sufficient length of time is allowed after the adsorption surface is cooled, the number of adsorbed molecules will reach an equilibrium value, and

$$n_m(t_{eq}) = n_m(0) \quad \text{(See figure 5)}$$

$$n_a(t_{eq}) = n_m(0)\left(\frac{T_a}{T}\right)^{1/2} \quad \text{(thermal transpiration)} \qquad (10)$$

Equation (9) now becomes

$$\sigma(t_{eq}) = - \frac{V_a}{A} n_m(0)\left[\left(\frac{T_a}{T}\right)^{1/2} - 1\right] + n_f \frac{c}{A} t_{eq} - \frac{c_o}{A}\int_o^{t_{eq}} n_m(t)\, dt \qquad (11)$$

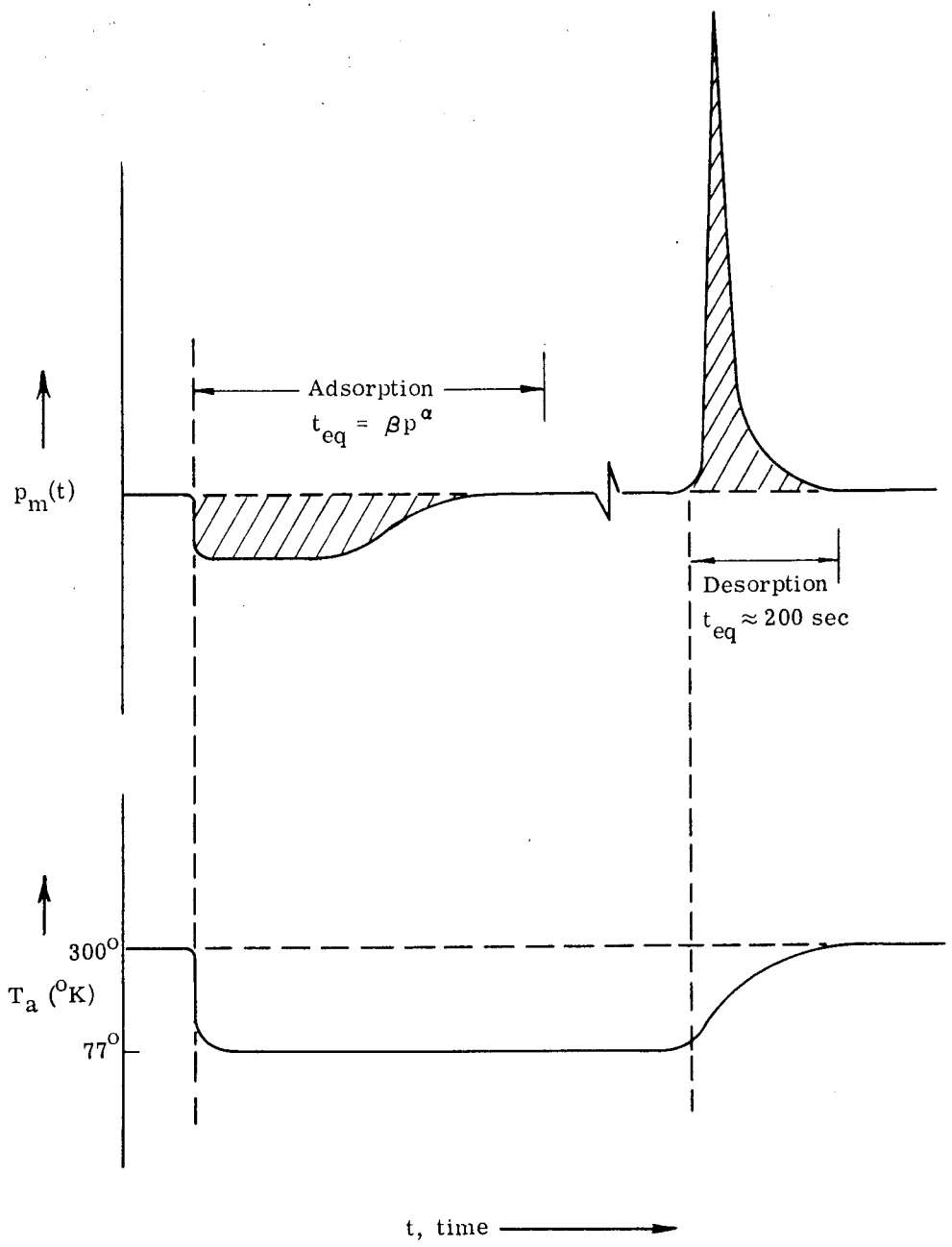

Figure 5.- Typical Pressure - Time and Temperature-Time Behavior Characteristic of the Dynamic Technique.

At low pressures ($p < 10^{-3}$ torr), the first term is negligible, so

$$\sigma(t_{eq}) \approx n_f \frac{c}{A} t_{eq} - \frac{c_o}{A} \int_o^{t_{eq}} n_m(t)\, dt \tag{12}$$

Now since $n_f c = c_o n_m(0)$ at equilibrium, equation (12) may be written

$$\sigma(t_{eq}) = \frac{c_o}{A} \int_o^{t_{eq}} \left[n_m(0) - n_m(t) \right] dt = \frac{c_o}{A} \int_o^{t_{eq}} \delta n_m(t)\, dt \tag{13}$$

In the dynamic technique, the equilibrium pressure is established by bleeding the test gas into the forechamber which, in turn, bleeds through the molecular leak into the main chamber at a flow rate, $n_f c$. The adsorption vessel surface to be studied is lowered to a prescribed temperature by immersion in a cryogenic bath. The adsorption then begins and the pressure in the main chamber decreases slightly. At equilibrium, the number of adsorbed molecules is constant, and the pressure returns to $n_m(0)$. The number density change integrated over this period of time is accounted for by the integral

$$\int_o^{t_{eq}} n_m(t)\, dt$$

The value of this integral is measured experimentally.

Equation (13) written in terms of pressure rather than number density becomes

$$\sigma(t_{eq}) = \frac{c_o}{AkT} \left[p_m(0) t_{eq} - \int_o^{t_{eq}} p_m(t)\, dt \right] \tag{13a}$$

$$= \frac{c_o}{AkT} \int_o^{t_{eq}} \delta p_m(t)\, dt \qquad (13b)$$

where k = Boltzmann's constant

$p_m(0)$ = pressure in main chamber at $t = 0$

$p_m(t)$ = pressure in main chamber at t

Finally, if the parameters in the above equation are replaced by their experimental equivalent then

$$\sigma(t_{eq}) = \frac{i_f^+ c_o}{i_m^+ s_f AkT} \left[IDVM\right] \equiv \sigma \qquad (14)$$

where

i_f^+ = the ion current indicated by the forechamber gage (amps)

i_m^+ = the ion current indicated by the main chamber gage (amps)

s_f = the sensitivity of the forechamber gage (amps/torr)

IDVM = the integrated result obtained from the desorption cycle (amp-sec)

B. Electron Impact Desorption

The laws of conservation of momentum and energy show that a chemisorbed molecule cannot be removed by low energy electron impact in an elastic process. Recent theories, based on the electron excitation and dissociation of gaseous molecules, have been presented which give plausible explanations of the EID phenomena. Since the time associated with excitation is much shorter than the time associated with nuclear movements (Franck-Condon principle) it has been theorized that incident

electrons cause electronic transitions in the adsorbed molecules[58]. Figure 6 shows the two states before and after excitation. Originally the adsorbed molecule is in the potential well described by the chemical interaction between adatom and the metal. After excitation, the ionized adsorbed molecule and metal have a new interaction that is repulsive. The result is that before the interaction can adjust to an attractive one, the adatom desorbs as an ion. A large fraction of these ions are neutralized before they can get away from the surface so that the major portion of desorbed particles are neutrals. Excited neutrals that are formed from the incident electron flux, desorb in a similar manner by being elevated to the anti-bonding curve. Additionally, since the Franck-Condon region has an effective width the desorbed neutrals and ions come off with a range of kinetic energies.

This, of course, is an extremely simplified explanation of the phenomena since there are many other influencing factors (e.g. Auger neutralization and transition back to the adsorbed bound state), but it serves to illustrate desorption not possible by direct energy transfer between incident electron and the adsorbed molecule.

Menzel and Gomer[58] have determined that the total probability of desorption, irrespective of mode, at a distance z_o from the surface is

$$P_T(z_o) = \exp\left\{- m^{1/2} \int_{z_o}^{z_c} \frac{R(z)}{\left[\Phi(z_o) - \Phi(z)\right]^{1/2}} dz \right\} \qquad (15)$$

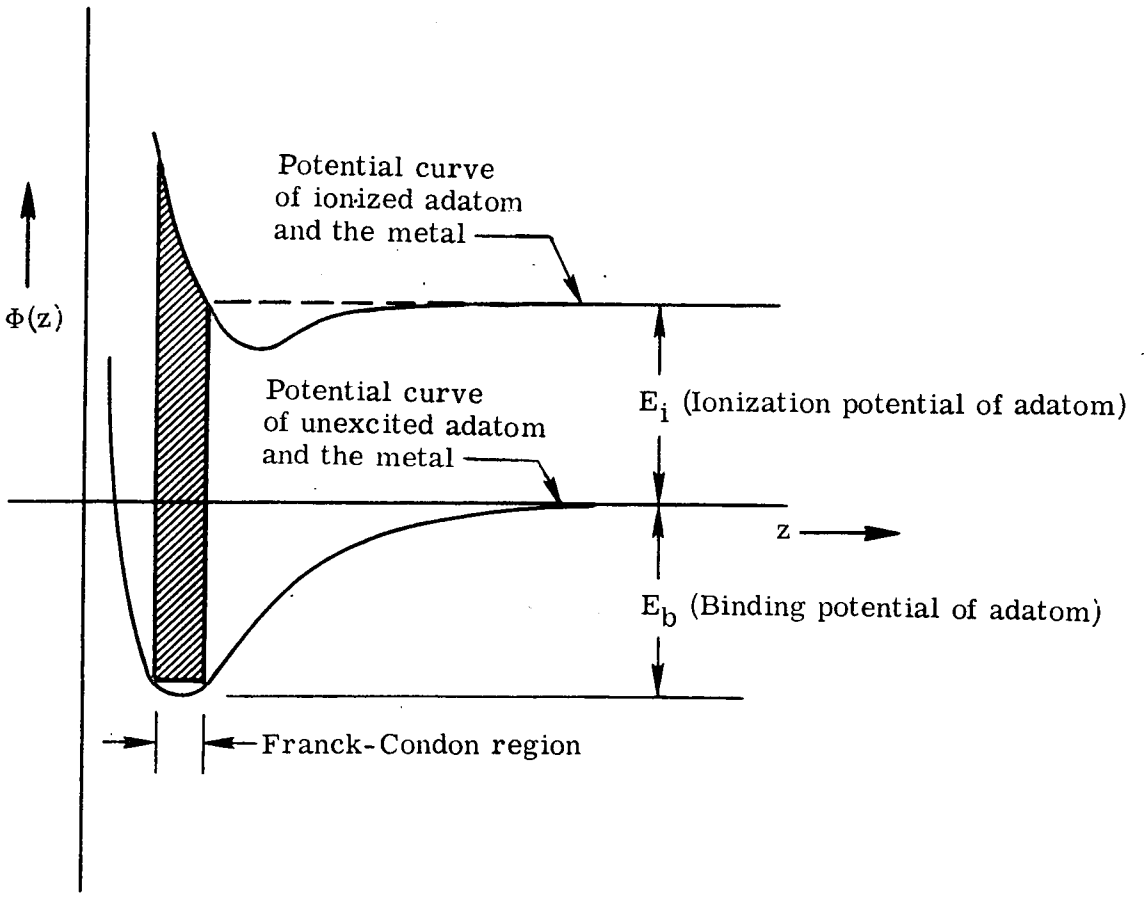

Figure 6.- Potential Diagram Illustrating the Phenomena of EID.

where $R(z)$ = rate of neutralization of ions at a distance z from the surface

$\Phi(z)$ = excited state potential function

m = mass of ion

z_c = critical recapture distance

If the energy spread of neutrals and ions is given by $f(E)$, then the total yield of neutrals and ions is

$$\psi_T = \frac{\int_o^\infty f(E)\, dE}{\int_o^\infty \frac{f(E)}{P_T(E)}\, dE} = \frac{\Omega}{\Omega^*} \tag{16}$$

where Ω is the cross section total for desorption and Ω^* is the cross section for excitation of the adsorbed species.

The integrals in equation (16) cannot be evaluated without detailed knowledge of the functional form of $f(E)$ and $P_T(E)$. Desorption yields must be determined experimentally.

Experimental determination of the first order desorption from an adsorbed layer with coverage θ is given by

$$\dot{\theta}(t) = \kappa(\theta)\gamma p - \frac{j}{e}\frac{\eta'}{\sigma_o}\theta(t) \tag{17}$$

where κ is the capture probability

γ is the incident gas flux

p is the pressure

j the current density

e the electronic charge .

σ_o the number of adsorption sites per unit area

η'/σ_o the desorption cross section ($\eta'/\sigma_o \equiv \Omega$)

If the background pressure of adsorbed gas is low the first term may be neglected and equation (17) is

$$\dot{\theta}(t) = - \frac{j}{e} \frac{\eta'}{\sigma_o} \theta(t) \tag{18}$$

Integration from an initial coverage, θ_o, gives

$$\theta(t) = \theta_o \exp\left[- \frac{j}{e} \frac{\eta'}{\sigma_o} t \right], \quad \eta' \neq \eta'(\theta) \tag{19}$$

or

$$\ln \frac{\theta(t)}{\theta_o} = - \frac{j}{e} \frac{\eta'}{\sigma_o} t \tag{19a}$$

Thus a semilog plot of $\ln \frac{\theta(t)}{\theta_o}$ versus $\frac{j}{e}$ t will give information about the desorption efficiency, η'.

Unfortunately, in this experiment the mass spectrometer is not in a line-of-sight to the adsorption vessel, so no direct identification of the desorbed molecules can be obtained. θ_o is also unknown. Quantitative variations can be inferred, however, by noting the change of peak heights in the mass spectrum during bombardment. The gas flux coming from the adsorption vessel is

$$q(t) = S\delta p(t) \tag{20}$$

where S = the system pumping speed for the particular gas specie

$\delta p(t)$ = the change in the partial pressure during bombardment

Since

$$\dot{\theta}(t) = -\frac{q(t)}{A\sigma_o} = -\frac{S}{A\sigma_o}\,\delta p(t) \tag{21}$$

then by combining (18) with (21) yields

$$\theta(t)\eta' = \frac{S\delta p(t)}{Aj/e} \tag{22}$$

or the unresolved electron desorption efficiency. Integration of equation (21)gives

$$(\Delta\theta)_{\Delta t} = -\frac{S}{A\sigma_o}\int_o^{\Delta t} \delta p(t)\, dt \tag{23}$$

Since the right hand of equation (23) can be obtained experimentally, the change in coverage for a given EID period can be determined.

The electrical schematic for the EID circuit is shown in figure 7.

C. Work Function Measurements

When an atom or molecule is adsorbed on a metal surface, a disturbance of the outer shell electrons occurs. This disturbance can be observed by measuring the change in work function of the metal. Basically, three different electronic interactions are possible

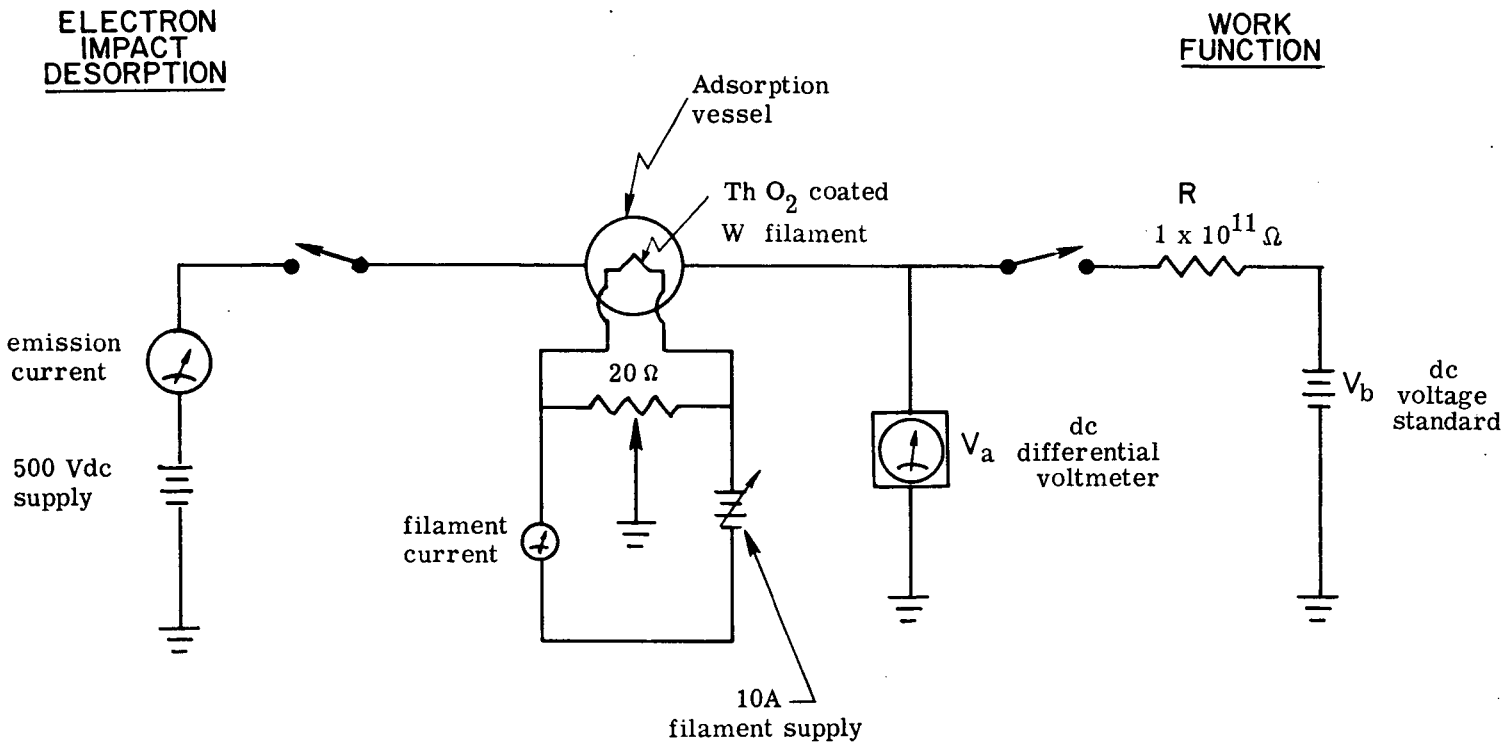

Figure 7.- Simplified Schematic of the EID and Work Function Circuitry to the Adsorption Vessel.

following the adsorption of the atom or molecule[59]. In the case of physically adsorbed gases, the atoms may tend to be polarized if the metal has a relatively large electron affinity. Second, weak chemical adsorption bonds, like hydrogen covalently bonded to nickel, change the work function. And finally, strong chemical adsorption bonds where electron transfer distances are significant, will give an increase or decrease of the work function (depending on the magnitude of the work function of the metal relative to the ionization energy of the adatom). Intermediate conditions are certainly possible between the above cases so that a physically adsorbed adatom may not only affect the work function by its polarization but also by overlapping of the electron states. This perturbation to the double layer of the metal lowers the work function proportionally by

$$\Delta\Phi \propto \frac{\phi}{I} - \frac{\xi}{\phi} \tag{24}$$

where I is the ionization potential

ξ is the electron affinity of the adsorbate

The work function should also be sensitive to coverage. If a classical electrostatic argument of the potential jump at the double layer is considered, the work function is given by[59]

$$\Phi = \Phi_o \pm 4\pi\, \sigma_1\, \mu_o\, \theta \tag{25}$$

where σ_1 is the adsorbed number per cm^2

μ_o is the dipole moment for the system

φ_o is the work function for clean metal

θ is the coverage

At low coverages ($\theta < 1/2$), theory predicts a linear relation between the change in work function and the change in coverage but at higher coverages theory predicts a nonlinear relation. Thus, at low coverages the surface state may be monitored as it is cleaned by EID.

A number of techniques to monitor the work function (and therefore, the coverage) were considered, but most of these methods required significant changes to the existing vacuum system. The cylindrical geometry of the adsorption vessel and the axial position of the EID cathode are compatible with the retarding field diode technique[48,60]. Basically, the cathode emits a flux of electrons which are incident on the adsorption vessel (anode). This electron flux density depends only on the cathode work function and the cathode temperature. The fraction of electrons received by the adsorption vessel depends only on the electron energy and the work function of the adsorption vessel metal. Therefore, if the cathode temperature is accurately controlled, the electron flux arriving at the adsorption vessel is dependent only on the work function difference and the voltage difference between the cathode and adsorption vessel. The applied voltage between cathode and adsorption vessel (V_a) determines the barrier height and the fraction of electrons reaching the adsorption vessel. If the voltage is such that the two surfaces have the same barrier height, all the electrons emitted from the cathode reach the adsorption vessel. (See

figure 8a) If the voltage is larger than this, the electron current reaching the adsorption vessel is unaltered since the field is essentially down hill (accelerating) as shown in figure 8b. If the voltage is smaller than the first case, the barrier is higher than the cathode barrier (retarding field region) as shown in figure 8c. Only that fraction of electrons with sufficient energy to go over the barrier are collected at the adsorption vessel.

The electronic flux leaving a cathode is given by

$$j_k = AT^2 \exp \frac{\varphi_k}{kT} \tag{26}$$

where A is a constant

T is the absolute temperature

φ_k is the cathode work function

The energy distribution of the above electrons is given by Fermi-Dirac statistics as

$$f(E) = C \exp\left(-\frac{E}{kT}\right) \tag{27}$$

where C is a constant.

If a retarding field exists outside the cathode, the fraction of electrons leaving the cathode with sufficient energy to overcome a potential barrier ΔU, is given by

$$j_r = j_k \exp \frac{-\Delta U}{kT} \tag{28}$$

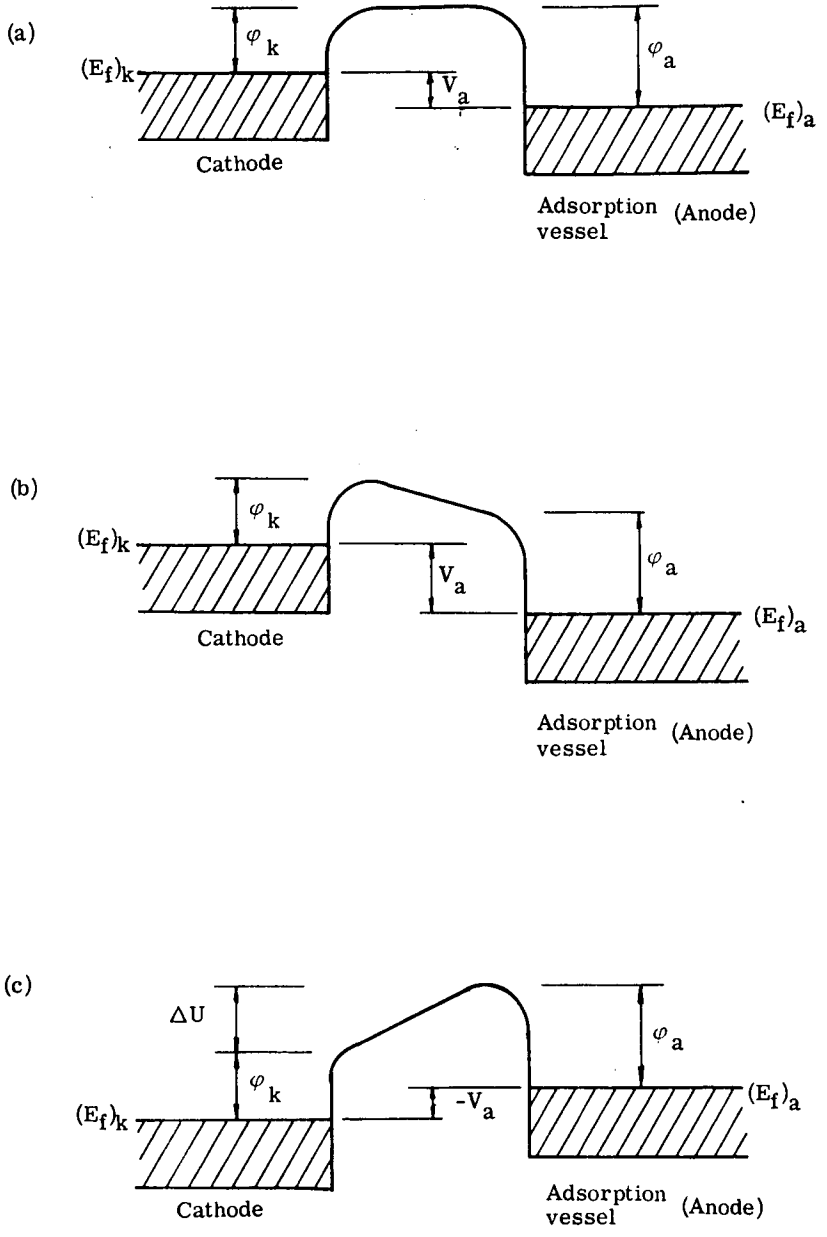

Figure 8.- Potential Diagram Illustrating the Retarding Field Region for this Adsorption Vessel Geometry.

As can be seen from figure 8c,

$$\Delta U = (\varphi_a - V_a) - \varphi_k \tag{29}$$

Combining equations (26), (28), and (29) gives

$$j_r = AT^2 \exp \frac{-1}{kT} (\varphi_a - V) \ , \ \Delta U \geq 0 \tag{30}$$

The last condition implies that $V \leq \varphi_a - \varphi_k$. The function $\ln j(V)$ thus has a knee at $V = \varphi_a - \varphi_k$. For the contact potential (surface potential difference) to be independent of the cathode work function $\Delta U > \delta$ where δ is the half width of the curved knee of a real $\ln j(V)$ curve. Therefore, $V_{a\ max} = \varphi_a - \varphi_k - \delta$. If the φ_a decreases then $V_{a\ max} = \varphi_{a\ min} - \varphi_k - \delta$. Even in nonideal geometry $\delta \leq 1$, the maximum anode voltage in practical situations should be $V_{max} = (\varphi_a - \varphi_k)_{min} - 1$.

In the retarding field region, the adsorption vessel (anode) current is given by

$$I = A' T^2 \exp \frac{-(\varphi_a - V_a)}{kT} \tag{31}$$

where V_a = anode-cathode voltage

φ_a = anode work function

The current through the diode is

$$V_b - V_a = IR = V_R \tag{32}$$

where V_b is the applied voltage. See figure 7.

Taking the logarithm of equations (31) and (32) and differentiating gives

$$\frac{dI}{I} = \frac{- d\varphi_a}{kT} + \frac{- dV_a}{kT} \tag{33}$$

$$\frac{dI}{I} = \frac{R}{V_b - V_a} \frac{-dV_a}{R} = \frac{-dV_a}{V_b - V_a} \tag{34}$$

combining equations (33) and (34) gives

$$\frac{- d\varphi_a}{kT} + \frac{- dV_a}{kT} = \frac{- dV_a}{V_b - V_a}$$

so that

$$\frac{d\varphi_a}{dV_a} = 1 + \frac{kT}{(V_b - V_a)} \tag{35}$$

and if

$$\frac{kT}{(V_b - V_a)} << 1$$

then

$$\Delta\varphi_a \approx \Delta V_a \tag{36}$$

A plot of ln i (or ln j) versus V_a, for a constant cathode temperature (in the retarding region) has the shape as shown in figure 9a. The contact potential difference is equal the voltage at the knee of the curve. Thus, in a given experiment, a change in the surface coverage of the adsorption vessel may be determined by a measurement of the cathode to adsorption vessel voltage at which saturation occurs. Although the actual experimental curves do not have the ideal shape as shown by the solid line in figure 9b, this is not necessary as long as the operating point,(ln j_o),is well within the retarding field region.

D. Procedure

The vacuum system was initially given a thorough bakeout to a temperature of about 450°C for 3-4 days. Subsequent bakes were limited to temperatures of about 350°C. During the bakeout, the gages, the QMS, the titanium sublimators, the injector filaments, and the adsorption vessel cathode were all properly degassed. After cooling to room temperature, EID/mass spectrometer and work function surface cleaning studies were started. Various electron energies and electron current densities were used to find the most efficient desorption of surface contaminants. Mass spectra and work function measurements were taken during and after each EID dose. The electron bombardment of the metal adsorption vessel was continued until the work function did not further change and until the mass spectrum indicated no significant gas release.

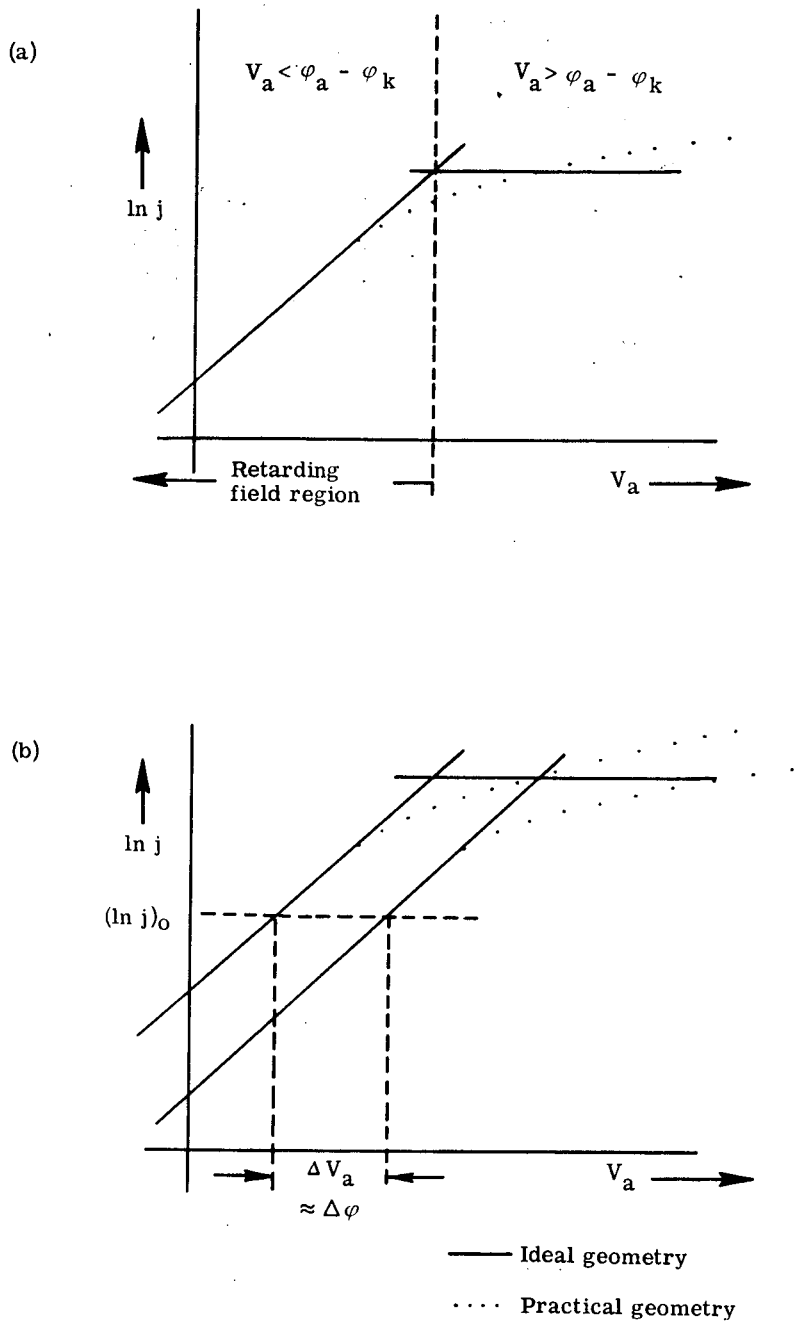

Figure 9.- Typical Emission Current Versus Anode Voltage Plots Illustrating Change in Work Function.

In the case of the stainless vessel, EID was discontinued when it appeared that the surface would be contaminated by the evaporated thorium from the cathode. At this point, the surface was considered relatively clean and physical adsorption studies were started. After degassing each gage for 5 mintes prior to taking data, the emission current of the forechamber gage was adjusted to 40 μA (to minimize variations in the gage constant occurring at high pressure) and the emission current of the main chamber gage left at 10 mA. Since hdyrogen and other background gases made up a residual pressure of approximately 2×10^{-12} torr, background adsorption data versus time plots (for each isotherm temperature) were first obtained in order to correct the low pressure adsorption data. The bottled, research grade nitrogen gas (< 10 ppm impurities) was admitted into the copper inlet line. The inlet line was previously degassed by torch and evacuated to a pressure of less than 1 micron. The inlet line was purged with the test gas several times and then pressurized to one atmosphere with nitrogen. The bleed valve was then opened to the forechamber and the forechamber pressure increased until the pressure in the main chamber reached the lowest equilibrium pressure desired for the isotherm (the main chamber was open to the forechamber through the molecular leak and valve c. Adequate time was allowed to assure that the flow thru was steady. The suppressor on the main chamber gage electrometer was adjusted to the equivalent current indicated to null out the equilibrium pressure signal. Any change due to adsorption would then be reported from a zero reference. The adsorption vessel was then immersed in the

cryogenic liquid. The time to reach adsorption equilibrium was found to be extremely long at low pressures. To shorten the time to reach adsorption equilibrium, the flow rate was raised several orders of magnitude for a given time interval to "force" adsorption equilibrium. The flow rate was then returned to the original value. If the pressure in the main chamber was still below the equilibrium value ($\sigma < \sigma_{eq}$) then the above procedure was repeated. If the pressure was above the equilibrium value ($\sigma > \sigma_{eq}$) the pressure was lowered to desorb the excess adatoms. Eventually equilibrium was attained. The integrating digital voltmeter (IDVM) was set for zero volt-seconds and turned to start. The cryogenic liquid was then removed and the surface was allowed to return to room temperature naturally. As the temperature increased the physically adsorbed molecules desorbed raising the pressure in the main chamber. The IDVM integrated the change in pressure over the total desorption interval. The IDVM output, which represents the brackets in equation (14), was recorded.

As is shown in figure 5, σ may be determined by measuring the area under the $p(t)$ curve either during adsorption or during desorption. In several preliminary experiments these two areas were separately measured and found to be equal. For example, at an equilibrium pressure of 10^{-9} torr it was found that the difference in the two areas was less than 1%. From the results of these experiments it was decided to determine σ from the integral of $p(t)\,dt$ during desorption only.

There is a question concerning σ resulting from "forcing." Specifically, is σ arrived at by the "forcing" technique the same σ arrived at naturally provided that the equilibrium pressures are the same? Several preliminary experiments were conducted in which σ was measured (during desorption) for both the "forcing" technique and the natural technique (at the same equilibrium pressure). It was found that the "forcing" technique yielded the same value for σ as the natural technique to within less than 1%. It was therefore decided to use the "forcing" technique for all σ determinations at very low equilibrium pressures.

Calculation of σ from equation (14) was done for a number of equilibrium pressures at the given isotherm temperature. Applying the thermal transpiration expression, equation (10) to the main chamber number density gave the number density in the adsorption vessel. The isotherm $\sigma = f(p)_T$ was constructed from these data.

Isotherms were constructed for two temperatures, corresponding to the free boiling temperature of liquid nitrogen and liquid argon being careful to take data when the barometer was very near 760 torr. Each determination of σ was corrected for background adsorption.

V. RESULTS AND DISCUSSION

The data obtained from the work function, EID, QMS, and physical adsorption studies of nitrogen on Pyrex, 347 stainless steel, and polycrystalline nickel are presented and discussed in this section.

A. N_2/Pyrex

The 77.4°K and the 87.4°K isotherms for nitrogen on the chemically cleaned surface of Pyrex are presented in figure 10. The data extends from σ values of 5×10^{10} to 3×10^{13} molecules/cm^2 corresponding to the pressure range 2×10^{-11} to 3×10^{-7} torr. This is the first low pressure data to be reported for nitrogen adsorption on chemically cleaned Pyrex. The background pressure was less than 1×10^{-11} torr, and, as indicated by the QMS, consisted of about 90% hydrogen and about 10% carbon monoxide. The shape of the isotherm is approximately that presented by others, but the value of σ for a given pressure, p, is almost twice the value of others[11-13]. The surface area was expected to be greater since the chemical cleaning of the solid would presumably have a leaching effect. The dashed lines on the isotherms, in the lower pressure range, indicate the shape of the isotherms after approximate corrections for the background were made. Only an approximate correction could be made since background data was not taken during this particular experiment. The data (solid line) in the 1×10^{-11} torr range is thus in error about 25% due to the uncertainty in the background gas composition.

C 2

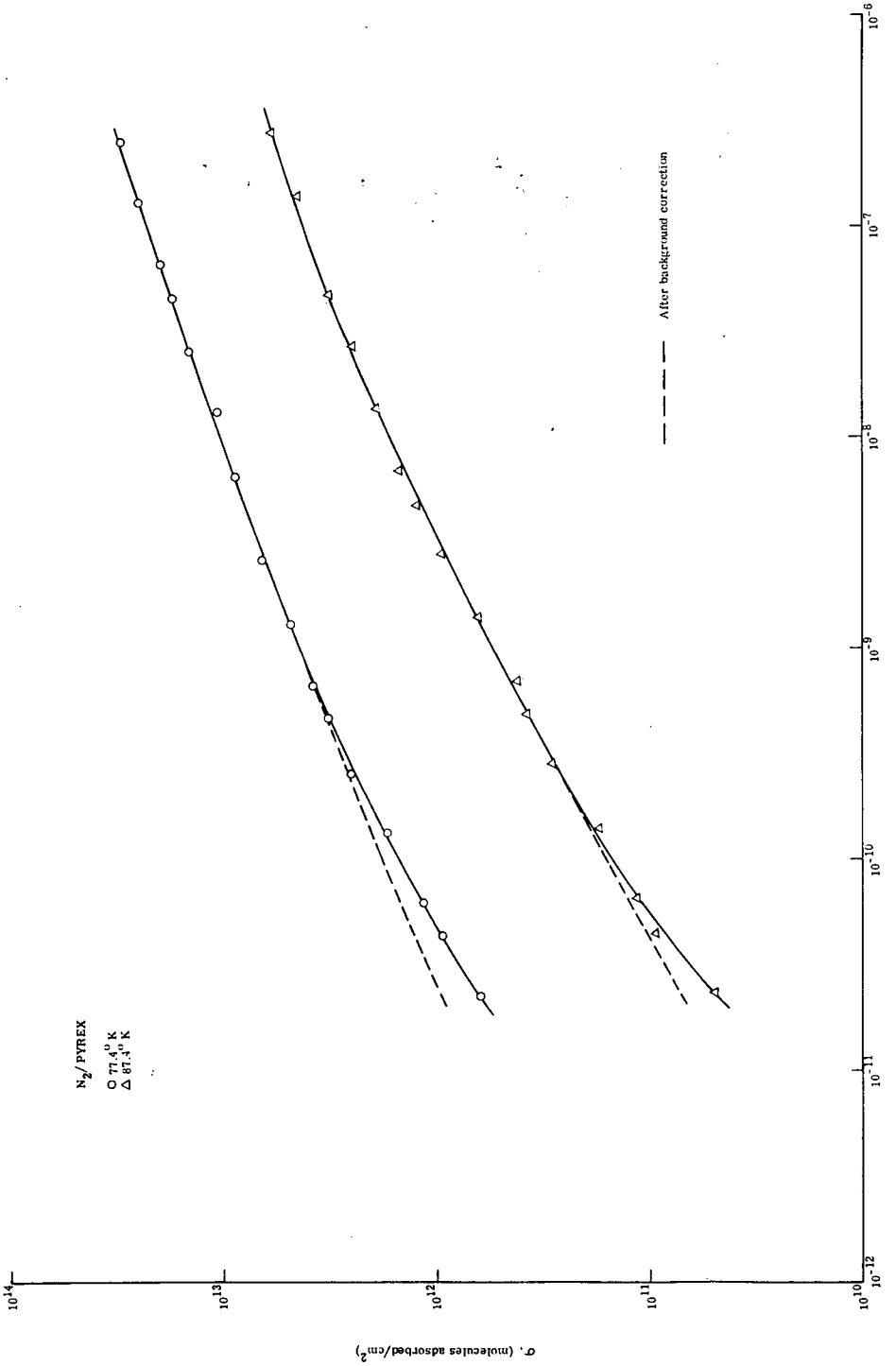

Figure 10.- Physical Adsorption Isotherms of Nitrogen on Pyrex.

Figure 11 shows a fit of the data to the D-R equation or equation (1). The value of p_o, the vapor pressure of the liquid adsorbate required to calculate ε^2, was determined from

$$p_o = 4.42 \exp \frac{-1333}{RT} \quad \text{reference 61} \tag{37}$$

A least squares analysis of all the D-R data is represented by the straight line. Separate least squares analysis were also run on the data for each temperature. The results are presented in table I. The correlation coefficients for both individual and combined isotherms are reasonably good, 0.998 for the combined data. There is some temperature variation of the constants $B^{-1/2}$ and σ_m, but the variation is well within experimental error. The combined data for both temperatures gives a value for $\sigma_m = 1.08 \times 10^{15}$ molecules/cm^2 and gives a value for $B^{-1/2} = 1.78$ kcal/mole. Comparing the value of σ_m found in this work with Hobson and Armstrong's[11] value of $\sigma_m = 6.2 \times 10^{14}$ molecules/cm^2 indicates a higher surface area by a factor of 1.7. The higher surface area would result from the leaching effect noted above. The higher value of the mean energy of adsorption, 1.78 kcal/mole compared to Hobson and Armstrong's value of 1.67 kcal/mole also supports the leaching effect. Another comparison was made by examining the value of the isosteric heat.

$$q_{st} = - R \left[\frac{\partial \ln p}{\partial (1/T)}\right]_{\sigma} \tag{38}$$

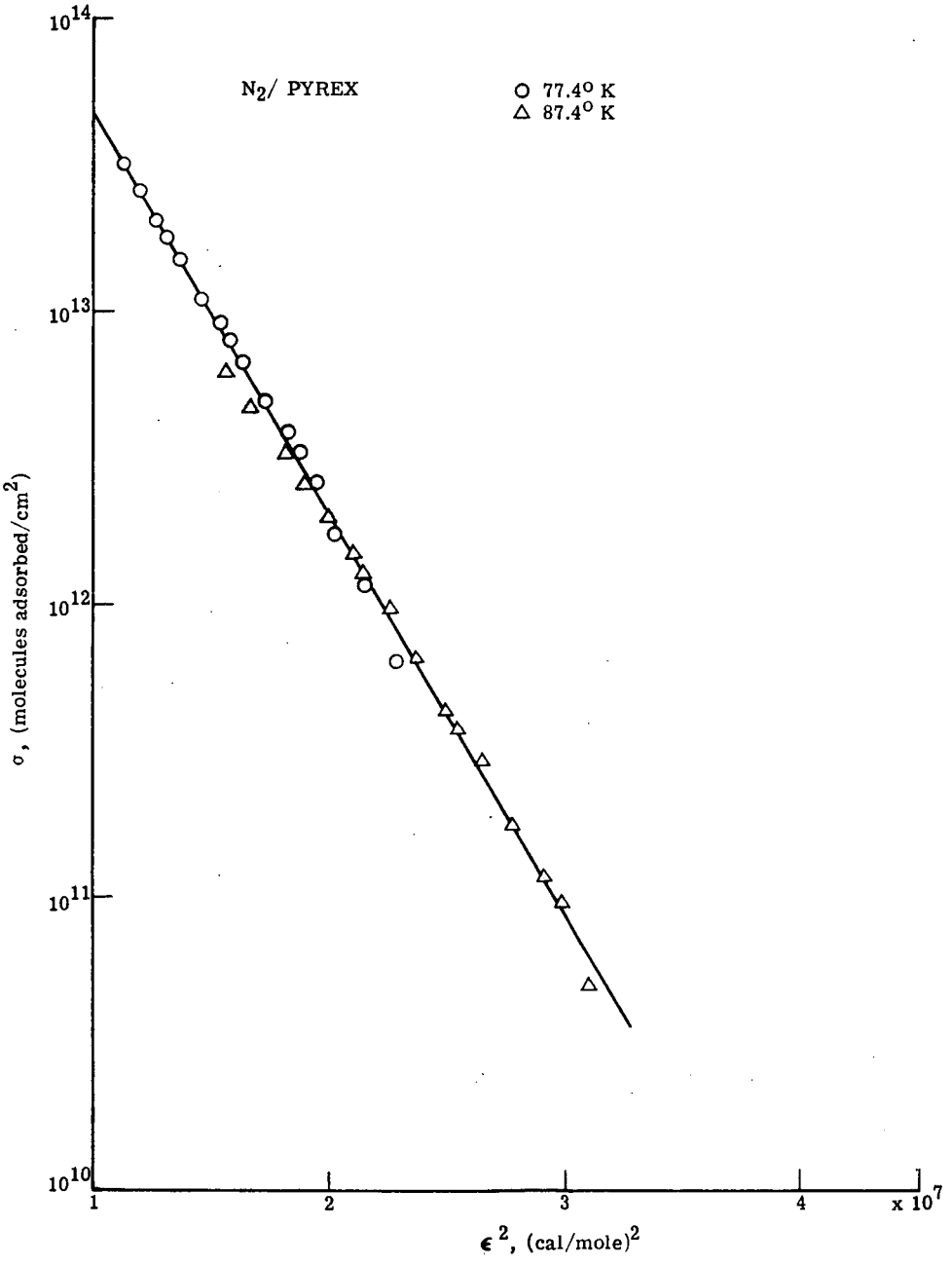

Figure 11. Dubinin- Radushkevich Plots of Nitrogen on Pyrex.

TABLE I.- TEMPERATURE DEPENDENCE OF D-R CONSTANTS FOR THE SYSTEM N_2/PYREX.

T (^oK)	No. data points	B $(mole/cal)^2$	$B^{-1/2}$ (kcal/mole)	σ_m ($molecule/cm^2$)	Cor. coef.
77.4	17	3.24×10^{-7}	1.76×10^3	1.28×10^{15}	0.998
87.4	16	3.04×10^{-7}	1.81×10^3	8.17×10^{14}	0.997
77.4 & 87.4	33	3.15×10^{-7}	1.78×10^3	1.08×10^{15}	0.998

In this work, the value of q_{st} was found to be 6.34 kcal/mole at a coverage of 5 x 10^{12} molecules/cm^2. Hobson and Armstrong found a value of 5.15 kcal/mole at the same coverage. The leaching would tend to remove the alkaline modifying ions from the alkaline rich phase of the glass and leave a slightly porous surface character. This porous structure would result in greater physical attraction between the adsorbed molecule and the increased number of nearest neighbors, thus giving rise to a higher binding energy. The isosteric heat at the lowest coverage, 9 x 10^{11} molecules/cm^2, was q_{st} = 6.56 kcal/mole.

B. N_2/347 Stainless Steel

An ultimate pressure of less than 2 x 10^{-12} torr was achieved following a 450°C bakeout with the 347 stainless steel vessel mounted on the system. The QMS indicated that the major residual gas was again mostly hydrogen (> 90%), and the remainder mostly carbon monoxide. In order to determine the outgassing contribution of the QMS itself, the adsorption vessel was cooled to 77.4°K for 20 minutes in order to enrich the residual gases by physically adsorbing them. The gases were then desorbed and their desorption spectra monitored by the QMS. This was done a number of times to monitor all suspected gases individually as they desorbed. Hydrogen was by far the largest signal observed even though its physical adsorption should be far less than the other residuals (boiling point of 20.4°K). Interestingly, carbon monoxide was not a significant adsorbate thus indicating that the QMS was generating its own CO.

The stainless adsorption vessel was then subjected to cleaning by EID. Work function indications were recorded at various dosages of bombardment in order to monitor the clean up of the surface. The electron energy for EID was set at 550 eV and this gave an emission current of 6 mA for a cathode heater current of 4.6 A. Figure 12 is a plot of the variation in work function with EID dosage. An increase in the work function of 1.1 eV occurred in about 3 hours of bombardment and then monotonically decreased from that point on. A possible explanation of such behavior could be the removal of carbon which was interspersed through the metal oxides. The carbon would tend to keep the overall work function lower than what it would be just with an oxide surface so that as the carbon was removed the work function would tend to go up. Then, as oxygen was desorbed from the surface the work function would go down. After 40 hours of EID, the work function had somewhat leveled off, but a negative slope was still apparent. Bombardment was halted at this point, because complete removal of oxygen from the high binding energy surface oxides like Cr_2O_3 and Fe_2O_3, would require a very great EID dosage. The thorium contamination on the adsorption vessel emanating from the cathode, would then become significant.

Figure 13B and 13A show typical spectra observed during, and after EID respectively. The total pressure eventually dropped to less than 1×10^{-10} torr during bombardment, indicating relatively little gas desorbing from the surface. The most prominent gases desorbed from the stainless were hydrogen, carbon monoxide, and a small amount of

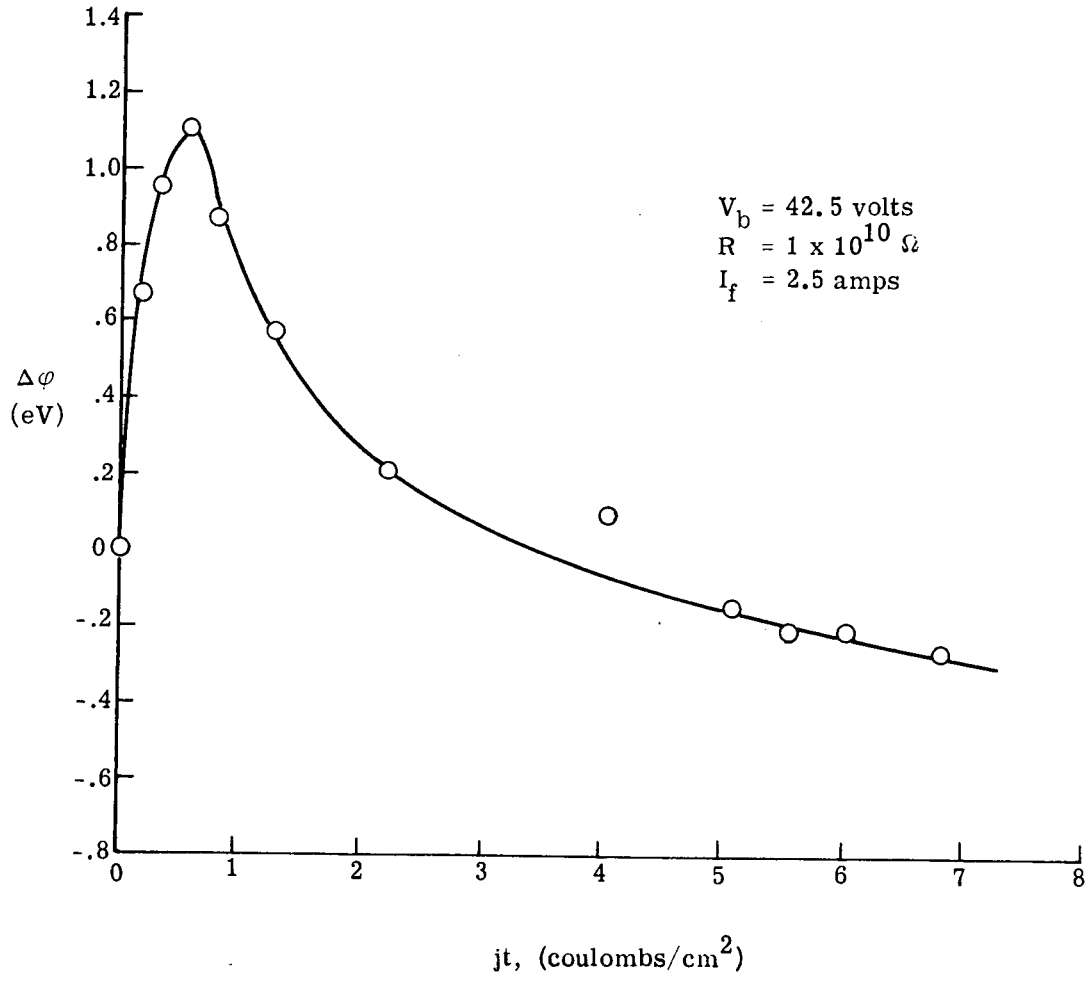

Figure 12.- Work Function Variation, $\Delta \varphi$, 347 Stainless Steel Versus EID Dosage, jt.

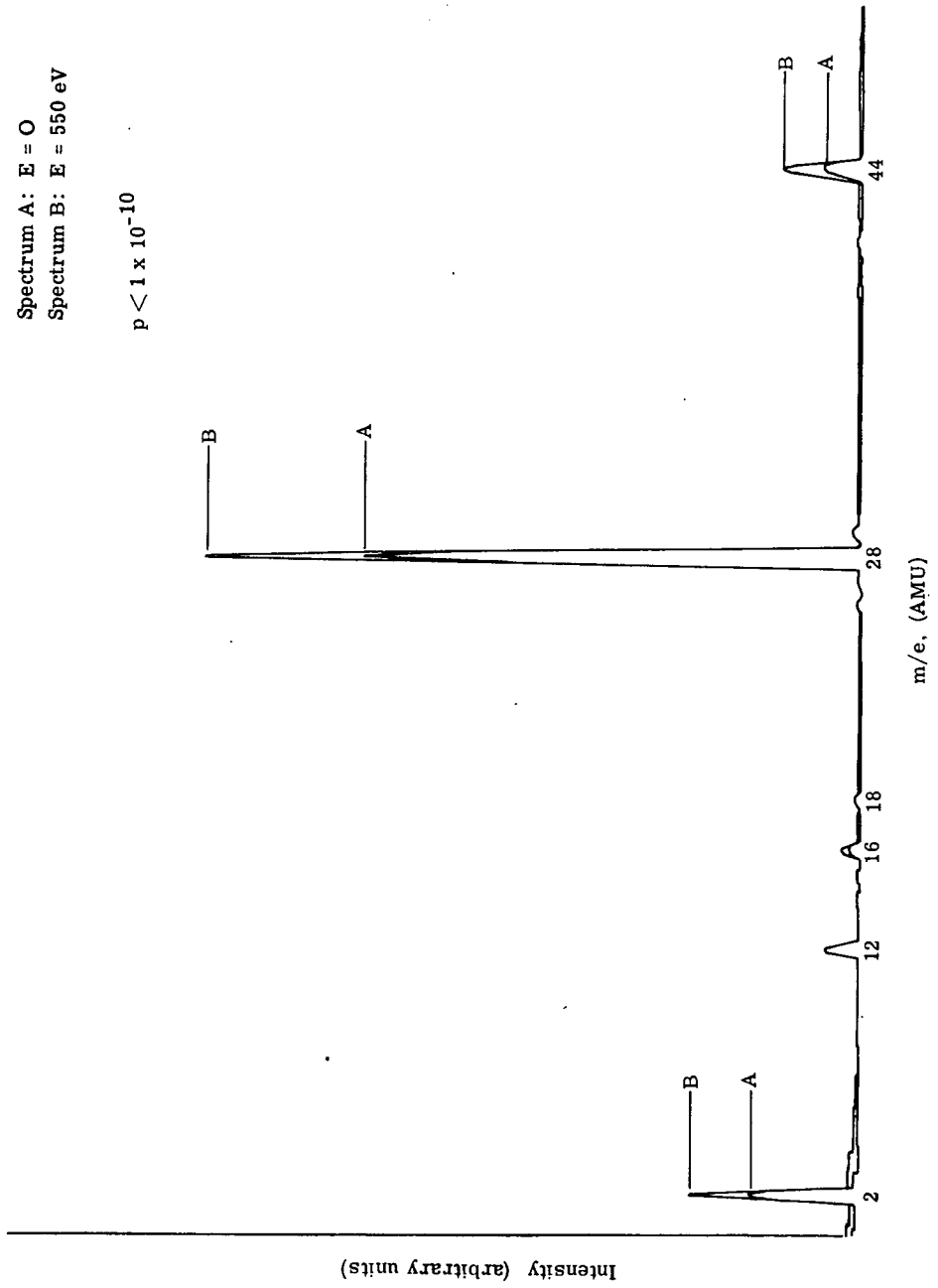

Figure 13.- Mass Spectra of the Gas Composition During and After EID of 347 Stainless Steel.

carbon dioxide. Since the QMS was not positioned in a line of sight to the surface, no firm statement can be made about the actual gases desorbing. Oxygen atoms and ions coming off the surface most likely combined with carbon atoms present on the vacuum chamber walls before arriving at the ion source of the QMS. Further, CO was probably also generated at the adsorption vessel surface. By taking the difference between curves A and B, for a particular m/e and employing the QMS sensitivity and main chamber pumping speed, an estimate of the gas desorbing from the stainless surface was made. Inserting these values into equation (20), a desorption flux of 1.6×10^{10} molecules/cm^2/sec was obtained for hydrogen and 7.5×10^{9} molecules/cm^2/sec was obtained for CO. These numbers correspond to values of $\theta\eta'$ (the unresolved electron desorption efficiency, equation (22)) equal to 6.0×10^{-5} molecules/electron and 2.6×10^{-5} molecules/electron, respectively, for an electron energy of 555 eV and a current density of 0.044 A/cm^2. The variation of $\theta\eta'$ with electron energy E, was determined for the stainless in its cleanest condition and is shown in figure 14. There is no data available on the electron desorption efficiency of CO on stainless, but Petermann[62] has determined a value of 8×10^{-8} molecules/electron for CO generated on nickel at 270 volts. $(\theta\eta')_{CO}^{270}$ from figure 14 is 1.75×10^{-5} molecules/electron, or about a factor of 200 greater. Petermann's nickel sample was a small filament of high purity and had been outgassed at 800°C so it was presumably a far cleaner material than the stainless used here. It is quite probable that the relatively higher carbon content in the stainless steel was a factor.

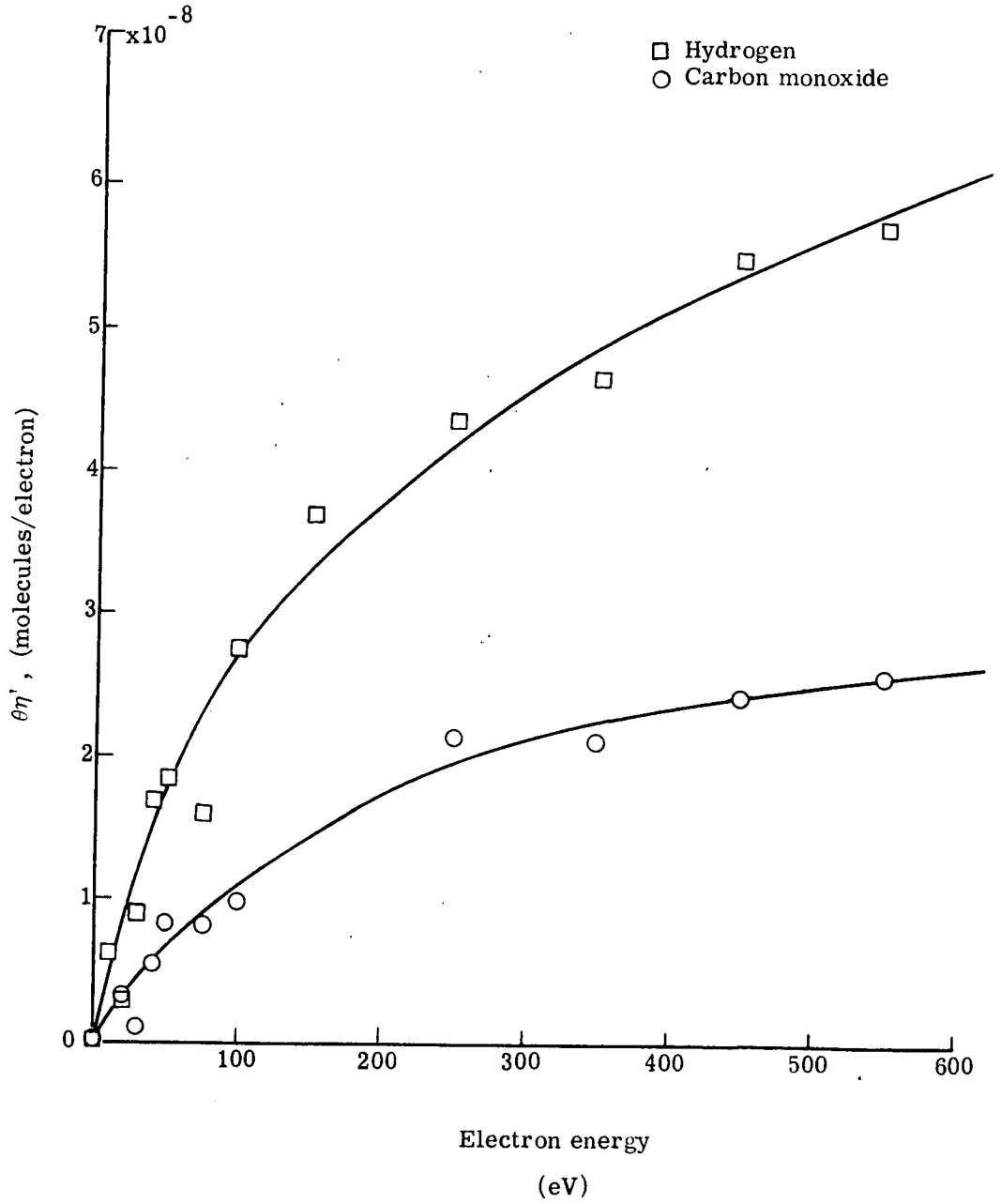

Figure 14.- The Unresolved Desorption Efficiency $\theta\eta'$, Versus Electron Energy, E, for 347 Stainless Steel.

Petermann also ignored the effect of coverage, θ, in his calculation which is clearly an error. There is no way of determining θ in this work so only an unresolved result can be given. The net change in the work function amounted to only about -0.3 eV, but the total amount of CO desorbed was on the order of 10^{17} molecules which, for an area of 135 cm^2, corresponds to monolayer coverage. Since the background pressure was mostly hydrogen and since the stainless bulk contained hydrogen, it is difficult to predict what was the extent of hydrogen removal. At any rate, considering the quantity of H_2 and CO desorbed, a work function change greater than -0.3 eV would be in order. It would thus appear that the rise of work function due to the loss of carbon, and the subsequent 1 eV decrease in work function due to the desorption of oxygen, is a plausible explanation.

The N_2/347 stainless steel isotherms for the EID cleaned and the oxygen treated surface are presented in figure 15. The data, corrected for background, covers a pressure range of 1×10^{-12} to 2×10^{-7} torr. This data represents the lowest pressure isotherms reported to date. The most striking feature of these isotherms is the small variation in σ with pressure. The isotherm flatness could be interpreted as an indication of the heterogeneity induced by the chemical cleaning and by the EID. The desorption of CO and H_2 probably has uncovered many high energy sites on the surface such as grain boundaries, dislocations, and vacancies in the surface oxide. If a high density of such heterogeneous sites existed, then an adsorbed nitrogen molecule would be slow in finding an equilibrium site because of its reduced surface

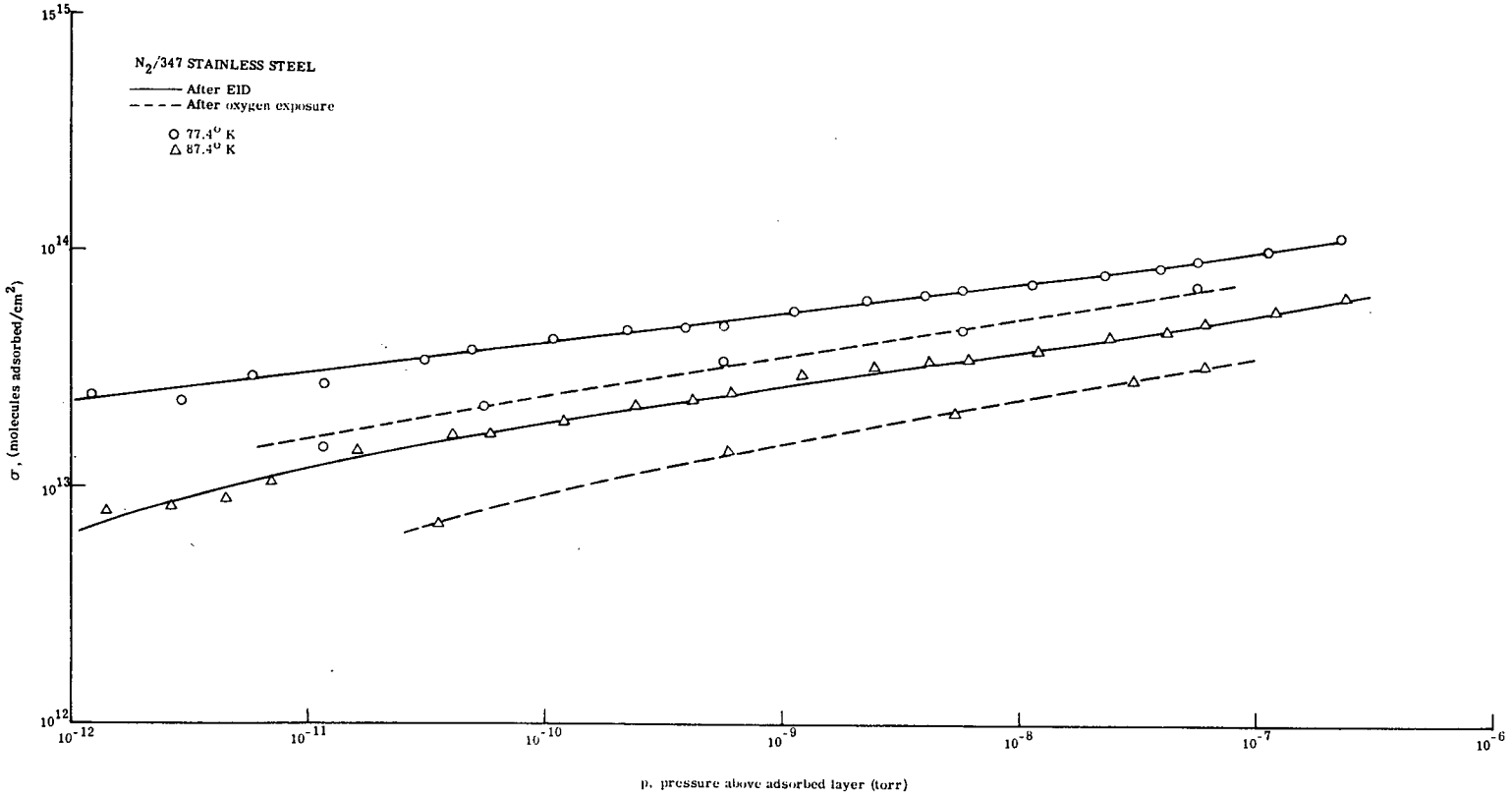

Figure 15.- Physical Adsorption Isotherms of Nitrogen on 347 Stainless Steel for Two Surface Conditions.

mobility. The very long equilibrium times observed, as compared to those for N_2 on Pyrex, support this argument. The number of molecules adsorbed at a pressure of 1×10^{-9} torr, $\sigma = 6 \times 10^{13}$ molecules/cm^2, is also evidence of a higher energy surface. Table II shows a comparison of physically adsorbed nitrogen on other adsorbents. Troy and Wightman's[24] data on uncleaned 304 stainless and Ricca and Medana's[63] data on Pyrex were extrapolated from their D-R plots to this pressure. These surfaces are evidently far less heterogeneous than the stainless in this work. In order to further establish the uncovering of energetic sites by EID, the surface was exposed to oxygen at a pressure of 1×10^{-7} torr for several hours. The permanent work function change observed during the exposure to oxygen exceeded several eV. In fact, the change was great enough to transgress the retarding field region. It was therefore necessary to change the work function parameters to again be in the retarding field domain. From this large work function change, it appears that a significant quantity of the surface gases was removed by EID. The isotherms obtained after the oxygen treatment, clearly show the effect of the change in surface condition. The isotherm slopes are greater and the value of σ, over the pressure range studied, was significantly lowered. The oxygen, very probably, reacted with the metal atoms, originally bared by EID, and reduced the number of energetic sites available to the N_2 molecules.

The data has been fitted to the D-R equation as shown in figure 16. Least squares analyses of the data are represented by the solid and dashed lines. The results of the D-R fit are tabulated in table III.

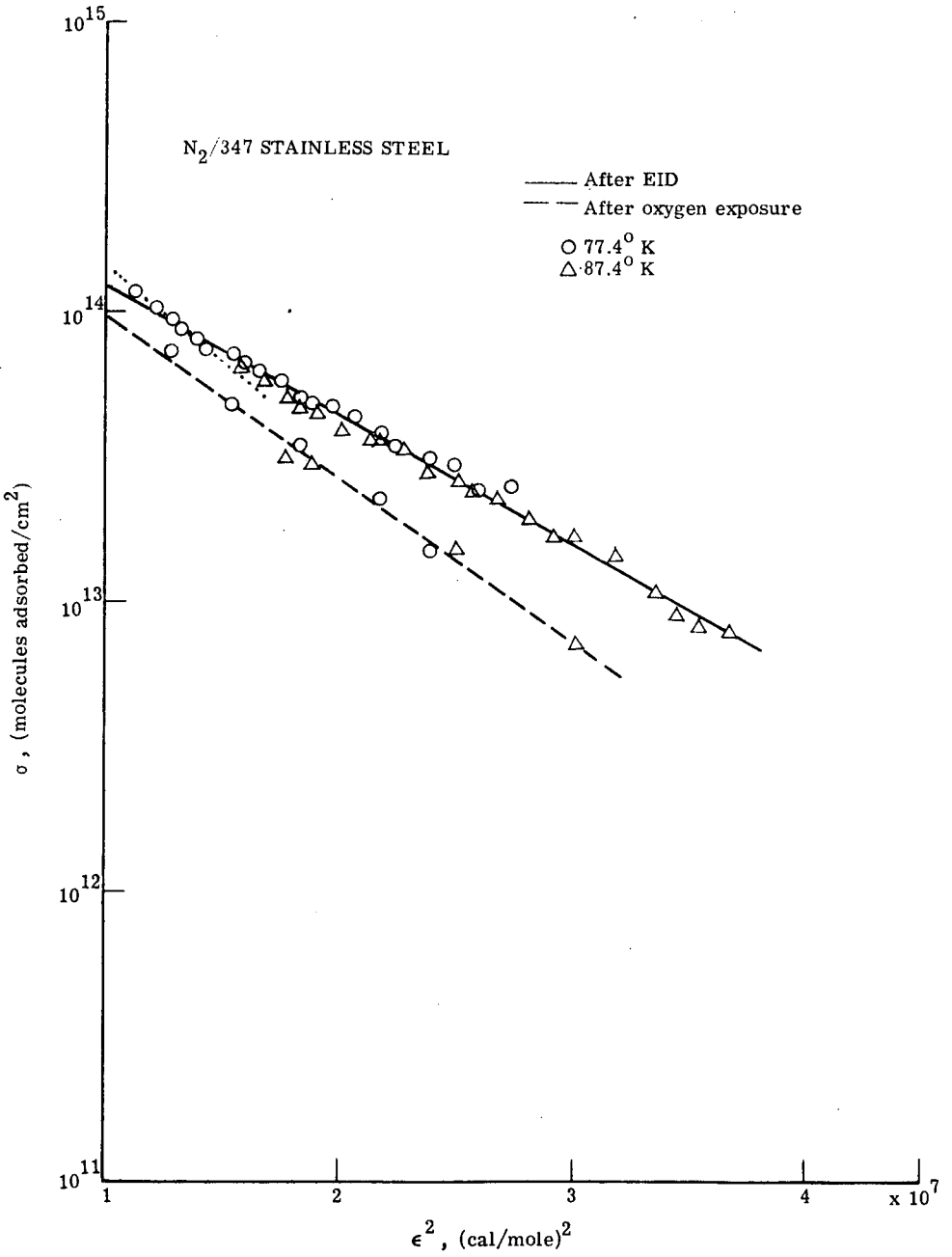

Figure 16.- Dubinin-Radushkevich Plots of Nitrogen on 347 Stainless Steel for Two Surface Conditions.

TABLE II.- A COMPARISON OF σ at 1×10^{-9} TORR

FOR N_2 ON SEVERAL ADSORBENTS

Adsorbent	Temperature °K	Technique	σ (molecules/cm^2)	Surface treatment	Author
347 SS	77.4	Dynamic	5.5×10^{13}	a,b,c	This work
347 SS	77.4	Dynamic	3.6×10^{13}	a,b,c,d	This work
Pyrex	77.4	Dynamic	4.5×10^{12}	a,b	This work
Pyrex	77.4	Static	1.2×10^{12}	b	Hobson & Armstrong
Pyrex	77.3	Dynamic	7×10^{11}	b	Ricca & Medana
304 SS	77.0	Static	3.2×10^{12}	b	Troy & Wightman

a. chemically cleaned

b. baked out

c. EID

d. exposed to oxygen

TABLE III.- TEMPERATURE DEPENDENCE OF D-R CONSTANTS

FOR THE SYSTEM N_2/347 STAINLESS STEEL

Surface Treatment	T (^oK)	No. of data points	B $(mole/cal)^2$	$B^{-1/2}$ (kcal/mole)	σ_m (molecules/cm^2)	Cor coef.
After EID	77.4	20	9.7×10^{-8}	3.34×10^3	3.17×10^{14}	0.990
	87.4	21	9.96×10^{-8}	3.17×10^3	3.09×10^{14}	.996
	77.4 & 87.4	41	1.02×10^{-7}	3.13×10^3	3.4×10^{14}	.994
After O_2	77.4	5	1.38×10^{-7}	2.69×10^3	4.22×10^{14}	.997
	87.4	5	1.21×10^{-7}	2.88×10^3	2.88×10^{14}	.996
	77.4 & 87.4	10	1.30×10^{-7}	2.78×10^3	3.56×10^{14}	.995

The values of σ_m are lower than the value expected for a flat surface (6.2×10^{14} molecules/cm^2)[64] but the majority of the data is for relatively low pressure and may not follow the D-R equation as well as data at higher pressures. This is indicated in figure 16 by the somewhat different slope of the higher pressure data. If an extrapolation to $\varepsilon = 0$ is made, a σ_m value of 6.5×10^{14} molecules/cm^2 is obtained, or near the expected value for monolayer coverage of a surface with a roughness factor of unity.

The variation in the values of the D-R constants for the different temperature isotherms was again noted, but it still was within experimental error. The magnitude of the mean energy of adsorption, $B^{-1/2}$, is quite different for the two surface conditions; 3.13 kcal/mole for the EID cleaned surface as compared to 2.78 kcal/mole for the oxygen treated surface. This is a decrease of about 11% in the mean energy. The isosteric heats for the two conditions give further evidence of the effect of oxygen treatment on the surface. Figure 17 is a plot of q_{st} versus σ. Since σ varied only slightly with pressure, the heats could only be obtained for a limited coverage. The magnitude of the heat for the EID cleaned condition varied from about 7.25 kcal/mole to 5.5 kcal/mole corresponding to a coverage of 3 to 7 $\times 10^{13}$ molecules/cm^2. At a coverage of 3.5×10^{13} molecules/cm^2, a value of 7.0 kcal/mole for the EID cleaned condition can be compared to a value of 6.2 kcal/mole for the oxygen treated condition. This decrease in binding energy of the nitrogen on stainless demonstrates the reduction in the number of energetic sites available. It is apparent, however,

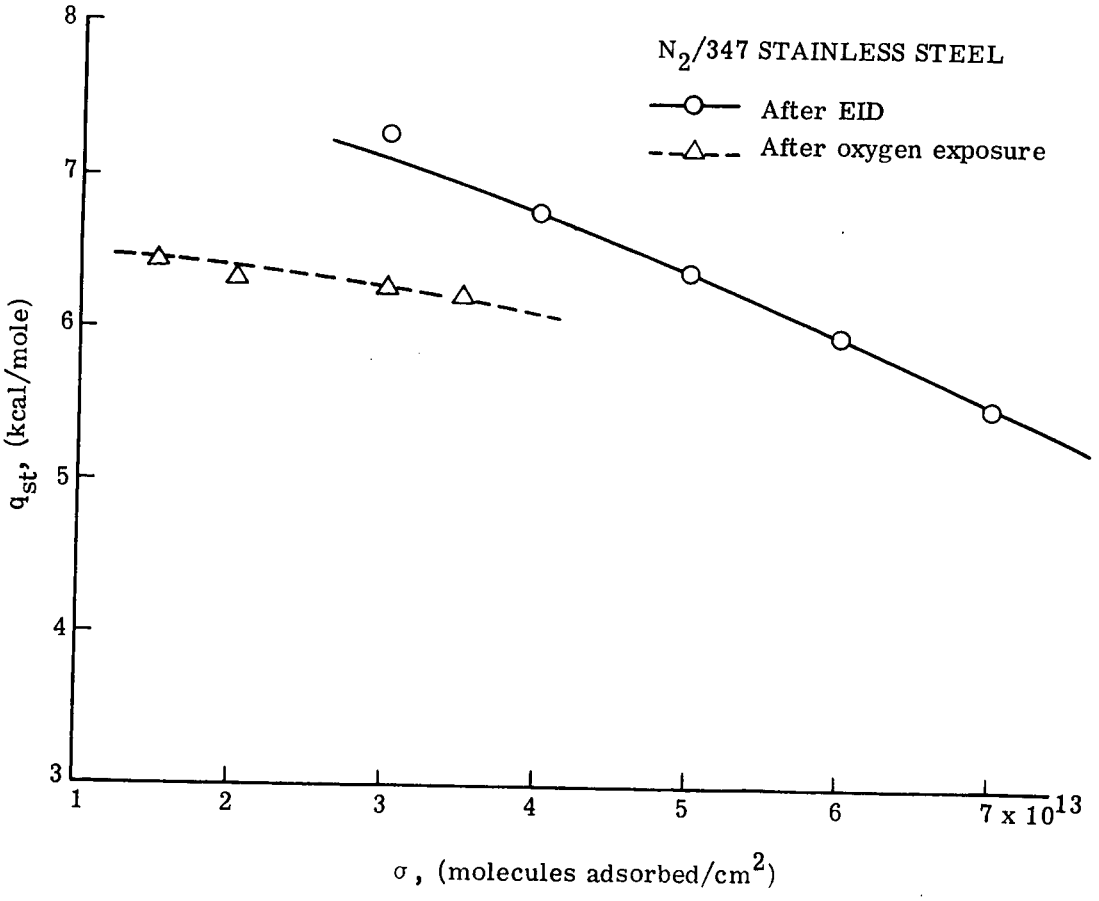

Figure 17.- Isosteric Heats of Adsorption, q_{st}, Versus σ of Nitrogen on 347 Stainless Steel for Two Surface Conditions.

that the oxygen treated surface is still quite heterogeneous if compared to the 304 stainless surface studied by Troy and Wightman[65]. They obtained a value of the isosteric heat of 4.4 kcal/mole that varied little with the range of coverage studied (0.025 to 0.08) or approximately 2 kcal/mole difference compared to the above data for oxygen treated 347 stainless. As can be seen from table II, there is also a factor of 17 in the amount of N_2 adsorbed on the two different steels at 1×10^{-9} torr. Since 347 and 304 are very similar in composition and since both surfaces are covered with oxide, it is possible that the greater heterogeneity of the 347 surface comes from the relatively cleaner surface conditions obtained in this work and/or from the chemical cleaning pretreatment. Consider, for example, the amount of gas adsorbed on the stainless surface following a good bake ($\simeq 450^{\circ}C$). At a background pressure of 1×10^{-11} torr, an initial pressure rise due to EID was observed to approach 1×10^{-7} torr. The pumping speed of the system was about 210 liters per second, so that a pressure of 1×10^{-7} torr corresponds to about 6×10^{14} molecules/second desorbing. Recalling that the surface area is 135 cm^2, it takes only about 2 minutes to desorb a complete monolayer. Because the pressure rise was so rapid for 100 eV electrons, the gas was probably chemically adsorbed in a weakly bound state. It seems probable then that the adsorbed background gases would, to some extent, cover the heterogeneous sites of the surface.

The chemical cleaning of the surface could also increase the heterogeneity by the effect of acid etching. The Fe, Cr, and Ni that

make up the stainless and the many grain orientations are quite susceptible to preferential chemical attack.

C. Oxygen Reactions With 347 Stainless Steel

During the oxygen treatment of the stainless (as mentioned earlier) the work function increased more than expected and transgressed the retarding field region. After adjusting the work function circuitry to again be within the retarding field region, the stainless was re-exposed to an oxygen pressure of 1×10^{-8} torr. A linear work function increase was noted. After an increase of approximately 1 eV, the O_2 was valved off and the system pumped down. The work function was then observed to slowly decrease. The surface was then bombarded with electrons for a short period (6 mA at 550 eV for 5 minutes) and the work function recorded. It had dropped several tenths of an eV to its original value before the O_2 exposure. The experiment was again repeated only to find that the work function always returned to the same value after EID. Now since there had been a permanent work function change of several volts, the surface should be completely covered by a strongly bound oxide which would not come off with such a light EID exposure. The amount of oxygen removed had to be very small, because no O_2 peak was observed in the mass spectrometer during the light bombardment and the CO peak was only about 1×10^{-10} torr. Since only a small amount of gas was desorbed, the oxygen was apparently incorporated (taken in) into the bulk. The amount of oxygen dissolved in the stainless was probably very low since it had been previously

vacuum fired (1000°C for 30 min) and then chemically cleaned. Figure 18 shows the linear rise of $\Delta\Phi$ when the stainless was exposed to a pressure of 1×10^{-8} torr (0_2). After the 0_2 was valved off a slight decrease in the work function was observed. A 2 minute dosage of electrons quickly returned the work function to its original value. After one oxygen exposure no following EID dosage was applied. The work function was monitored for over an hour and it continued to slowly decrease but it would have required many hours for the work function to have returned to its original value. Figure 19 shows the variation in work function at several different exposure pressures. The work function increase was most rapid at the higher exposure pressure (1×10^{-7}) and was repeatable for all pressures. The exposure was not maintained for very long, however, because of the time and difficulty in adequately cleaning the vacuum system in order to take the physical adsorption data of N_2 on oxygen treated stainless. It was noted, however, that the work function change at 1×10^{-7} torr (0_2) approached 1 eV without appearing to change in slope.

Oxygen incorporation into 347 stainless steel has not been previously reported.

D. N_2/ Polycrystalline Nickel

After bakeout an ultimate pressure of less than 1×10^{-12} torr was achieved with the nickel vessel mounted on the system. The residual gases were completely predominated by H_2, but a larger quantity of CO (~ 5%) was observed than for the stainless steel experiment .

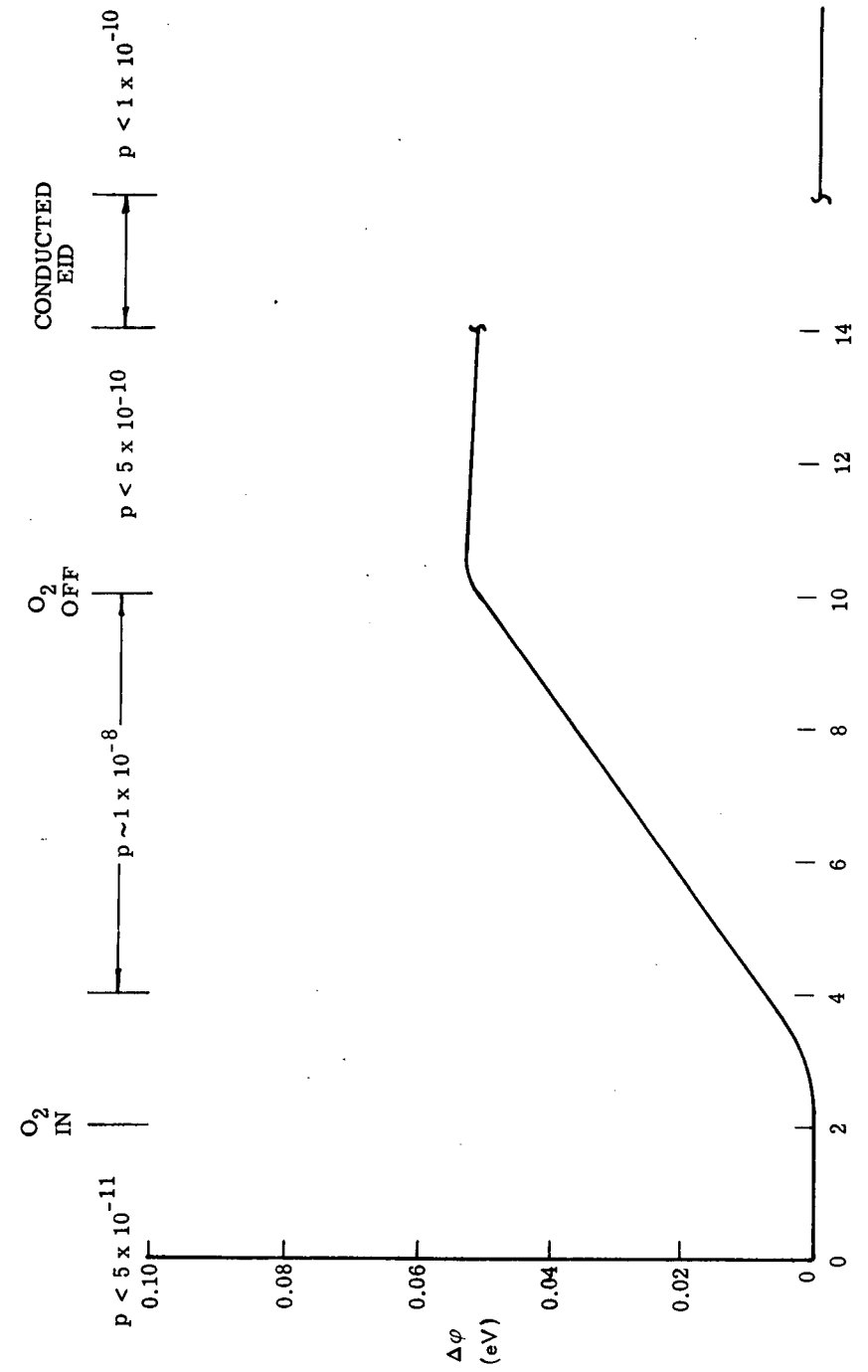

Figure 18.- Work Function Variation, $\Delta\varphi$, Versus Exposure Time, t, of Oxygen on 347 Stainless Steel at 298° K.

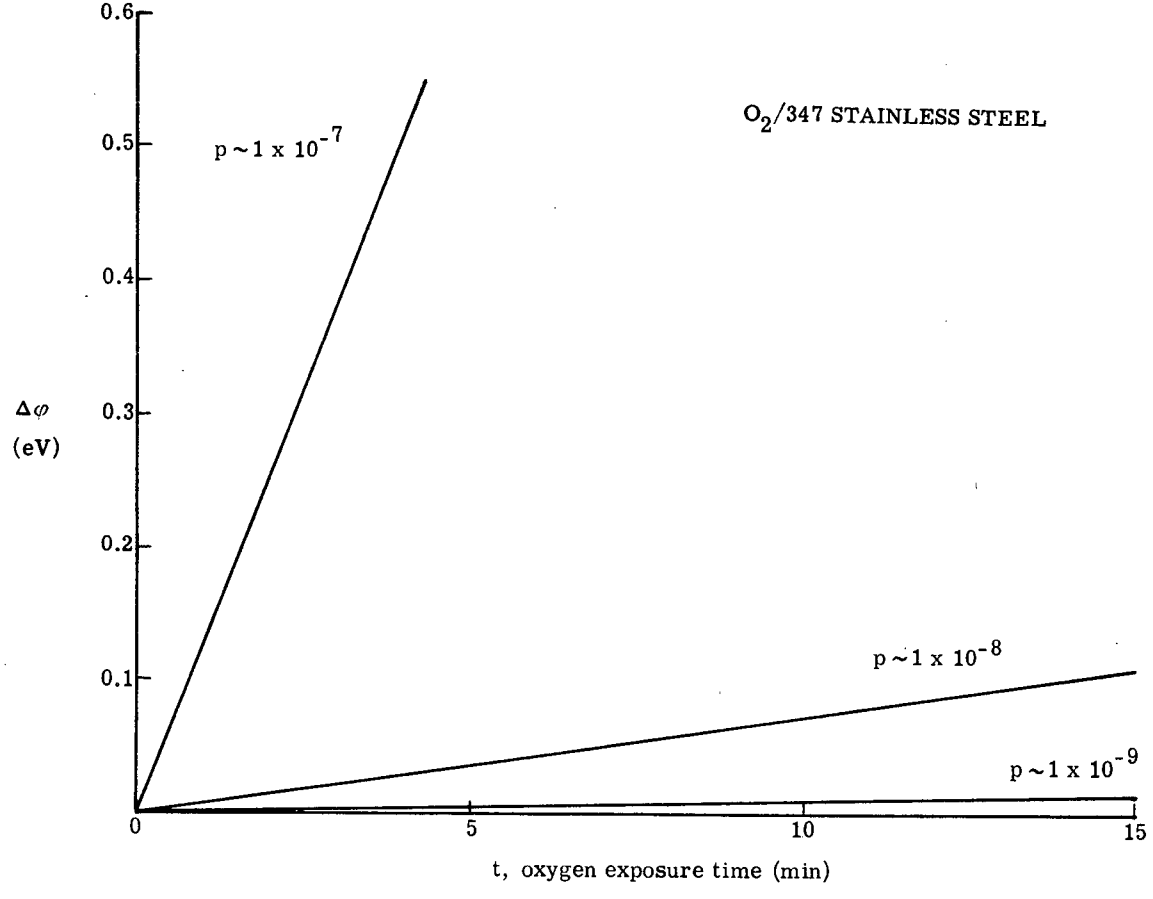

Figure 19.- Work Function Variation, $\Delta\varphi$, Versus Exposure Time, t, of Oxygen on 347 Stainless Steel at Several Pressures (298° K).

EID cleaning of the nickel was then started. An electron energy of 100 eV at a current density of 0.10 ma/cm^2 was initially used. After the rapid desorption of the weakly bound gases (~ monolayer), the electron energy was increased to 300 eV and finally to 555 eV. Figure 20 shows a plot of the pressure change, δp, due to EID, versus the EID dosage, jt. H_2 and CO partial pressures make up about 95% of the total gas flux desorbing from the nickel surface. As mentioned earlier, since the QMS was not in a line of sight to the adsorption vessel, it cannot be stated whether the desorbing gases were adsorbed H_2 and CO or whether the gases were generated at the surface. The initial high gas flux coming off in the first minutes from EID is most likely the former case and the subsequent gas desorbed the latter case. The total quantity of gas desorbed and therefore the change in surface coverage can be obtained from equation (23). By comparing the QMS indication with the total pressure indication the amount of CO and H_2 desorbed for an EID dosage of jt ~ 27 coulombs/cm^2 was found to be, $q_{CO} = 2.67 \times 10^{14}$ molecules/cm^2 which corresponds to $\Delta\theta = 0.38$ monolayers and $q_{H_2} = 1.30 \times 10^{15}$ molecules/cm^2 which corresponds to $\Delta\theta = 1.85$ monolayers. Since hydrogen is present in the bulk of the nickel and permeates through from the outside of the adsorption vessel it is difficult to determine the significance of the change in H_2 coverage. The value of $\Delta\theta$ obtained for CO, however, seems to be a very reasonable one. If the CO were generated at the surface rather than desorption of adsorbed CO, then $\Delta\theta$ would be even larger than 0.38.

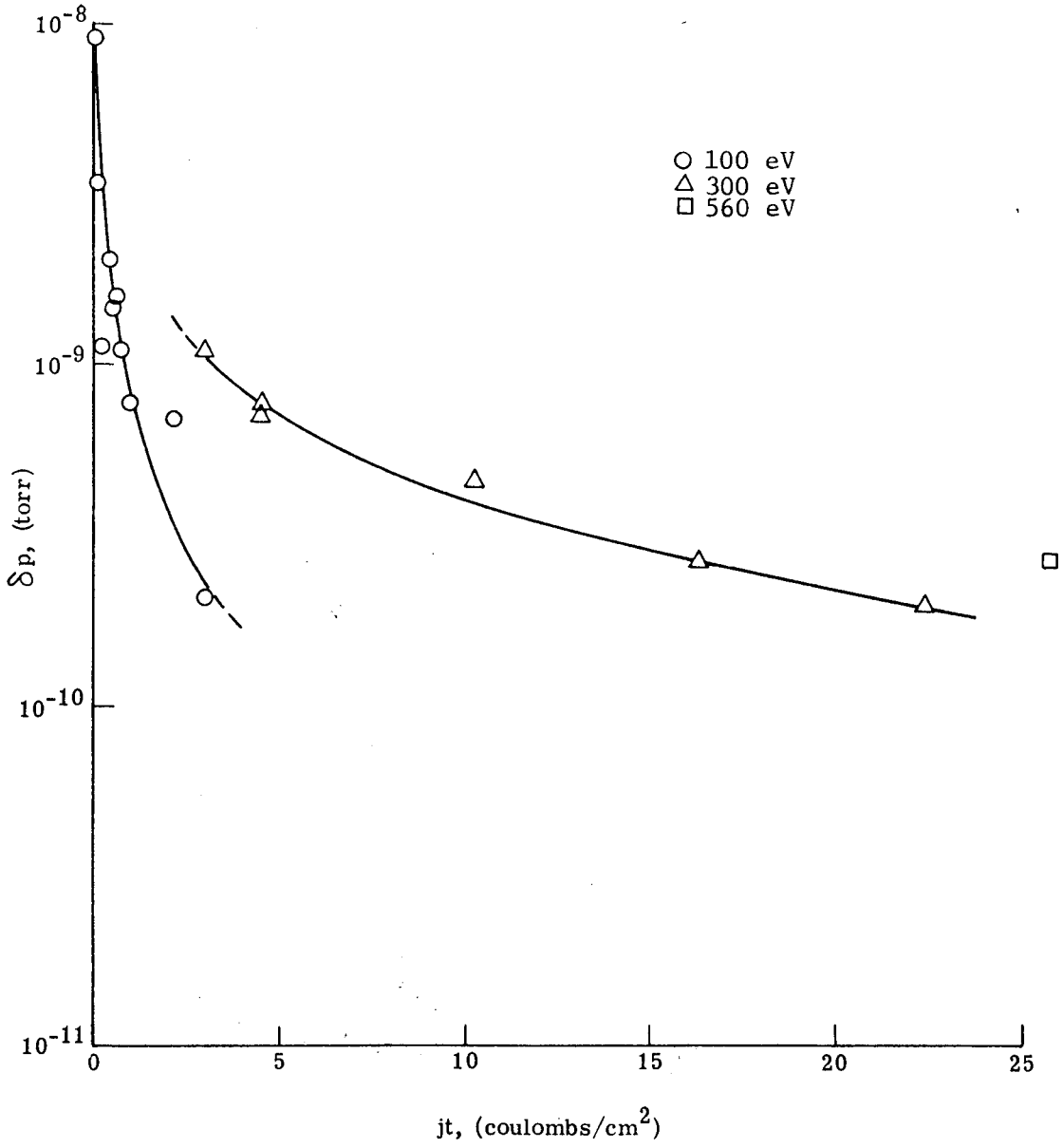

Figure 20.- The Variation in Pressure δp, Versus EID of 100 eV, 300 eV, and 560 eV Electron Energies.

As determined earlier for stainless, a measure of the unresolved desorption efficiency for CO, $(\theta\eta')_{CO}$, was made after the work function indicated little change with additional EID dosage. A value of 4.1 x 10^8 molecules/cm^2/sec was obtained for an electron energy of 555 eV and a current density of 0.11 ma/cm^2. This gas flux desorbed corresponds to a value of $(\theta\eta')_{CO}^{555}$ = 6 x 10^{-7} molecules/electron. This value may be compared with Petermann's[62] result by assuming a similar variation of gas desorption with electron energy observed on the stainless, so for 270 eV $(\theta\eta')_{CO}^{270}$ = 4.6 x 10^{-7} molecules/electron or about a factor of 6 greater than Petermann's value of 8 x 10^{-8} molecules/electron. Considering the difference in geometric area between the two conditions, 135 cm^2 in this case compared to 0.5 cm^2, the agreement is not too bad.

Figure 21 shows the variation in work function, $\Delta\varphi$, versus jt. Surprisingly, only a very small work function change was observed. The shape of the curve is similar to that obtained for the stainless steel, but the maximum variation is less than 0.30 eV as opposed to 1.10 eV obtained on the stainless. Klopfer[40] has reported very small EID efficiencies for oxygen on nickel at coverages less than a monolayer, $\eta' \sim 1 \times 10^{-7}$ molecules/electron at a coverage of 7.5 x 10^{14} molecules/cm^2, and indicated that this might be explained by an incorporation effect where the oxygen diffusing into the lattice is actually promoted by EID. The occurrance of this phenomena would imply that the nickel surface in this work, is bare of oxygen so that a significant change in the work function would occur when the surface

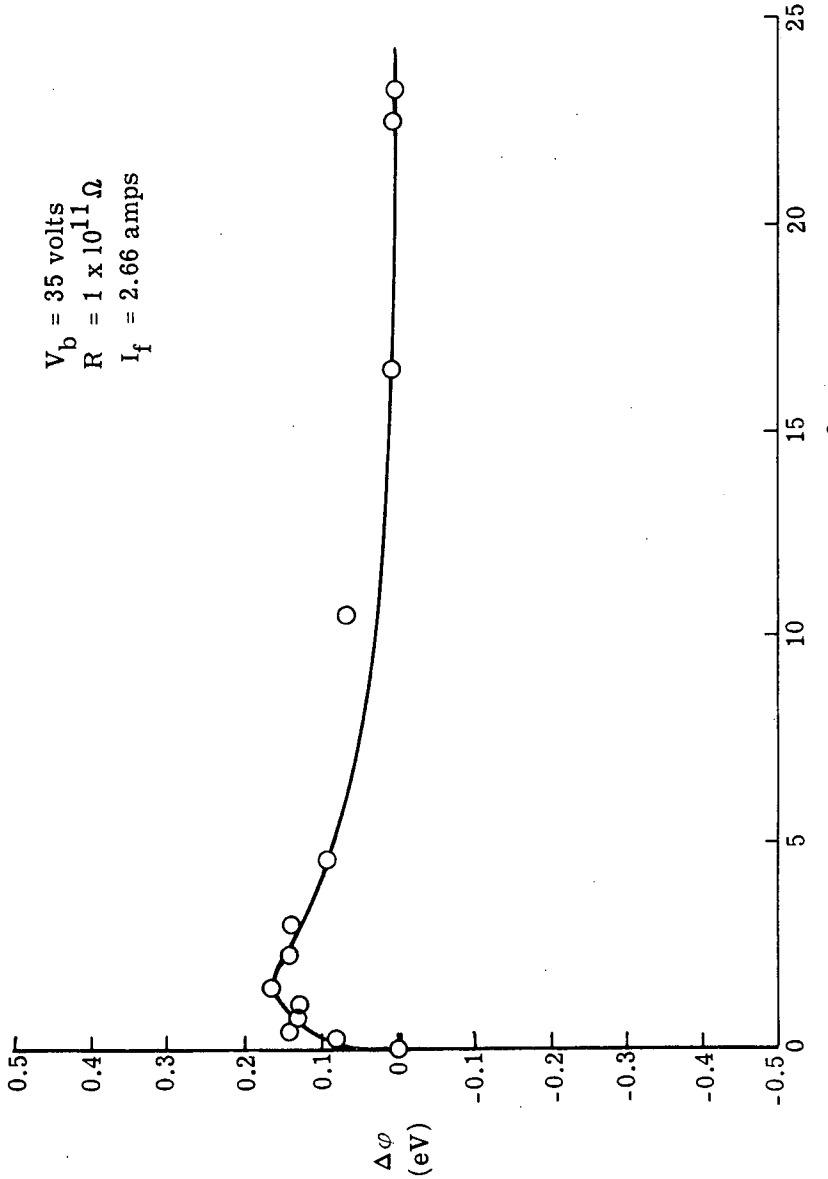

Figure 21.- Work Function Variation, $\Delta\varphi$, of Nickel Versus EID Dosage, jt.

was exposed to oxygen. A change of only 0.20 eV was observed when this experiment was conducted.

On the other hand, Bradford[66] observed only a 0.30 eV decrease when a polycrystalline nickel sample was Ar ion bombarded. Oxygen should have been quickly desorbed in that experiment considering the desorption efficiencies for Ar ion bombardment, $\eta' \sim 1$. Ion bombardment would lower the work function just due to the disordering of the surface, so a value of 0.20 eV does not seem to be unrealistic[51].

An ancillary AES experiment was conducted on a polycrystalline nickel sample to determine the effect of the cleaning procedure used in the primary experiment. The results of that study indicated that contaminants sulfur and carbon which remained after the chemical cleaning can efficiently be reduced, but the results obtained for oxygen are not clear. There is also some question as to what part the effect of surface temperature played in the apparent removal of surface oxygen. It appears that EID does not efficiently desorb oxygen, but that heating of the nickel promotes incorporation. Unfortunately, no chemical analysis (e.g., AES) was possible with the primary apparatus, so the composition of the surface is not known. It can be stated, however, that since a great deal of gas was desorbed by EID, the nickel was in a far cleaner condition than it would have been without EID. See Appendix A.

Figure 22 shows the nitrogen on nickel isotherms. It is immediately apparent that the isotherms are steeper than those observed for the stainless, indicating a more homogeneous surface. It should be

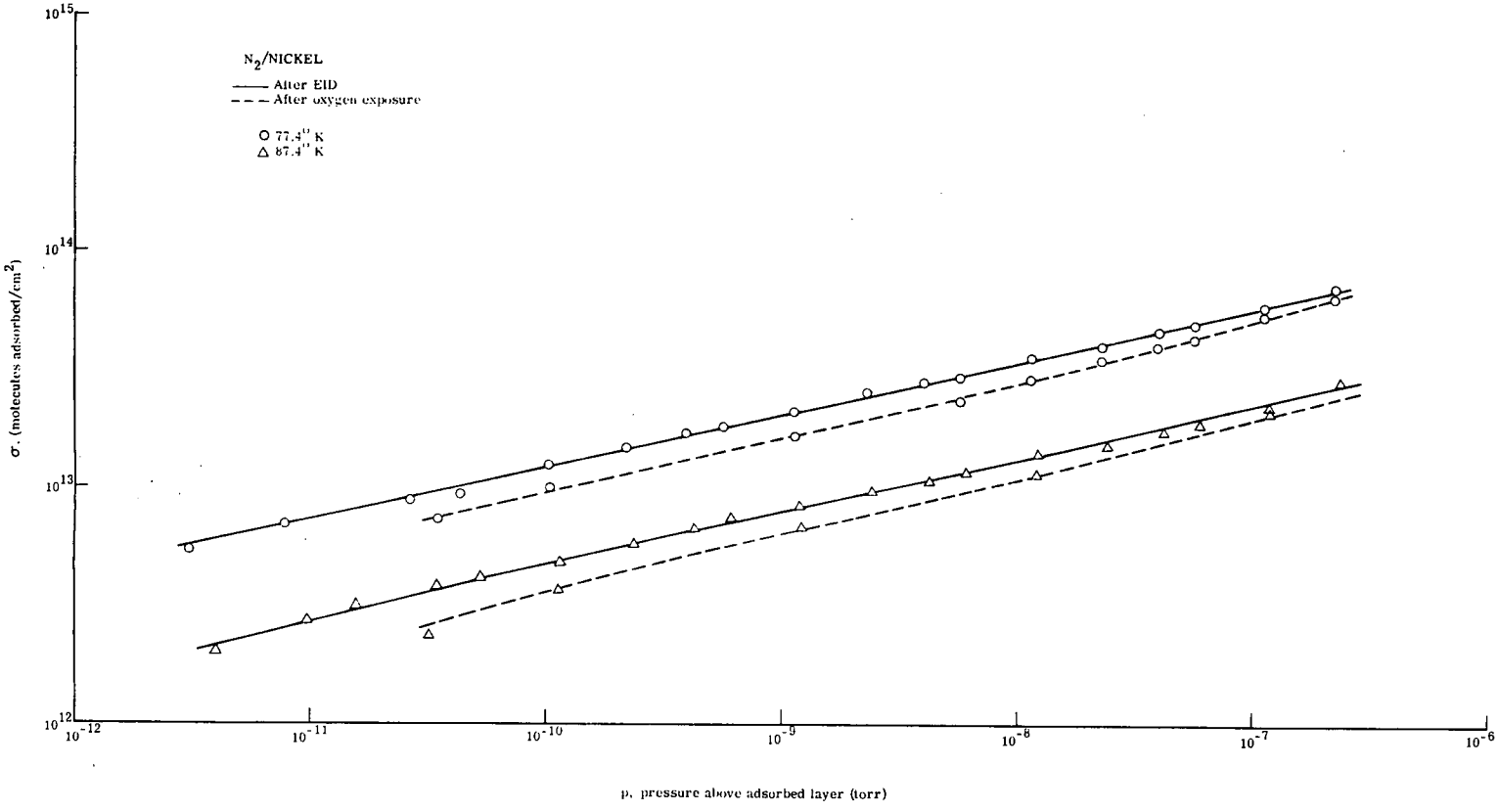

Figure 22.- Physical Adsorption Isotherms of Nitrogen on Nickel for Two Surface Conditions.

pointed out that the total amount of surface metal removed by the chemical etching was a factor of 10 less on the nickel than the amount removed from the stainless. (See page 25 .) The EID treatment on the nickel was more extensive however, since a total electron dosage was about 27 coulombs/cm^2 as compared to 7 coulombs/cm^2 on the stainless. A more active thoria coating on the EID cathode permitted much higher values of jt for a given heater current. The nitrogen isotherms obtained after the nickel was exposed to oxygen show only a small change at the higher equilibrium pressures but becomes noticeably different at the lower pressure end.

The fit of the data to the D-R equation is shown in figure 23. The results of this fit are presented in table IV. As is apparent from the correlation coefficients, the data reveals a large temperature effect between the two isotherms taken after EID. The coefficients for each temperature are quite good, both 0.998, but for the combination the coefficient drops to 0.991. This clearly indicates some distinct dependence upon the temperature. The low number of points taken for the isotherms following oxygen exposure prevents any reasonable conclusions from being made on the observance of a temperature effect in this data.

As was also observed on the stainless, it is apparent from the 77.4^{o}K data that the higher pressure data points ($> 10^{-9}$ torr) have a different slope than the lower pressure points. If only these points are considered a higher value of σ_m results, one that is a more reasonable value for monolayer coverage $\sigma_m \approx 7 \times 10^{14}$ molecules/cm^2.

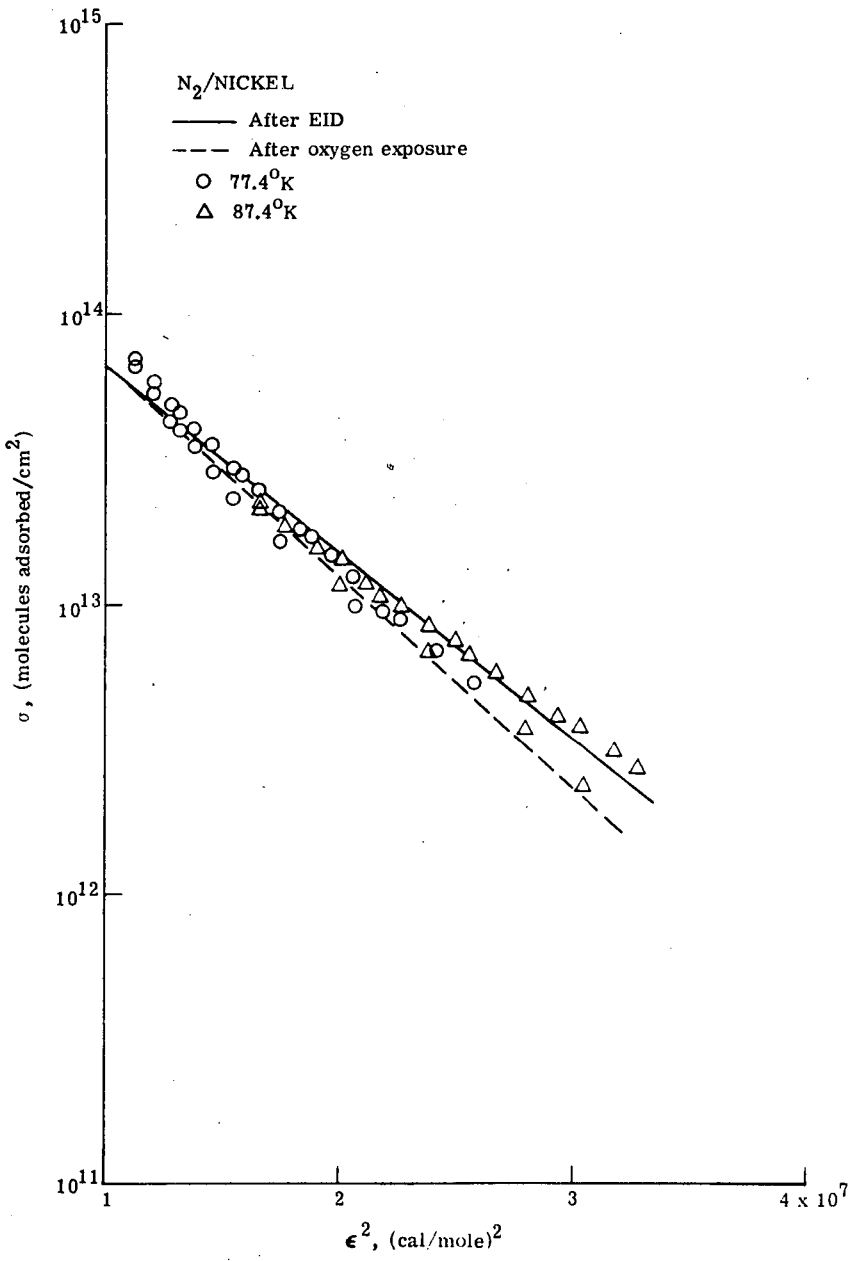

Figure 23.- Dubinin-Radushkevich Plots of Nitrogen on Nickel for Two Surface Conditions.

TABLE IV.- TEMPERATURE DEPENDENCE OF D-R CONSTANTS

FOR THE SYSTEM N_2/NICKEL

Surface treatment	T ^oK	No. of data points	B $(mole/cal)^2$	$B^{-1/2}$ (kcal/mole)	σ_m (molecules/cm^2)	Cor. coef.
After EID	77.4	18	1.75×10^{-7}	2.39×10^3	4.67×10^{14}	0.998
	87.4	18	1.31×10^{-7}	2.76×10^3	1.96×10^{14}	0.998
	77.4 & 87.4	36	1.48×10^{-7}	2.60×10^3	2.90×10^{14}	0.991
After O_2	77.4	09	2.02×10^{-7}	2.22×10^3	5.93×10^{14}	0.993
	87.4	05	1.55×10^{-7}	2.54×10^3	2.75×10^{14}	0.999
	77.4 & 87.4	14	1.67×10^{-7}	2.45×10^3	3.56×10^{14}	0.994

The data taken following oxygen exposure at 77.4°K gives a similar value for σ_m. It therefore appears that the D-R data changes slope at lower pressures, at least in this case of nitrogen on 347 stainless and on pure nickel.

The plots of isosteric heats of adsorption versus coverage for the nitrogen on nickel are presented in figure 24. Very little change is observed with coverage for either surface condition. The mean values are about 5.7 kcal/mole for the surface following EID dosage and about 5.2 kcal/mole for the surface following oxygen exposure. Comparison of the slopes and magnitudes of these curves to those of figure 17 reveals the greater heterogeneity of the stainless and the greater effect of the oxygen exposure on the stainless. The 5.7 kcal/mole heat of adsorption at a coverage of approximately 5×10^{12} molecules/cm^2 may be indirectly compared to the data of Baker and Fox[15] for krypton on nickel films using the ratio $q_{st}(N_2)/q_{st}(Kr) = 1.15$[67]. Baker and Fox found the heat of adsorption at a coverage of 5×10^{12} molecules/cm^2 to be 5.0 kcal/mole which implies that they would find for nitrogen on nickel a heat of about 5.75 kcal/mole. This agreement is very good but it is a very approximate comparison and done only because of the absence of N_2/Ni data.

During the time nitrogen was present in the system, the EID/work function cathode was not heated in order to eliminate the possibility of exciting the nitrogen molecule by a hot filament. This procedure prevented activated nitrogen from chemisorbing on the nickel. When the nitrogen had been evacuated, work function measurements were made

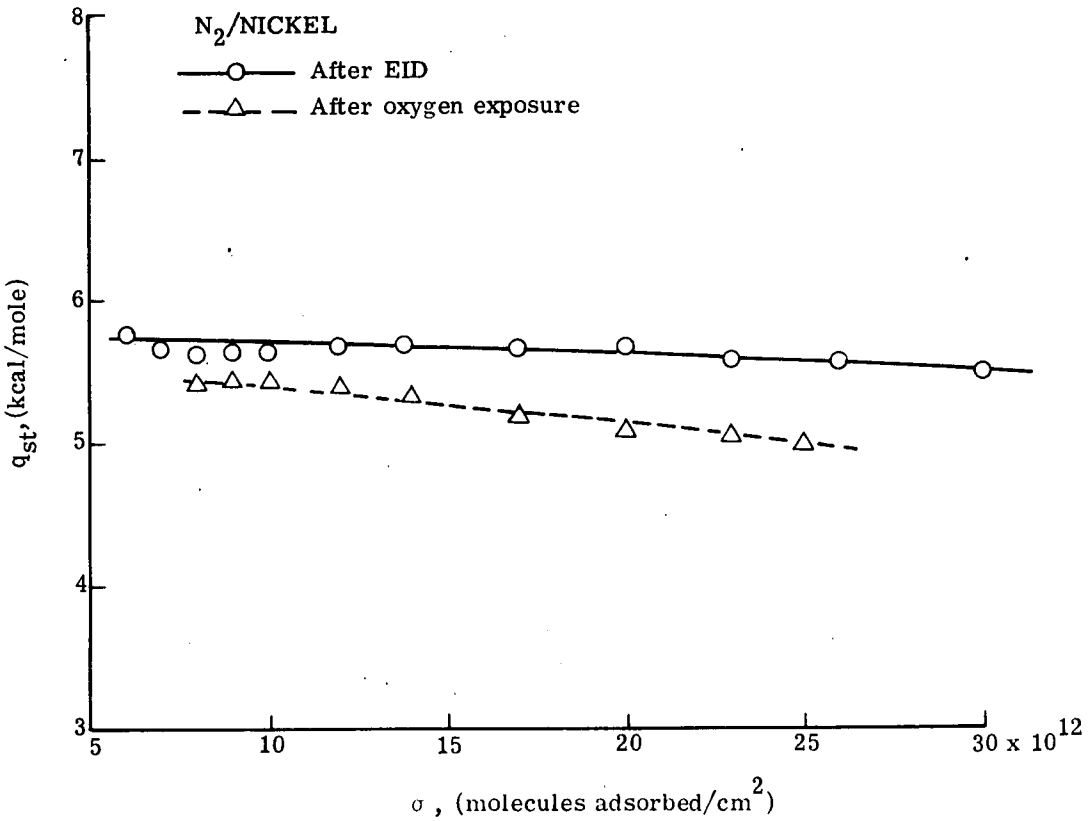

Figure 24.- Isosteric Heats of Adsorption, q_{st}, Versus σ of Nitrogen on Nickel for Two Surface Conditions.

to see if ground state nitrogen had chemisorbed on the nickel. No work function change was observed.

E. Oxygen Reaction with Nickel

Following the physical adsorption studies of nitrogen on the EID cleaned nickel, the vacuum system was prepared for studies of oxygen adsorption on nickel. Before exposing the surface to O_2, valve (a) was throttled down considerably and the predominant residual gas pressure (H_2) was observed to increase from 5×10^{-12} torr to 1×10^{-10} torr. Coincident with this pressure rise, the nickel work function increased by 0.05 eV, most likely corresponding to the well known interaction of atomic hydrogen on nickel. This work function change did not disappear when the valve was opened to its original position, but did vanish with a light EID dosage. The importance of this observation is that even at 1×10^{-10} torr, surface reactions can contaminate the surface.

O_2 was then admitted into the main chamber to a pressure of 1×10^{-7} torr. The QMS indicated a small peak at m/e = 28 (CO) in addition to the large 16 (O) and 32 (O_2) peaks. Figure 25 shows the work function response versus time for the oxygen on nickel at 1×10^{-7} torr. The work function sharply increased 0.05 eV within the first 30 seconds, probably corresponding to the saturation of bare sites. The work function then increased at a continually faster rate up to about 1 eV where it reached an inflection point and then at a continually slower rate, increased to about 1.40 eV. Here the rate of increase became

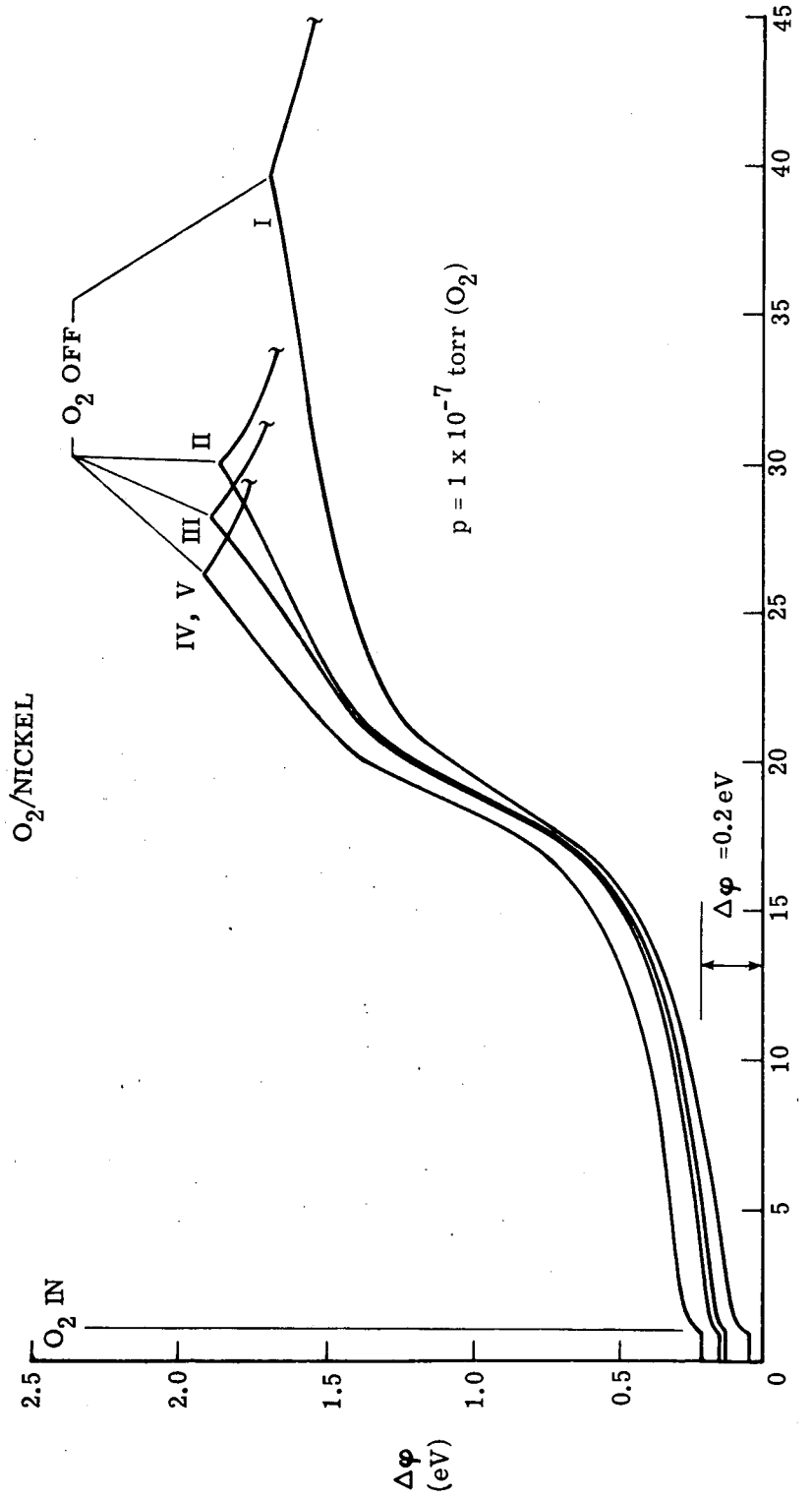

Figure 25.- Work Function Variation, $\Delta\varphi$, Versus Exposure Time, t, of Oxygen on Nickel at 298° K.

constant. The oxygen was valved off after the work function reached 1.60 eV and was observed to reversibly decrease similar to that of the O_2/347 stainless steel system. The rate of decrease became so slow, it was necessary to use a light EID dose. This returned the work function almost to its original value; a permanent change of 0.065 eV had occurred. This same experiment was repeated four times until the permanent work function reached a constant value. As indicated earlier, a total permanent change of only +0.20 eV was observed. Run II of this experiment again repeated the initial rise lasting about 60 seconds, and then continued in the same manner as before except it increased at a faster rate above the inflection point. Runs III, IV, and V are slightly different, indicating some permanent effect taking place.

Delchar and Tompkins[42], and Quinn and Roberts[68] have observed an oxygen incorporation into the bulk of nickel films. Delchar and Tompkins saturated their nickel film with O_2 at 77°K and then rapidly heated the film to a series of constant, higher temperatures. They observed the work function to increase and then decrease as the oxygen was incorporated into the bulk and formed a reverse dipole layer. They also determined that the number of adatoms incorporated is proportional to the work function change. Quinn and Roberts noted a similar work function response when they admitted O_2 at 298°K into their system in individual dosages. They observed the work function to change a net of +0.8 volts for a series of 11 dosages (8×10^{17} molecules/dose), each dose causing a sudden work function increase and then a decrease. The ultimate pressure of their vacuum system was only about 10^{-7} torr however,

so the films were probably partially contaminated. Horgan and King[41] have described three stages of the oxygen reaction with nickel. They concluded that oxygen forms into a nondissociatively bound state with a heat of about 50 kcal/mole (state I) and then forms into a more strongly bound stage with an ordered structure and a higher heat of adsorption (110 kcal/mole). The final stage is characterized by the formation of an oxide film at the nickel surface.

Since the exposure pressure was two decades higher in this experiment, most likely the first stage was not observed. The bulge at the inflection point, occurring at about an exposure time of 20 minutes, might be attributed to the reordering of the surface oxide[69]. Although the work function decreased when the oxygen was valved off, corresponding to the oxygen going into the bulk (incorporation) it did not decrease below its original value. The reason for this is not understood. An experiment was conducted to see if the work function would return to its original value naturally, figure 26 . After nearly 3 hours, $\Delta\Phi$ had decreased to within 0.33 eV of the original work function, but the rate of decrease was very slow. It therefore appeared that a very long time would be required for $\Delta\Phi$ to return to its original value. Finally, only a very small quantity of gas was observed to come off during the light EID doses. No oxygen, either atomic or molecular, was indicated by the QMS, only the small magnitudes of CO and H_2 characteristic of the clean state. It therefore appears that the adsorbed oxygen was incorporated into the bulk .

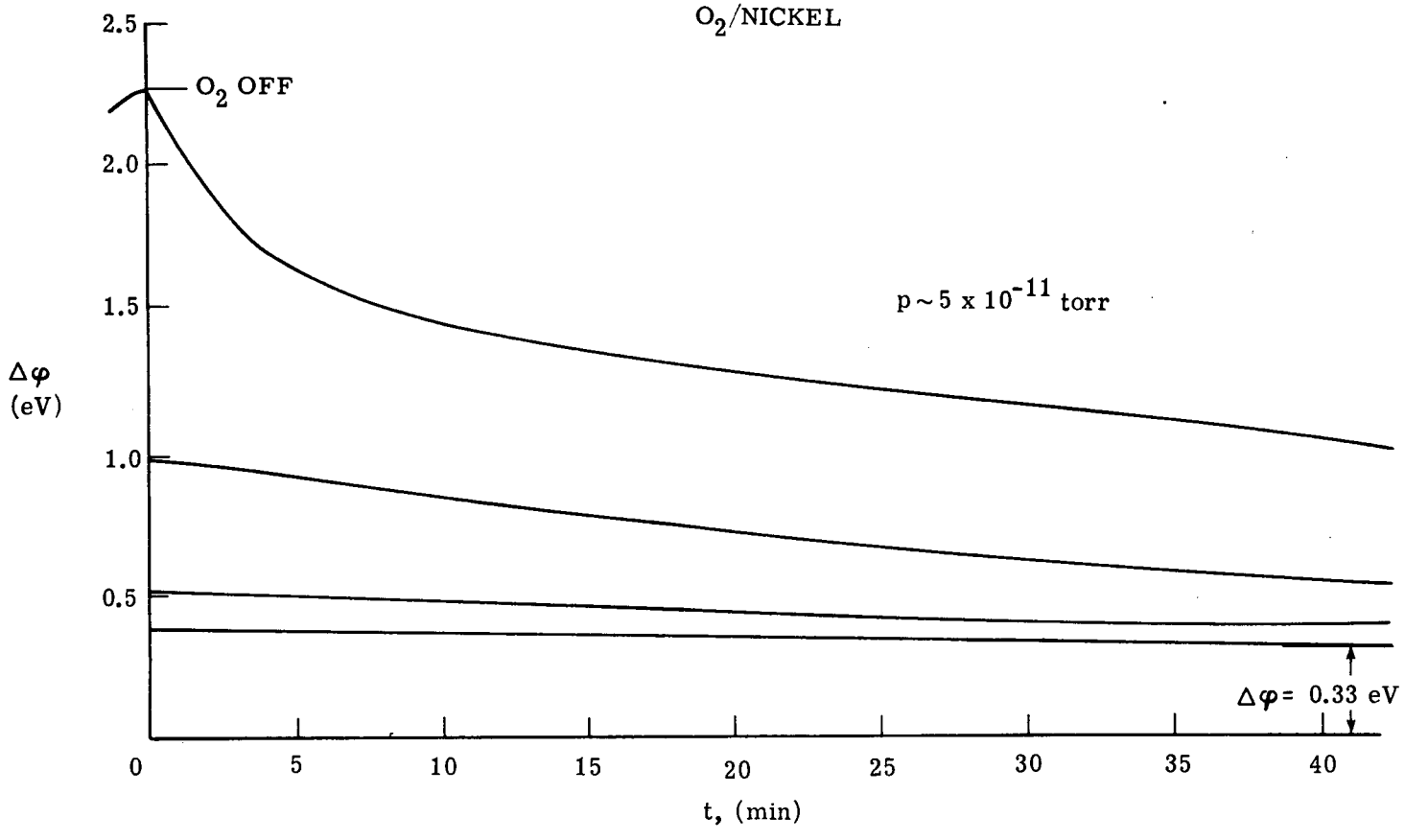

Figure 26.- Work Function Variation, $\Delta\varphi$, Versus Time, t, Following Oxygen Exposure on Nickel at 298° K.

F. Equilibrium Time Study

1. N_2/Pyrex

At the beginning of the physical adsorption/desorption studies of nitrogen on Pyrex it was found that a time greater than 60 minutes was required for adsorption equilibrium to be obtained at 1×10^{-9} torr. At higher pressures, the time to reach equilibrium was obtained far more rapidly (< 2 minutes at 2×10^{-7} torr). This apparent pressure dependence had to be determined and understood if the isotherm data was to be completed in a reasonable period of time. Further, it was necessary to know at what pressure the equilibrium time became excessive so that the "forcing" technique, described in the procedure, could be employed. Plots of the number of molecules adsorbed per cm^2, $\sigma(t)$, versus time, t, were constructed for four separate equilibrium pressures as shown in figure 27. The amount of nitrogen adsorbed continually increased with time until eventually a plateau was formed. The plateau indicated that no further change of σ with t was occurring, i.e., equilibrium had been obtained. The onset of that plateau was defined as t_{eq}, the equilibrium time. The value of t_{eq} varied from less than 2 minutes at an equilibrium pressure of about 9×10^{-8} torr to about 4 hours at 9×10^{-11} torr. The trend to extremely long equilibrium times at the lower pressures would indeed make data taking arduous. A log-log plot of t_{eq} (minutes) versus the pressure, above the adsorbed layer, p(torr), was found to be linear as shown in figure 28 and can be expressed as

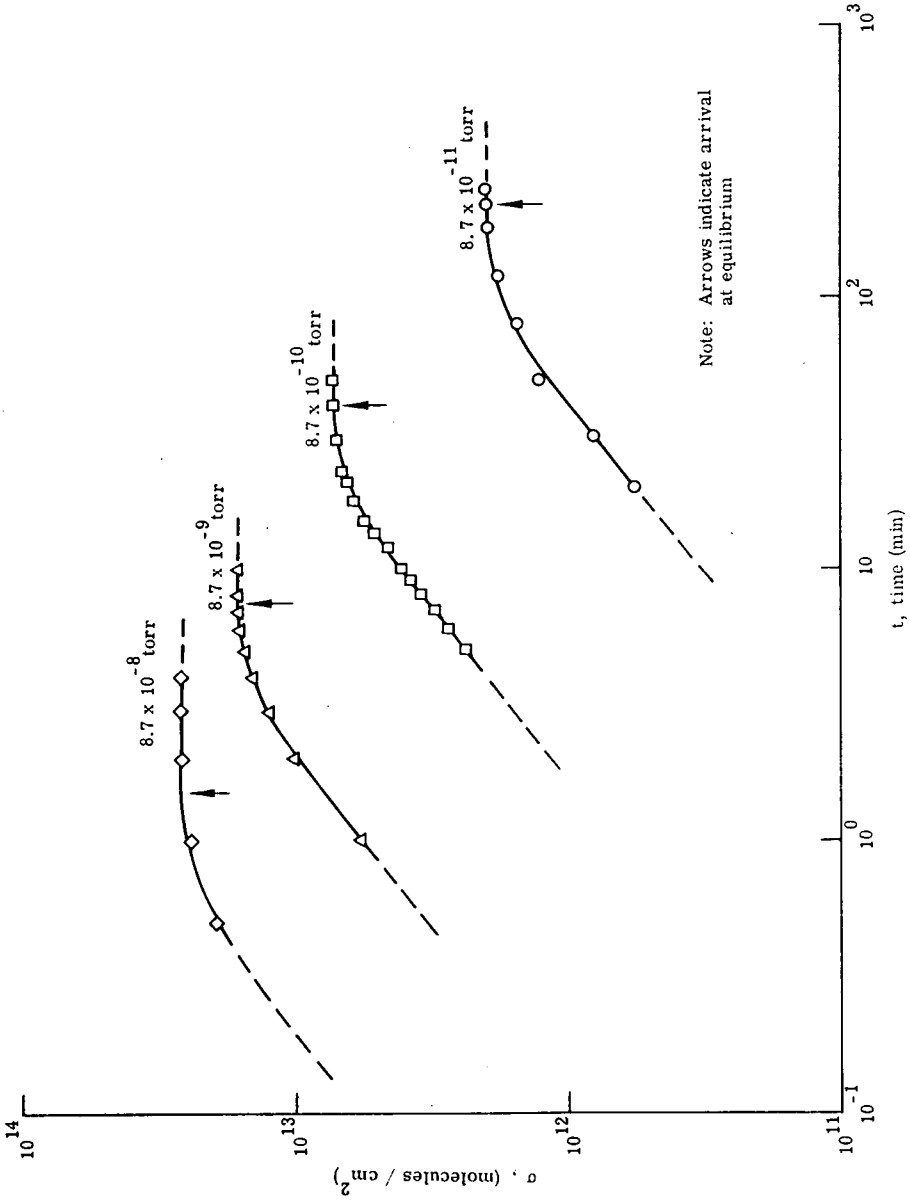

Figure 27.- Equilibrium Time, t_{eq}, Determination of Nitrogen on Pyrex for Several Equilibrium Pressures.

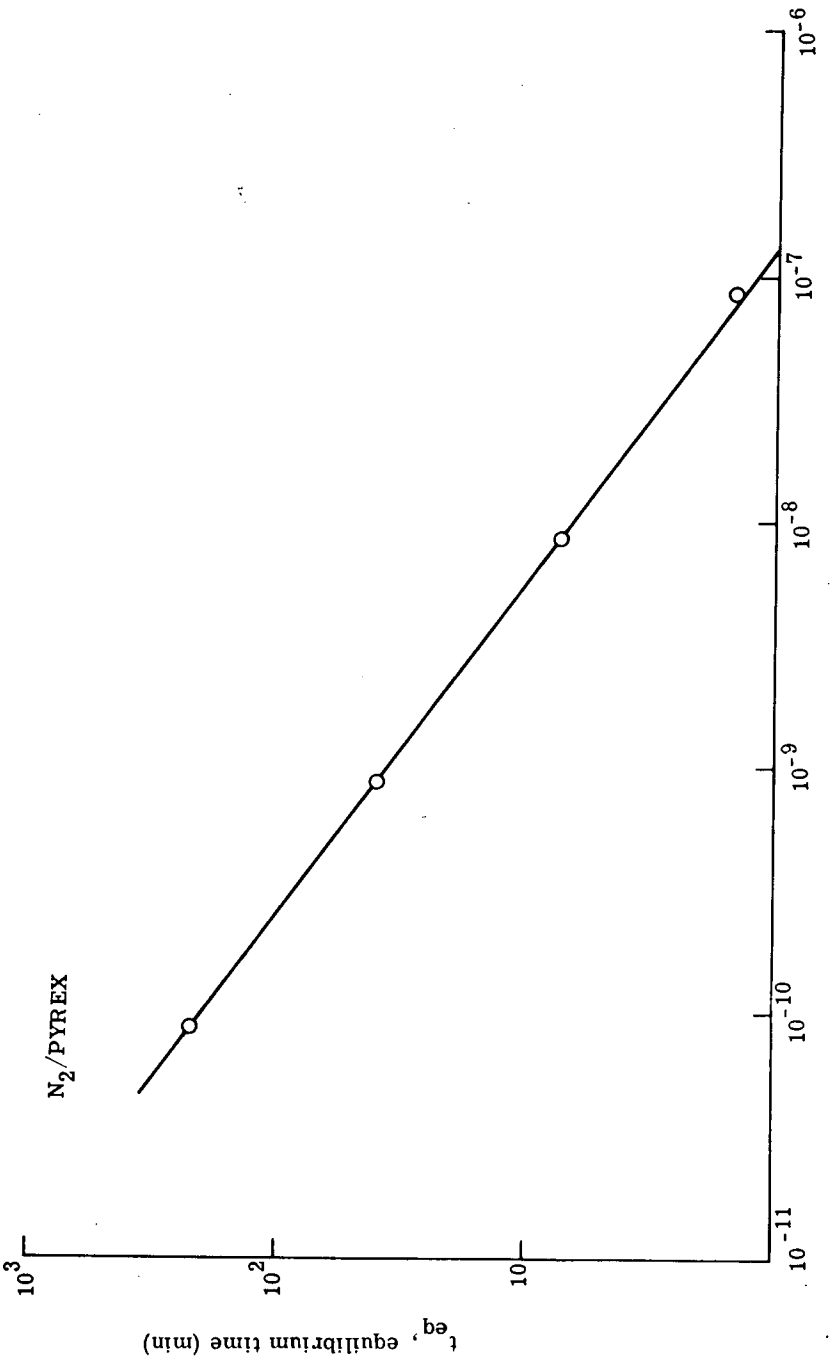

Figure 28.- Linear Relationship Between the Equilibrium Time, t_{eq}, and the Pressure Above the Adsorbed Layer, p, of Nitrogen on Pyrex.

$$\ln t_{eq} = \alpha \ln p + \ln \beta \tag{39}$$

or

$$t_{eq} = \beta p^{\alpha} \tag{39a}$$

where α and β are constants.

Extrapolation of this curve to a pressure of 1×10^{-11} torr gives a $t_{eq} \approx 18$ hours and to a pressure of 1×10^{-12} torr, a $t_{eq} \approx 97$ hours. The constants for the Pyrex surface were found to be

$$\alpha = -0.736$$

$$\beta = 8.57 \times 10^{-6} \text{ (min/torr) at } T = 77.4^{\circ}K;\ S = 100 \text{ l/s}$$

This relationship between t_{eq} and p, equation (39), has not been previously reported.

The utility of equation (39), other than a convenient indicator of the time required for equilibrium, may be found in the constant α. The constant α appears to be insensitive to pumping speed and surface temperature but does appear to vary with changes in surface heterogeneity or surface condition. Additional evidence to support this statement was not obtained with the Pyrex surface but was obtained on the stainless steel surface.

2. N_2/347 Stainless Steel

Since the stainless steel was given different surface treatments, i.e., cleaned by EID and then exposed to oxygen, an opportunity was available to study the variation of α. In addition, the constant β was also studied to empirically determine on what factors it depended. Four equilibrium time experiments were run on the oxygen treated surface at two different temperatures and at two different pumping speeds. An earlier experiment had been conducted following the EID cleaning. The results of the experiments are presented in figure 29. The data for curves A and D were taken at the same surface temperature, 77.4°K, and the data for curves C and E at 87.4°K. The data for curves A and C were taken at a pumping speed of 10 liters/sec while the data for curves E and D were taken at 110 liters/sec. These curves are all parallel but displaced from each other. For a given pumping speed and pressure, the data taken at 87.4°K indicates a more rapid approach to equilibrium since the adsorbed molecules have a higher surface mobility at this temperature. For a given temperature and pressure, the data at a pumping speed of 10 liters/sec would require longer to reach equilibrium because the pressure differential across the conductance leading into the adsorption vessel is smaller, indicating that less molecules are entering the adsorption vessel per unit time. The constant β has been found to be dependent on temperature and pumping speed in the following way:

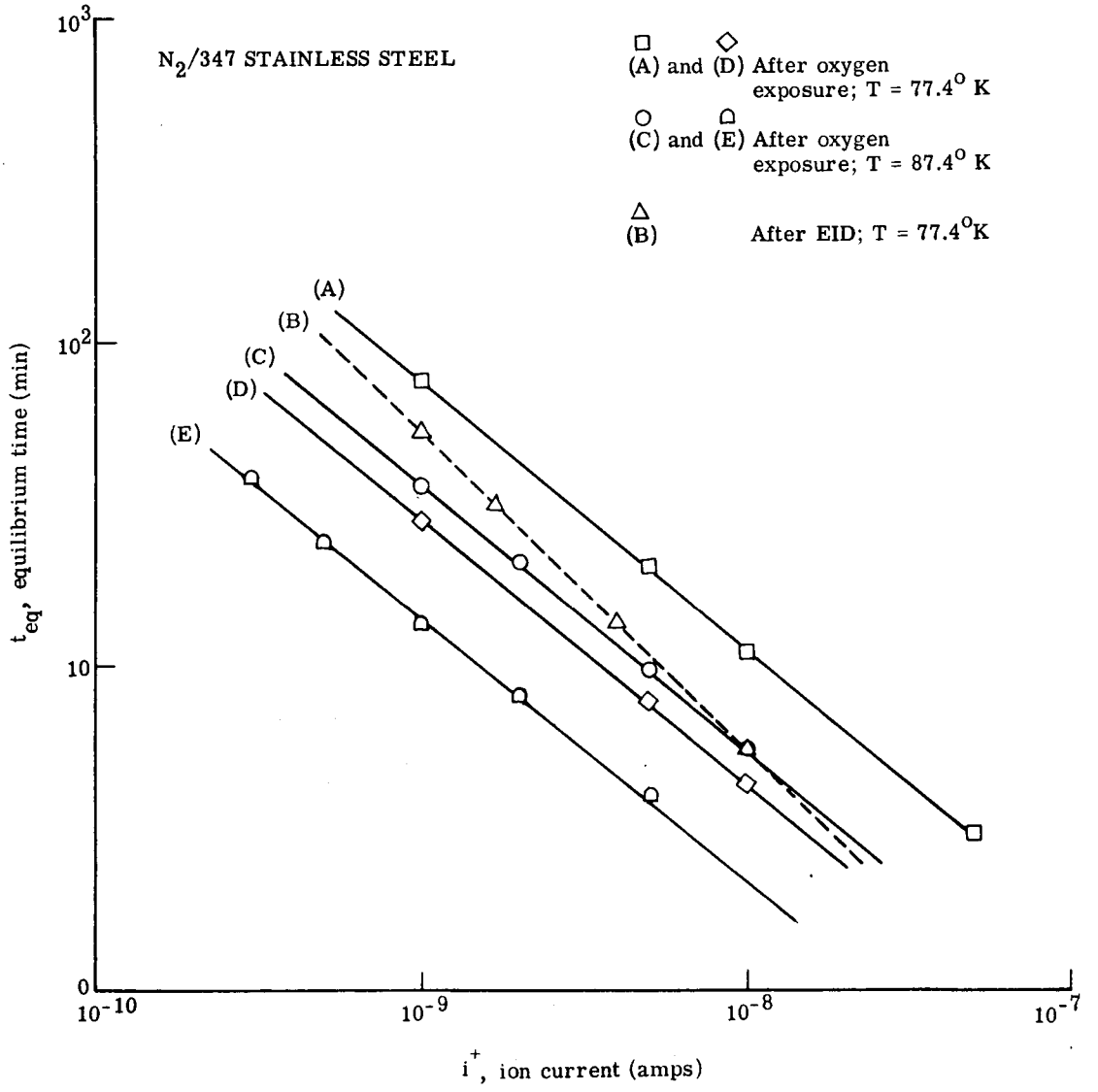

Figure 29.- Variation in Equilibrium Time, t_{eq}, With Ion Current, i^+, Of Nitrogen on 347 Stainless Steel for Different System Conditions.

$$\beta \propto \frac{S}{S + C}$$

$$\beta \propto \frac{1}{T}$$

The data for curve B was taken at a surface temperature of 77.4°K and at 110 liters/sec. Curve B may be compared to curve D since they are for the same temperature and pumping speed. It is apparent that the slopes corresponding to the two surface conditions are quite different. Curve B, representing the EID cleaned surface, has a greater negative slope so that, for a given pressure, t_{eq}, would be longer. Curve D, representing the oxygen treated surface,would have a lesser number of energetic sites and would allow the adsorbed molecule more mobility to find an equilibrium position. It thus seems probable that

$$\alpha \propto f(E_d)$$

where E_d is the barrier to surface diffusion.

Curves B and D tend to approach each other at higher pressures (10^{-7} torr) where the number of adsorbed molecules is sufficient to obscure the effect of surface diffusion.

3. N_2/Nickel

An equilibrium time experiment was also conducted for nitrogen on nickel at 77.4°K for each of the two surface conditions. It is apparent

from figures 22, 23, and 24 that the oxygen had not significantly changed the surface of the nickel and this is further supported by the equilibrium time data presented in figure 30. The two curves are very near the same indicating that there is no essential difference in the mobility of the adatoms. This contrasts strongly to the equilibrium time data observed on the stainless surface for the two surface conditions. The utility of this technique for observing surface condition changes does not seem as great as that of the heat of adsorption determination but it may provide information on surface mobility that is not attainable from the heats alone. At any rate, it is still an interesting tool for studying surfaces.

G. Surface Mobility and Clustering

The diffusion of adatoms over the surface is dependent, among other factors, upon the surface temperature and the surface heterogeneity. For example, if an atom is adsorbed on the surface at $80^{o}K$ with a heat of adsorption greater than 4 kcal/mole the residence time of the adatom is greater than 1 second. If the barrier to surface diffusion is small the adatom will migrate over the surface from site to site within that residence time as regulated by its own energy and the surface site energy distribution. If the migration is extensive, collisions between adatoms are possible and clustering may result. The formation of a number of clusters over the surface as opposed to quasi-localized adsorption of individual atoms may be reflected in the overall thermodynamic measurement of the heat of adsorption. The energy associated with the adsorbate-adsorbate interaction would be

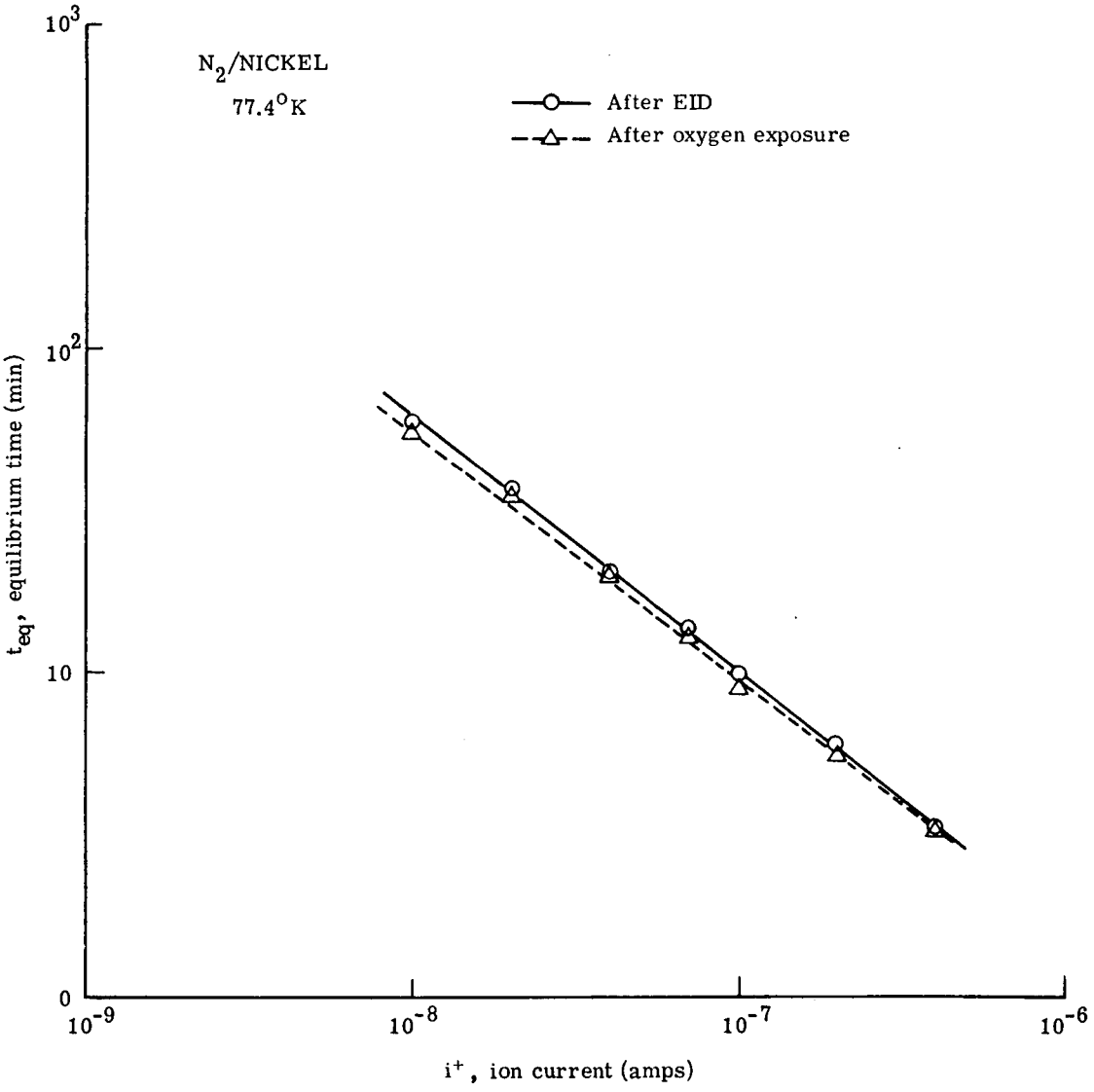

Figure 30.- Variation in Equilibrium Time, t_{eq}, With Ion Current, i^+, of Nitrogen on Nickel for Two Surface Conditions.

present in a cluster, for example. The effect of clustering would also be the approach of the adsorbate to a "liquid-like" state with the properties characteristic thereof. The knowledge of such an effect would obviously be of help in interpretation of experimental results.

The question of whether an adatom would have a significant probability of colliding with another adatom may be first approximated by assuming a random walk migration over the surface and determining the influx of adatoms into a capture area of atomic dimensions. The surface is also assumed to be a homogeneous one, i.e., all surface sites are energetically equal.

Assuming the above conditions, Halpern[70] has determined the total growth rate of a cluster of radius Rd to be

$$G_t(R) = \frac{\frac{\pi}{2} Jd^2\lambda^2}{\ln \frac{\lambda}{R}} + \pi J(Rd)^2 \qquad \frac{R}{\lambda} \to 0 \tag{40}$$

Where d = the lattice parameter

J = the incident flux

R = the radius multiplier of the capture center

and λ, the surface diffusion multiplier is given by

$$\lambda = \left\{ \frac{\nu_1}{\nu_0} \exp\left[(E_a - E_d)/RT\right] + 1 \right\}^{1/2}$$

where E_a = the activation energy for desorption

E_d = the activation energy for surface diffusion

ν_1, ν_0 = characteristic frequencies of the adatom ~ 10^{12} sec^{-1}

Now in the case of low pressure ($< 1 \times 10^{-6}$) the second term in equation (40) may be neglected. Assuming $\nu_1 \approx \nu_0$ and that

$$\exp\,[(E_a - E_d)/RT] >> 1$$

then equation (40) becomes

$$G_t(R) \approx \frac{\frac{\pi}{2} Jd^2\lambda^2}{\ln \frac{\lambda}{R}} \tag{41}$$

where $\lambda = \exp\,[(E_a - E_d)/2RT]$

For surface temperatures 87.4°K and 77.4°K and $E_a - E_d$ = 4, 3, 2, and 1 kcal/mole, table V shows the variation of cluster growth rate with pressure. If there is a difference of 4 kcal/mole between adsorption and diffusion energies, clusters are possible (at a chosen site with a radius of 3.5×10^{-8} cm) for any pressure below 1×10^{-13} torr and residence times of about 1 second. For an energy difference between 1 and 2 kcal/mole, which is conservative for physical adsorption,[71], clustering is probable at pressures above 1×10^{-9} torr at 77.4°K and is probable at pressures above 1×10^{-8} torr at 87.4°K.

It is apparent from table IV that the lower surface temperature gives considerably higher growth rates for the same pressure and energy difference, $E_a - E_d$. Certainly these energies will change, because the lower temperature would decrease the mobility of the adatom in addition to increasing its residence time. These two conflicting arguments are not reflected in the above theory. There is also no

inclusion of surface heterogeneity or an accurate relationship between gas phase and the adsorbed state. The theory is still instructive however, even with its shortcomings, for indicating a strong possibility of clustering.

TABLE V.- THE GROWTH RATE OF CLUSTERS* AS A FUNCTION OF PRESSURE

T (^{o}K)	P (torr)	$E_a - E_d$ (kcal/mole)	$G_t(R)$ (molecules/sec) = 4	3	2	1
87.4	1×10^{-7}		3.78×10^{7}	1.63×10^{5}	7.54×10^{2}	4.76×10^{0}
87.4	1×10^{-8}		3.78×10^{6}	1.63×10^{4}	7.54×10^{1}	4.76×10^{-1}
87.4	1×10^{-9}		3.78×10^{5}	1.63×10^{3}	7.54×10^{0}	4.76×10^{-2}
87.4	1×10^{-10}		3.78×10^{4}	1.63×10^{2}	7.54×10^{-1}	4.76×10^{-3}
87.4	1×10^{-11}		3.78×10^{3}	1.63×10^{1}	7.54×10^{-2}	4.76×10^{-4}
87.4	1×10^{-12}		3.78×10^{2}	1.63×10^{0}	7.54×10^{-3}	4.76×10^{-5}
77.4	1×10^{-7}		6.56×10^{8}	1.31×10^{6}	2.96×10^{3}	8.87×10^{0}
77.4	1×10^{-8}		6.56×10^{7}	1.31×10^{5}	2.96×10^{2}	8.87×10^{-1}
77.4	1×10^{-9}		6.56×10^{6}	1.31×10^{4}	2.96×10^{1}	8.87×10^{-2}
77.4	1×10^{-10}		6.56×10^{5}	1.31×10^{3}	2.96×10^{0}	8.87×10^{-3}
77.4	1×10^{-11}		6.56×10^{4}	1.31×10^{2}	2.96×10^{-1}	8.87×10^{-4}
77.4	1×10^{-12}		6.56×10^{3}	1.31×10^{1}	2.96×10^{-2}	8.87×10^{-5}

*$d = 3.5 \times 10^{-8}$ cm

R = 1

VI. CONCLUSIONS

1. The nitrogen adsorption data on Pyrex, 347 stainless steel and nickel were linearized by the Dubinin-Radushkevich equation. A significant temperature dependence was observed for the system nitrogen on nickel. The adsorption data at higher pressures (> 1 x 10^{-9} torr) for the systems nitrogen on stainless and nitrogen on nickel at 77.4°K have a different slope than the lower pressure data.

2. The relative order of binding of the nitrogen molecule to the three solids studied was stainless > Pyrex > nickel at 1 x 10^{-11} torr.

3. The effect of the chemical cleaning and the EID doses increased the binding energy between the nitrogen and the solids. The data indicates that the heterogeneity of the stainless was very high and indicates that the surface of Pyrex had been leached.

4. EID is a useful tool in cleaning metal surfaces for ultrahigh vacuum applications when used in conjunction with vacuum firing and chemical cleaning pretreatment. At least a monolayer of gas was observed to desorb from the two metals prior to physical adsorption studies. A net work function change of -0.3 eV as a result of EID was observed on the stainless, but very little work function change was noted on the nickel.

5. Oxygen incorporation was observed to occur naturally following adsorption and appears to be rapidly promoted by electron impact.

6. The logarithm of the time to arrive at equilibrium, t_{eq}, was found to vary linearly with the logarithm of the pressure above the adsorbed layer, p. The constant α from equation (39a) was observed to be sensitive to the heterogeneity of the surface and may be related to the activation energy for surface diffusion of physically adsorbed molecules.

7. The probability of clustering of the physically adsorbed gases on the surface for $E_a - E_d \geq 2$ is significant according to present theory. The effect of clustering may be a factor causing the temperature dependency observed in the fit of the nitrogen on nickel data to the Dubinin-Radushkevich equation.

8. The chemical adsorption of nitrogen on nickel at surface temperatures of 298°K and below was not found to occur.

VII. BIBLIOGRAPHY

1. Young, D. M.; and Crowell, A. D.: Physical Adsorption of Gases, Butterworth, London, 1962.

2. Flood, E. A., ed.: The Solid-Gas Interface, Volumes I and II, Marcel Dekker, New York, 1967.

3. Ross, S.; and Olivier, J. P.: On Physical Adsorption, Interscience Publishers, New York, 1964.

4. Hayward, D. O.; and Trapnell, B. M. W.: Chemisorption, 2nd ed., Butterworth, London, 1964.

5. Green, M., ed.: Solid State Surface Science, Marcel Dekker, New York, 1969.

6. Saltzburg, H.; Smith, J. N., Jr.; and Rogers, M., ed.: Fundamentals of Gas-Surface Interactions, Academic Press, New York, 1967.

7. Samorjai, G. A., ed.: The Structure and Chemistry of Solid Surfaces, Wiley, New York, 1969.

8. de Boer, J. H.: The Dynamical Character of Adsorption, Oxford, 1953.

9. Kaminsky, M.: Atomic and Ionic Impact Phenomena on Metal Surfaces, Academic Press, New York, 1965.

10. Hobson, J. P.: Can. J. Phys., 37, 300 (1959).

11. Hobson, J. P.; and Armstrong, R. A.: J. Phys. Chem., 67, 2000 (1963).

12. Ricca, F.; Medana, R.; and Bellardo, A.: Z. Physik, Chem., 52, 276 (1967).

13. Ricca, F.; Bellardo, A.; and Medana R.: Ric. Sci. 36, 460, 1966.

14. Tuzi, Y.; and Saito, T.: J. Vac. Sci. Technol., 6, 238, (1969).

15. Baker, B. G.; and Fox, D. G.: Trans. Faraday Soc., 61, 2001, (1965).

16. Kaganer M.G.: Proc. Acad. Sci., USSR, 116, 251, (1957).

17. See reference 11, pg. 2003.

18. See reference 11, pg. 2006.

19. Misra, D. N.: Surface Sci., 18, 367, (1969).

20. Cerofolini, G. F.: Surface Sci., 24 , 391 (1971).

21. Schram, A.: Sup. Al Nuovo Cim., 5, 309 and 5, 291, (1967).

22. See reference 1.

23. See reference 11, pg. 2002.

24. Troy, M.; and Wightman, J. P.: J. Vac. Sci. Technol., 8, 84 (1971).

25. Degras, D. A.; Schram, A.; Lux, B.; and Petermann, L. A.: Trans. 8th Nat. Vac. Symposium, Pergamon Press, 177, (1961).

26. Hobson, J. P.: Brit. J. Appl. Phys., 14, 544, (1963).

27. Zettlemoyer, A. C.; Yung-Fang Yu; and Chessik, T. T.: J. Phys. Chem., 59, 588 (1955).

28. See reference 21, pg. 291.

29. See reference 24.

30. See reference 15, pg. 2004.

31. Germer, L. H.; Scheibner, E. J.; and Hartman, C. D.: Phil. Mag., 5, 222, (1960).

32. Gundry, P. M.; Haber, J.; and Tompkins, F. C.: J. Catalysis, 1, 363, (1964).

33. Germer, L. H.; and MacRae, A. U.: J. Chem. Phys., 36, 1555 (1962).

34. See reference 7, pg. 53-1.

35. See reference 7, pg. 56-1.

36. King, D. A.: Surface Sci., 9, 375, (1968).

37. Winters, H. F.; Horne, D. E.; and Donaldson, E. E.: J. Chem. Phys., 41, 2766, (1964).

38. Steinrisser, F.; and Sickafus, E. N.: Int. Conf. Solid Surfaces, Boston, (1971).

39. Madey, T. E.; Yates, J. T., Jr.: J. Vac. Sci. Technol., 8, 525, (1971).

40. Klopfer, A.: J. Vac. Sci. Technol., 9, 301, (1972).

41. Horgan, A. M.; and King, D. A.: Surface Sci., 23, 259, (1970).

42. Delchar, T.; Tompkins, F. C.: Surface Sci., 8, 165, (1967).

43. Klopfer, A.: Sup. Al Nuovo Cim., 5, 607, (1967).

44. Sickafus, E. N.: Surface Sci., 19, 181, (1970).

45. Coad, J. D.; and Riviére, J. C.: Surface Sci., 25, (1971).

46. Williams, D. P.; and Gasser, R. D. H.: Surface Sci., 25, (1971).

47. See reference 5, pg. 179.

48. Shelton, H.: Phys. Rev., 107, 1553 (1957).

49. Baker, B. G.; and Johnson, B. B.: Vacuum, 21, 91, (1970).

50. Suhrmann, R.; and Wedler, G.: Z. Angew, Phys., 14, 70, (1962).

51. Farnsworth, H. E.; and Madden, H. H., Jr.: J. Appl. Phys., 32, 1933 (1961).

52. Cardwell, A. B.: Phys. Rev., 76, (1949).

53. Riviére, J. C.: Proc. Phys. Soc., (London), 70, 676, (1957).

54. Clausing, P.: Ann. Der Physik, 12, 961,(1932).

55. Buckingham, J. D.; and Thorne, P. N.: Third Cz. Conf. on Electronics and Vacuum Phys. Trans., 375 (1965).

56. See reference 10.

57. Hansen, N.: Vacuum-techik, 11, 70, (1962).

58. Menzel, D.; and Gomer, R.: J. Chem. Phys., 41, 3311, (1964).

59. See reference 9, pg. 10; reference 5, pg. 179.

60. Brock, F. J.: NASA CR-66273, U.S. Government Printing Office, Washington, D.C., (1967).

61. See reference 11, pg. 2002.

62. Petermann, L. A.: Sup. Al Nuovo Cim., 1, 601, (1963).

63. Ricca, F.; and Medana, R.: La Ric. Sci., 4, 617, (1964).

64. Hobson, J. P.: J. Chem. Phys., 34, 1859, (1961).

65. Troy, M.; and Wightman, J. P.: J. Vac. Sci. Technol., 7, 429, (1970).

66. Bradford, J. M.: Ph. D. Thesis, N. C. State University, (1968).

67. See reference 24.

68. Quinn, C. M.; and Roberts, M. W.: Trans. Faraday Soc., 60, 899, (1964).

69. MacRae, A. U.: Surface Sci., 1, 319, (1964).

70. Halpern, V.: J. Appl. Phys., 40 , 4627, (1969).

71. Barrer, R. M.; and Strachan, E.: Proc. Roy. Soc. (London), A231, 52, (1955).

VIII. APPENDICES

A. An AES Experiment

The question of whether EID would efficiently clean the surface of the polycrystalline nickel is important to the interpretation of the results of the nitrogen adsorption on nickel discussed earlier. In order to answer this question, a separate AES experiment was conducted. The AES instrument permitted the determination of the chemical composition of the surface but because the instrument was difficult to calibrate no quantitative information was obtained. Changes in the signal intensity following individual EID doses were observed however, to determine the effectiveness of EID as a surface cleaning tool.

The polycrystalline nickel sample was prepared in the exact same manner as the nickel adsorption vessel. After mounting the sample inside the vacuum system, the system was baked out to 200°C for 24 hours. The ultimate pressure attained was less than 1×10^{-10} torr. The cylindrical energy analyzer was operated at voltages sweeping from 0 to 1000 V and the incident electron beam of 150 μA was operated at an energy of 2000 eV.

An Auger spectrum was taken on the nickel prior to any EID dosage and is presented in figure A1-a. The derivative of the electron energy distribution $dN(E)/dE$ in arbitrary units was plotted versus sweep voltage, E_s, in volts. The actual energy of the Auger electrons (E_a) can be found by dividing E_s by 0.593. The largest contaminants observed were sulfur at E_s = 90 V (E_a = 152 eV), carbon at E_s = 160 V

C3

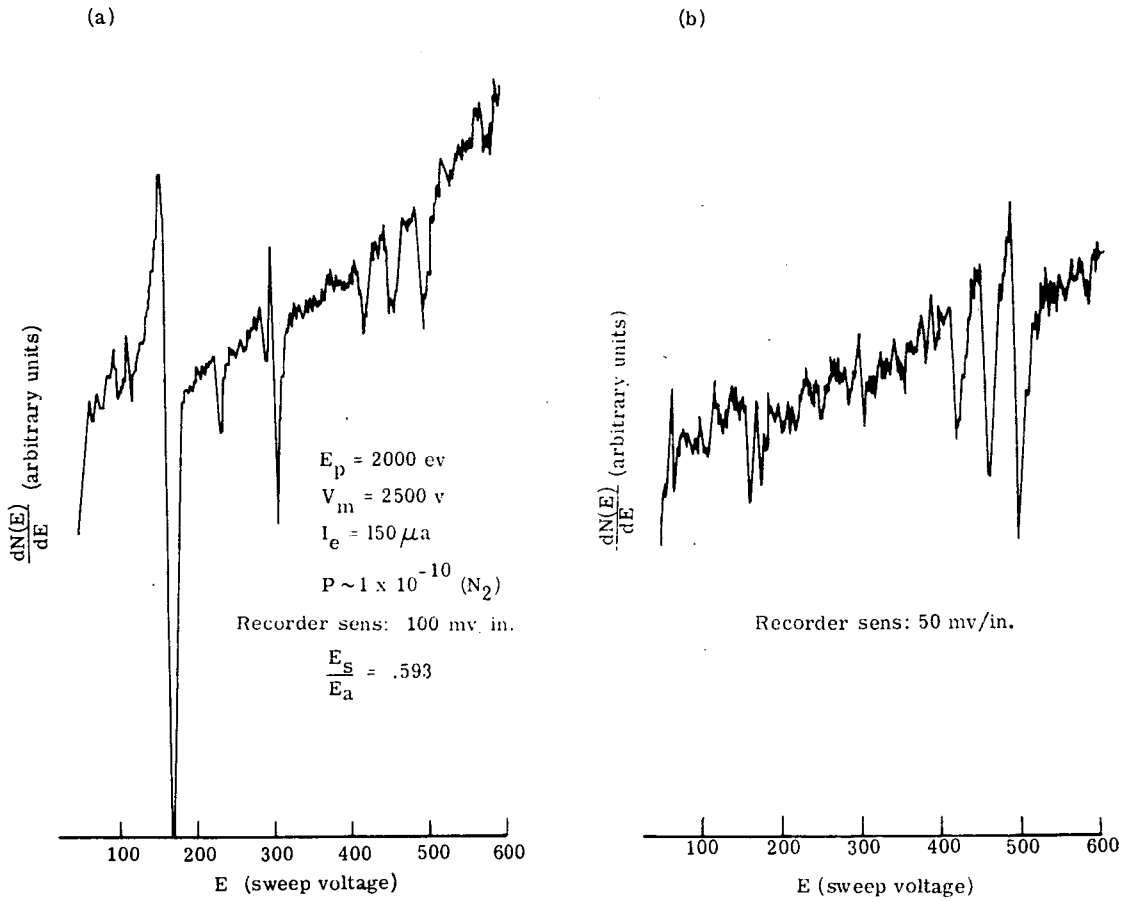

Figure A-1.- Auger Spectrum of Polycrystalline Nickel Before (a) and After (b) EID Cleaning.

(E_a = 270 eV), oxygen at E_s = 298 V (E_a = 505 eV) and titanium at E_s = 230 V (E_a = 388). The three peaks on the right of the spectrum are characteristic nickel peaks. The nickel was then subjected to low energy electron bombardments (EID) at current densities up to 1 ma/cm^2 and electron energies up to 1100 eV. Initially a current density of 0.1 mA/cm^2 and an electron energy of 600 eV were used. After a total of 33 hours of EID the sulfur, carbon, and titanium contaminants were gone and the oxygen was reduced to a small signal. Figure A1-b is the Auger spectrum showing the relatively clean state of the nickel surface. The characteristic nickel peaks are sharper and cleaner even though the sensitivity was increased by a factor of two. Two new peaks appearing at E_s = 150 V and E_s = 170 eV are a result of the deposition of thorium on the nickel. During the electron bombardment the thoria coated tungsten filament of the electron gun was run at an excessively high temperature causing the accumulation of thorium. It may be that the low level of oxygen is associated with these peaks.

Figure A2 is a time history of the AES patterns for oxygen, carbon, and sulfur. Titanium was removed after the first few EID doses. The peak-to-peak Auger signal of the contaminants relative to the nickel peak at E_s = 450 V are plotted versus EID time. The sulfur was removed in approximately 3 hours of EID and the carbon signal reduced about 90% in 5 hours. Simultaneously with the decrease in carbon the oxygen signal increased. A possible explanation of this observation is that the carbon signal initially covered the surface and was the predominant source of Auger electrons. As the carbon was removed

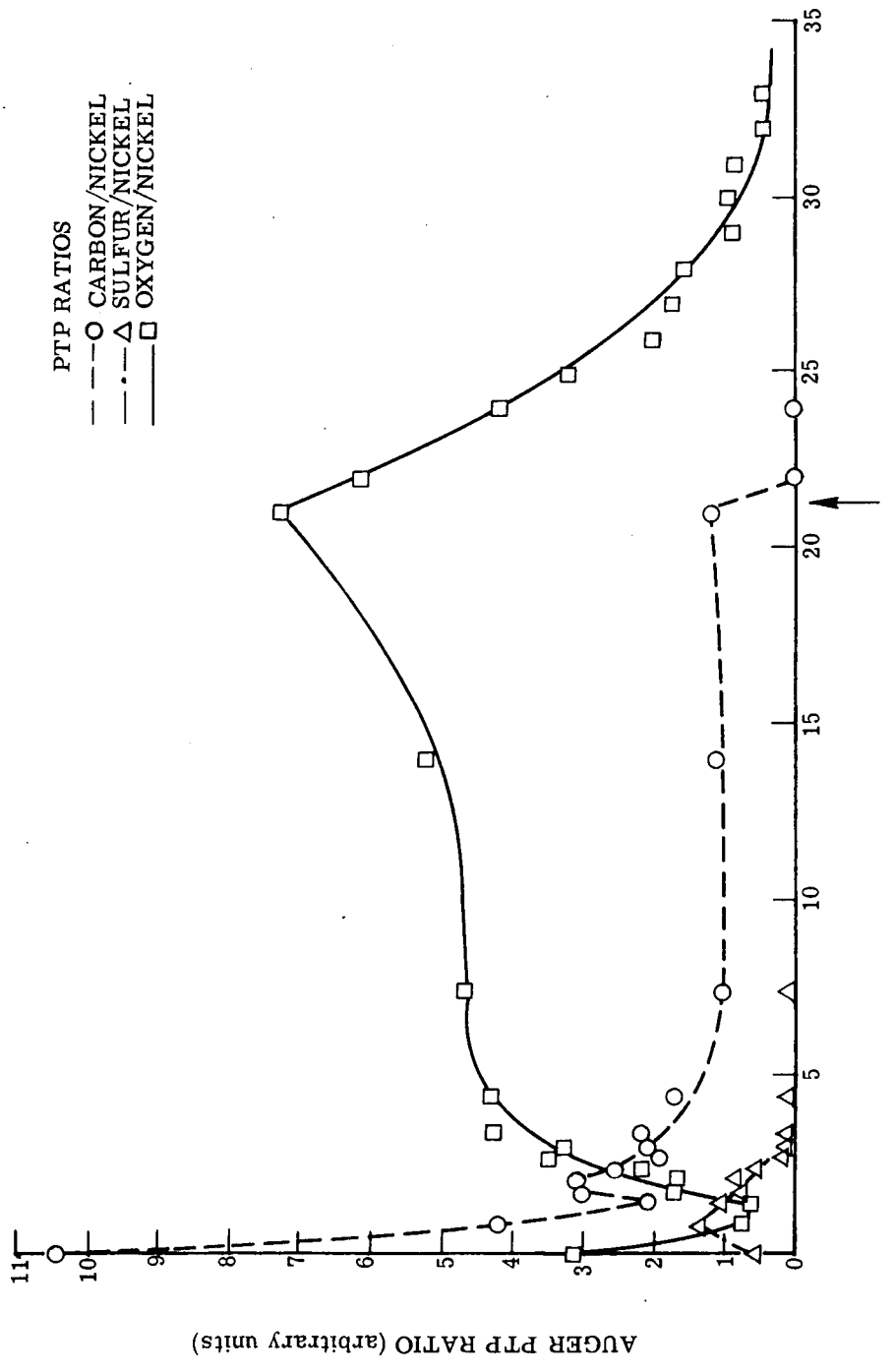

Figure A-2.- Variation of Auger Peak to Peak (PTP) Signals of Carbon, Sulfur, and Oxygen Relative to Nickel with EID Time.

(probably as CO) the oxygen was uncovered and produced a higher flux of Auger electrons. After 21 hours of EID, the oxygen signal actually increased, possibly emanating from the hot filament of the electron gun. The electron energy was then increased from 600 eV to 1100 eV. Immediately the carbon signal decreased to zero. The oxygen signal decreased continually to its lowest level after an additional 11 hours of EID. The temperature of the nickel with the higher energy electrons increased to 600°C. Since no significant pressure increase was observed during this period, the oxygen is thought to have diffused into the nickel as a result of the increase in temperature rather than desorbed by the higher energy electron impact. Carbon is also thought to have diffused into the bulk.

The results of this experiment indicate that the chemical cleaning procedure employed, followed by a 600°C bakeout in combination with EID, will clean a nickel surface.

B. Error Analysis

The question of whether the measurements made in this experiment are of reasonable precision can be answered by determining the relative probable error. The relative probable error of a function $f(x_1, x_2, \ldots x_n)$ is given by

$$\frac{\delta f}{f} = \left\{ \sum_n \left[\frac{\left(\frac{\partial f}{\partial x}\right)_n \delta x_n}{f} \right]^2 \right\}^{\frac{1}{2}} \qquad \text{(B-1)}$$

assuming that the variation in the functional parameters, x_n, is small and independent for all n.

The determination of the number of molecules adsorbed per cm^2, σ, involves several independent measurements of pressure, temperature, time, area, and conductance. Equation (14) was used to make these measurements and is repeated here for convenience:

$$\sigma = \frac{i_f^+ \, c}{i_m^+ \, s_f \, AkT} \quad \text{[IDVM]}$$

The maximum uncertainties for these parameters are:

Parameter	Maximum Uncertainty (%)
$\frac{\delta i_f^+}{i_f^+}$	3.0
$\frac{\delta i_m^+}{i_m^+}$	3.0

$\frac{\delta c}{c}$		3.0
$\frac{\delta s_f}{s_f}$		11.0
$\frac{\delta A}{A}$		1.0
$\frac{\delta T}{T}$		1.0
$\frac{\delta[IDVM]}{[IDVM]}$		10.0
	TOTAL	32.0

These values correspond to a relative probable error of

$$\frac{\delta\sigma}{\sigma} = 15.8\% \text{ (percent of decade)}$$

The maximum uncertainty in a given pressure measurement was found to be about 14% corresponding to a relative probable error of

$$\frac{\delta p}{p} = 9\% \text{ (percent of decade)}$$

Finally relative probable errors of 12.4% and 2.0% were determined for q_{st} and $\Delta\varphi$, respectively.

IX. VITA

The author, Ronald Allen Outlaw, was born [redacted]. He attended school at Hampton High, Hampton, Virginia, and was graduated from there in June 1955.

Following graduation, he entered the Norfolk Division of William and Mary to pursue a degree in electrical engineering under the Co-operative Engineering Program.

In the summer of 1958, the author transferred to Virginia Polytechnic Institute and switched his curriculum to physics. In June 1960 he completed the requirements for the Co-operative Program and for a B.S. degree in physics and was graduated.

Upon graduation, the author was employed by the National Aeronautics and Space Administration, Langley Research Center, Hampton, Virginia, where he had also worked during the industrial work periods of the Co-operative Program.

In January 1961 the author left Langley Research Center to go in the U.S. Navy. After graduation from Naval O.C.S., May 1961, in Newport, Rhode Island, he was commissioned as an Ensign, U.S.N.R.

Following a tour of 2 years aboard a destroyer, the Navy assigned him to work at Langley in the same position he had left. He resigned from the Navy in May 1965 and continued to work at Langley. In the fall of 1966, he entered the graduate school at Virginia Polytechnic Institute to study physics. After receiving an M.S. in Physics in June 1969, the author entered the Materials Engineering Science program.

The author is a member of Kappa Theta Epsilon, Alpha Sigma Mu, Sigma Pi Sigma and Phi Kappa Phi.